

---

Structures Research Report No. BB-512  
FINAL PROJECT REPORT

March, 2000

UF Project No. 4910 4504 618 12  
State Job No. 99700-3592-119  
Contract No. BB-512  
WPI No. 0510836

---

**USE OF GROUT PADS  
FOR SIGN AND LIGHTING STRUCTURES  
PART 1 - STRUCTURAL EVALUATION**

---

Principal Investigators:

Ronald A. Cook, Ph.D., P.E.  
Mang Tia, Ph.D., P.E.

Graduate Research Assistants:

Kevin B. Fischer  
Daniel D. Darku

Project Manager:

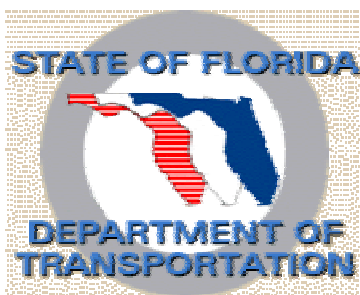
Marcus H. Ansley, P.E.

---

Department of Civil Engineering  
College of Engineering  
University of Florida  
Gainesville, Florida 32611

Engineering and Industrial Experiment Station

---



USE OF GROUT PADS  
FOR SIGN AND LIGHTING STRUCTURES

State Job No. 99700-3592-119  
Contract No. BB-512  
WPI No. 0510836  
UF No. 4910 4504 618 12

Principal Investigators:	R. A. Cook M. Tia
Graduate Research Assistants:	K. B. Fischer D. D. Darku
FDOT Technical Coordinator:	M. H. Ansley

Engineering and Industrial Experiment Station  
Department of Civil Engineering  
University of Florida  
Gainesville, Florida

## DISCLAIMER

“The opinions, findings, and conclusions expressed in this publication are those of the authors and not necessarily those of the Florida Department of Transportation or the U.S. Department of Transportation.

Prepared in cooperation with the State of Florida Department of Transportation and the U.S. Department of Transportation.”

## LIST OF FIGURES

<u>Figure</u>	<u>page</u>
2.1 Rigid plate behavior.....	5
2.2 Flexible plate behavior.....	8
2.3 Procedure based on ultimate strength concrete beam design .....	10
2.4 Procedure based on working stress method.....	15
2.5 Components of total deflection.....	21
3.1 Base plate and pipe dimensions .....	25
3.2 Anchor bolt detail .....	28
3.3 Anchor bolt patterns.....	32
3.4 Typical shop drawing.....	33
3.5 FDOT grout pad requirement.....	34
3.6 Position of plate stiffeners .....	36
3.7 Typical test block.....	37
3.8 Schematic diagram of typical test setup .....	38
4.1 Coupons for pipe tensile strength tests .....	44
4.2 Detail for typical compression bolt.....	45
4.3 Grout application formwork .....	48
4.4 Typical stiffener .....	50
4.5 Typical test setup .....	51
4.6 Compression bolt load cells.....	52
4.7 Tension bolt load cells .....	54

4.8 Load cell placement .....	55
4.9 Template for LVDTs.....	56
4.10 Position of pipe displacement LVDT relative to test block.....	57
4.11 Points at which elevation of deformed plate was measured .....	59
5.1 Deformed shape at axis of bending of Specimen #1.....	64
5.2 Deformed shape in tension region of Specimen #1 .....	64
5.3 Plot of deformed shape of Specimen #1 .....	65
5.4 Bolt deformations observed during failure loading of Specimen #1 .....	66
5.5 Deformation of tension bolt during loading of Specimen #2 .....	67
5.6 Deformed shape at axis of bending of Specimen #2.....	68
5.7 Deformation in tension region of Specimen #2 .....	68
5.8 Plot of deformed shape of Specimen #2 .....	69
5.9 Deformed shape at axis of bending of Specimen #3.....	70
5.10 Deformed shape in tension region of Specimen #3 .....	71
5.11 Plot of deformed shape of Specimen #3 .....	72
5.12 Deformed shape at axis of bending of Specimen #4.....	73
5.13 Deformed shape in tension region of Specimen #4 .....	73
5.14 Plot of deformed shape of Specimen #4 .....	74
5.15 Elastic range load-displacement for Specimen #1 .....	77
5.16 Elastic range load-displacement for Specimen #2.....	77
5.17 Elastic range load-displacement for Specimen #3 .....	78
5.18 Elastic range load-displacement for Specimen #4 .....	78
5.19 Full-scale load-displacement for Specimen #1 .....	78
5.20 Full-scale load-displacement for Specimen #2.....	79
5.21 Full-scale load-displacement for Specimen #3 .....	79

5.22 Full-scale load-displacement for Specimen #4.....	79
6.1 Four bolt diamond arrangement.....	84
6.2 Plot of movement of grout reaction resultant during loading for 8-3/4-4s-G.....	88
7.1 Typical stiffness determination by linear regression analysis .....	96
7.2 Rotation of system due to bolts.....	102
7.3 Power relationship trend for large FDOT-type plate specimens .....	106
7.4 Plot of calculated to predicted plate rotations vs. $r_{\Delta}/t_{plate}$ ratio .....	107

## LIST OF TABLES

<u>Table</u>	<u>page</u>
3.1 Test dimensions .....	32
4.1 Concrete cylinder strengths at 28 days .....	40
4.2 Concrete cylinder strengths at 141 days .....	40
4.3 Anchor bolt tensile strengths .....	41
4.4 Grout cube strengths .....	42
4.5 Flow cone results .....	43
4.6 Pipe tensile strength test results .....	44
5.1 Predicted yield and plastic moments in pipe .....	75
5.2 Comparison of predicted plastic moment and maximum moment in pipe .....	75
5.3 Maximum applied moments and recorded bolt loads .....	80
6.1 Results of plate thickness design equations .....	83
6.2 Design analysis for plates from Cook (1995) study .....	85
6.3 Load carried by grout pad .....	86
6.4 Calculated location of compressive reaction acting on the grout pad .....	87
6.5 Comparison of predicted and measured bolt loads at service load level .....	90
6.6 Comparison of predicted to measured bolt forces at ultimate load level .....	90
6.7 Grout bearing stress evaluation .....	93
7.1 Connection stiffnesses .....	97
7.2 Comparison of predicted connection rotations .....	100
7.3 Components of calculated connection rotation using equation (2-31) .....	101

7.4 Evaluation of predicted bolt rotation .....	104
7.5 Comparison of prediction equation to FEM predictions and test values.....	105
7.6 Comparison of predicted plate rotations to $r_{\Delta}/t_{\text{plate}}$ ratio .....	108
7.7 Evaluation of predicted plate rotation.....	108
7.8 Comparison of measured to predicted rotations .....	109
7.9 Evaluation of predicted plate rotation for three specimens with grout pads .....	110
7.10 Evaluation of serviceability design equation for base plates with grout pads .....	111
7.11 Evaluation of design equation for base plates with grout pads and stiffeners.....	112
7.12 Evaluation of final rotation equation for plates with grout pads and stiffeners.....	113

## CHAPTER 1 INTRODUCTION

### 1.1 General

Base plates are structural elements used to connect structural members to their foundations. They are commonly used in conjunction with tubular high mast poles, roadway light poles, and traffic mast arms. The base plate connects the sign or lighting structure to its foundation with anchor bolts using a double nut installation.

The Florida Department of Transportation (FDOT) recommends that a grout pad be placed beneath the base plates of all of its sign and lighting structures. Many states are eliminating this requirement from their specifications for these structures. The main argument for eliminating grout pads is that they prevent the visual inspection of the anchor bolts for possible corrosion due to weathering. Currently, there is very little information available pertaining to both the structural and serviceability benefits of placing a grout pad beneath base plates.

### 1.2 Objective

The primary objective of this study was to evaluate the structural behavior of sign and lighting structure base plates with and without grout pads and to develop design criteria for evaluating strength and serviceability.

### 1.3 Scope

This project was divided into four main tasks:

- 1) A literature review.
- 2) Development of the testing program.
- 3) Structural strength and serviceability tests.
- 4) Development of strength and serviceability design recommendations.

The objective of the literature review was to determine the testing procedures used, what results have been obtained and what has not already been covered by similar studies.

The second part of the project involved the development of a testing program designed to experimentally evaluate the strength and serviceability behavior of base plates exposed to large bending moments.

The third part of the project implemented the testing program. This phase concluded with the application of a bending moment to the plate and measurement of load distribution, bolt displacements and pipe displacement.

Analysis of the recorded experimental data and a recommendation of a strength and serviceability design procedure for grouted base plates based on this data encompassed the fourth and final phase of the project.

## CHAPTER 2 BACKGROUND

### 2.1 Introduction

Few experimental studies have been performed to examine the structural behavior of steel base plates loaded with large bending moments. Most of the previous base plate work has focused on the effect of applied axial load with little or no eccentricity of the axial load in column-type connections. This type of loading results in a small bending moment combined with large axial compression.

This investigation concentrates on the development of strength and serviceability design criteria for base plates loaded primarily by large bending moment constructed with grout pads beneath the base plate. These design criteria were derived for base plate systems exposed to loading dominated by bending moment

### 2.2 Previous Research

The following subsections contain background information pertaining to previous research performed on steel base plates.

#### 2.2.4 Annular Base Plates Subjected to Moment from Eccentric Shear Load

Cook et al. (1995) studied annular base plates with a gap between the bottom of the base plate and the face of the concrete. Much of this current investigation is patterned after this previous study. They applied an eccentric shear load to a tubular member

welded to plates with four, six, and eight bolt arrangements, to create a loading scenario dominated by moment.

Cook et al. (1995) performed yield line analyses for all of the failed plates. The yield line mechanisms analyzed were chosen based on the observed deformed shape of each plate. The yield line analysis was used to determine two simple design models for annular base plates.

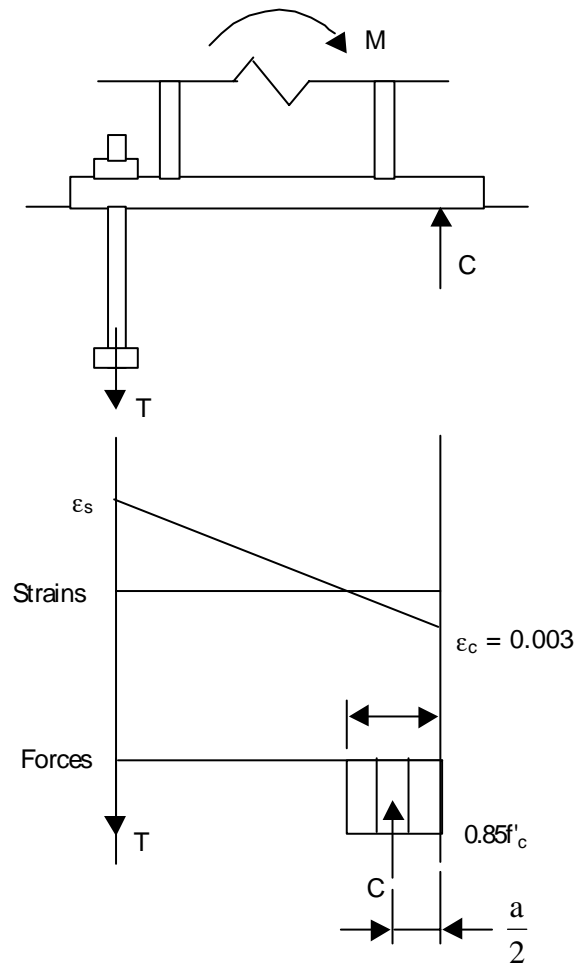


Figure 2.3 Procedure based on ultimate strength concrete beam design

The first design model was an equation for the overall moment capacity of the plate based on the plastic moment capacity of the base plate from equation (2-2) and is valid for plates with four bolts only. The first design equation was:

$$M_{\text{plate}} = \frac{\pi}{2} m_p (2r_b) \quad (2-5)$$

where  $m_p$  = plastic moment capacity of the base plate and  $r_b$  = distance from the center of the pipe to the center of the bolt.

The second design equation was once again based on the plastic moment capacity of the plate found in equation (2-2). The second design equation, valid for plates with any number of bolts, was as follows:

$$M_{\text{plate}} = 2\lambda m_p r_b \quad (2-6)$$

where:

$$\lambda = 2 \frac{\sqrt{r_{\text{pl}}^2 - r_p^2}}{(r_b - r_p)} \left( \frac{r_p}{r_b} \right) f_r \quad (2-7)$$

$$f_r = e^{\left(1 - \frac{4}{n}\right)^2} \quad (2-8)$$

$n$  = number of bolts

$r_{\text{pl}}$  = radius of plate

$r_p$  = radius of the pipe to the centerline of the pipe wall thickness

$m_p$  = plastic moment capacity of the base plate

$r_b$  = distance from the center of the pipe to the center of the bolt

### 2.3 Summary of Existing Design Methods

The following section contains a discussion of the derivation of the available formulas for determining the loads carried by base plate anchor bolts and for the required base plate thickness. These formulas were used for an analysis of the results observed during the experimentation phase of this project.

### 2.3.1 Anchor Bolt Loads

A previous study by Cook et al. (1995), as discussed earlier, yielded two strength equations for base plate design. All of the base plates connections in that study were constructed with a gap beneath the base plate and were held in place with leveling nuts. Equation (2-5) was developed for base plates with four anchors only. However, the equation can be modified to work for plates with any number of anchors:

$$P_{\text{bolt}} = \frac{2Mc}{nr_b^2} \quad (2-13)$$

The previous studies mentioned earlier in this chapter showed that the loads within the anchors are not the same for base plate connections with leveling nuts and base plates that are flush mounted or have grouted connections. A compressive reaction develops in the concrete or grout beneath the base plate as the plate rotates during loading. This reaction may result in an amplification of the loads that would normally be experienced in the tension bolts for plates with a gap beneath them.

One method for determining the compressive reaction involves placing the reaction at the outermost edge of the attached compression element. The procedure is

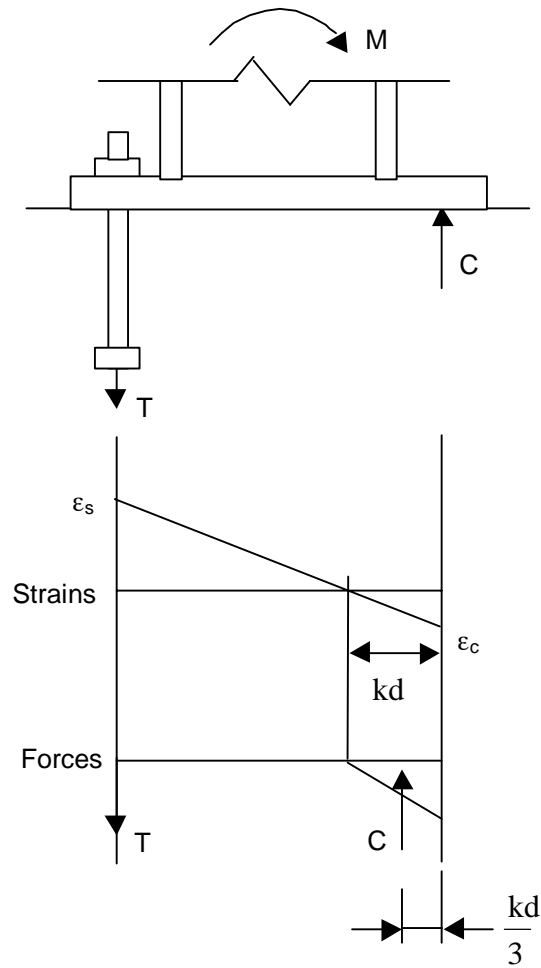


Figure 2.4 Procedure based on working stress method

illustrated schematically in Figure 2.1 for rigid base plates and in Figure 2.2 for flexible base plates. Cook and Klingner (1989) accepted this method as the most reliable method for determining the compressive reaction.

### 2.3.2 Plate Thickness

A design equation for determining the thickness of an annular base plate is currently used by FDOT. The equation was derived from a simplified yield line analysis of the base plate. The equation can be modified for any number of bolts.

$$t = \sqrt{\frac{16M}{\pi n r_b (\phi F_y)}} \quad (2-17)$$

Two additional base plate thickness design equations can be derived from the work done by Cook et al. (1995).

$$t = \sqrt{\frac{4M}{F_y \pi r_b}} \quad (2-20)$$

$$t = \sqrt{\frac{2M}{\lambda F_y r_b}} \quad (2-22)$$

$$t = \sqrt{\frac{8M}{F_y \pi n r_b}} \quad (2-28)$$

## 2.4 Deflections

Background information pertaining to the serviceability (deflection) considerations of annular base plate design is detailed in the following subsections. Included are the results of previous research, deflection prediction models, design equations, and deflection limitation specifications.

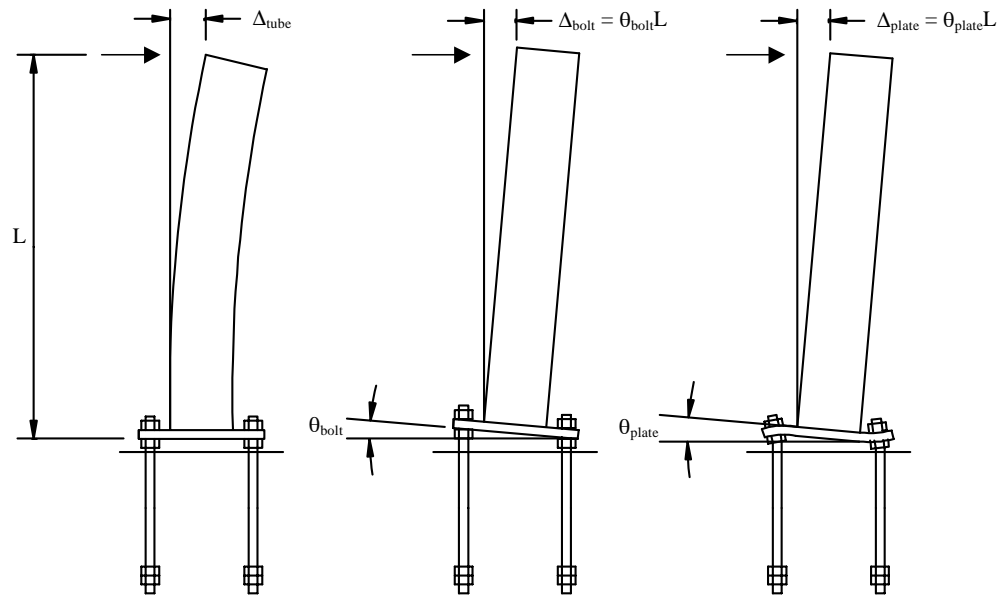


Figure 2.5 Components of total deflection

#### 2.4.2 Deflection Calculation Model for Structures with Annular Base Plates

Cook et al. (1998) used finite element analysis to further study the deflection results analyzed by Cook et al. (1995). Cook et al. (1995) determined that the deflection at the end of a base plate connection cannot simply be calculated as a cantilevered beam, fixed at one end. They found additional deflection that they theorized was probably related to the rotation of the bolts and plate.

Cook et al. (1998) sought to quantify these rotation values, and improve on the rotation assumptions made by Cook et al. (1995). The finite element analysis was compared to the experimental results measured by Cook et al. (1995). The total rotation in an annular base plate exposed to a large bending moment was found to be:

$$\theta_{\text{total}} = \left[ \frac{3M}{Er_b^2 b} \left( \frac{r_{\Delta}}{t_{\text{plate}}} \right)^3 + \frac{55M}{Er_b^2 b} \left( \frac{r_{\Delta}}{t_{\text{plate}}} \right) \right] + \left[ \frac{1.5ML_b}{s_g A_b E_b r_b} \right] \quad (2-31)$$

where:

$M$  = applied moment

$E$  = modulus of elasticity

$r_b$  = distance from the center of the pipe to the center of the bolt

$r_p$  = outside radius of the pipe

$$b = 2\sqrt{r_b^2 - r_p^2}$$

$r_{\Delta}$  = distance between the edge of the pipe and the center of the bolt

$t_{\text{plate}}$  = thickness of the base plate

$s_g$  = unit section modulus of bolt group relative to the axis of moment application

$L_b$  = length of bolt under tension or compression

$A_b$  = cross sectional area of bolt

$E_b$  = modulus of elasticity of bolt

The first term of equation (2-20) represents rotation from flexural deformation, the second term rotation from shear type deformations, and the third term rotation caused by axial deformations in the bolt.

### 2.4.3 Deflection Limitations

The proposed draft of the 1997 AASHTO Standard Specifications provide guidelines for limiting the horizontal deflection for vertical supports, such as streetlighting poles, traffic signal structures, and sign structures. The limitations are as follows: “Under Group I load combination (dead load only), deflection at top vertical

support shall be limited to 1.5 percent of the structure height. For luminaire support structures under Group II load combination (dead load + wind), deflection shall be limited to 15% of the structure height.”

## CHAPTER 3 DESCRIPTION OF EXPERIMENTAL PROGRAM

### 3.1 Introduction

This chapter contains a description of the objectives of the experimental program, the reasons for the selection of the test specimens and their dimensions, a description of the test setup, and the purpose of each test.

### 3.2 Objectives of Experimental Program

The objectives of the experimental program were:

- 1) To develop strength design standards for grouted annular base plate connections.
- 2) To develop serviceability design standards for grouted annular base plate connections.

The variables considered in the development of this testing program included:

- base plate thickness,  $t$
- base plate radius,  $r_{pl}$
- bolt quantity,  $n$
- moment,  $M$ , applied through and eccentric shear force,  $P$
- pipe radius,  $r_p$
- distance to applied shear force from bottom of base plate,  $L$
- distance between outside of pipe and center of anchor bolt,  $r_{\Delta}$

- distance from center of pipe to center of bolt,  $r_b$

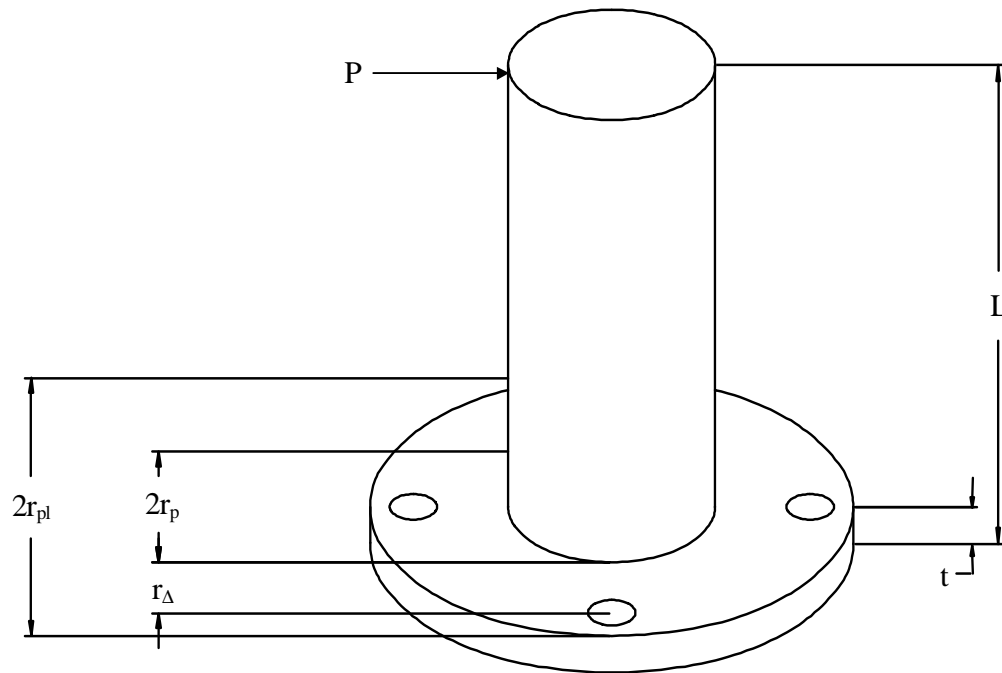


Figure 3.1 Base plate and pipe dimensions

### 3.3 Selection of Typical Base Plate Loads

The main forces felt by a sign and lighting structure base plate are the result of the self-weight of the structure and the overturning moment caused by the mast arm. It was determined prior to testing that the stresses from the bending moment far exceed the stresses from the axial load for even a short mast arm. Thus, the experimentation was developed such that the applied loading was dominated by bending moment. This was accomplished by the application of an eccentric shear load.

#### 3.4.1 Materials

The basis for selecting the particular concrete, particular grout, anchor bolt material, base plate material, and pipe material used in this study are given below:

- 1) Concrete: The concrete chosen for the experimental program was a ready-mix concrete designed to meet Florida DOT Specifications for Class II concrete. This is typical of FDOT structures. The minimum design compressive strength of Class II concrete is 23.45 MPa (3400 psi) at 28 days.
- 2) Grout: The grout was chosen directly from the FDOT approved product list for use in FDOT structures. Master Builders Technologies's Masterflow 928 Grout was the grout selected. This is a high precision, nonshrink, natural aggregate grout. This Masterflow 928 grout was selected because of its quick set time and favorable compressive strength. The FDOT specifications for sign and lighting fixtures require a minimum 28-compressive strength of grout to be 35 MPa (5075 psi).
- 3) Anchor Bolts: The anchor bolts were fabricated at a local shop in accordance with ASTM F1554.
- 4) Base plates: The base plate material was ASTM A36 clean mill steel. FDOT uses galvanized plates consistent with ASTM 123. However, since galvanization would have no bearing on the outcome of the experimentation, these plates were left black.
- 5) Pipes: Structural steel pipes were used to model the tubular sections used by FDOT for their sign and lighting structures. The pipes were ASTM A53 Type E, Grade B, Extra Strong. Extra Strong pipes were selected to decrease the chances of a failure mechanism developing in the pipe before the grout pads. The pipes were socket-welded to the base plates in accordance with FDOT specifications.

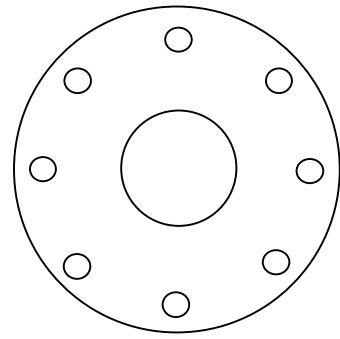
- 6) Plate stiffeners: The stiffeners were cut to size from 12.7 mm (0.50 inch) thick A36 steel plate. This strength is considered standard for plate stiffeners.

#### 3.4.2.1 Anchor Bolts

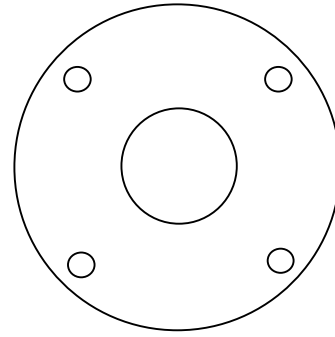
The anchor bolts were 25.4 mm (one inch) diameter cold-rolled structural steel rods that were threaded on each end. The bolts were 749.3 mm (29.5 inches) long with 88.9 mm (3.5 inches) of thread on the embedded end and 228.6 mm (9 inches) of thread on the exposed end (see Figure 3.2).

#### 3.4.2.2 Base Plates

The four base plate specimens examined in this study were chosen to all be 19.1 mm (0.75 inch) thick because of what was learned during testing in the study by Cook et al. (1995). The tests in that study were all originally performed with base plates 25.4 mm (one inch) thick. However, it became obvious during testing that both the plate and the pipe were yielding. Thus, the remainder of the tests were conducted on plates 19.1 mm (0.75 inch) thick in order to have initial yielding occur in the plate. The same base plate thickness was chosen throughout this study to increase the chances of the base plates, and more importantly the grout pads, failing before the pipe.



(a) Eight bolt arrangement



(b) Four bolt square arrangement

Figure 3.3 Anchor bolt patterns

Table 3.1 Test dimensions

Specimen #	Test	Bolt $\phi$ mm (inches)	Pipe $\phi$ mm (inches)	Bolts	Plate Thickness mm (inches)	$r_{\Delta}/t$
1	8-3/4-8-U	292 (11.5)	219 (8.63)	8	19.1 (0.75)	1.88
	8-3/4-8-G	292 (11.5)	219 (8.63)	8	19.1 (0.75)	1.88
2	8-3/4-4s-U	292 (11.5)	219 (8.63)	4s	19.1 (0.75)	1.88
	8-3/4-4s-G	292 (11.5)	219 (8.63)	4s	19.1 (0.75)	1.88
3	6-3/4-4sW-U	292 (11.5)	168 (6.63)	4s	19.1 (0.75)	3.21
	6-3/4-4sW-G	292 (11.5)	168 (6.63)	4s	19.1 (0.75)	3.21
	6-3/4-4sW-GS	292 (11.5)	168 (6.63)	4s	19.1 (0.75)	3.21
4	6-3/4-4s-U	292 (11.5)	168 (6.63)	4s	19.1 (0.75)	3.21
	6-3/4-4s-G	292 (11.5)	168 (6.63)	4s	19.1 (0.75)	3.21
	6-3/4-4s-GS	292 (11.5)	168 (6.63)	4s	19.1 (0.75)	3.21

### 3.4.2.3 Grout Pads

The gap between the bottom of the base plates and the exterior face of the test block was 38.1 mm (1.5 inches). This entire region had to be filled with grout and evacuated of all air voids. The FDOT design specifications for the foundations of cantilever signal structures require that the grout pad be flush against the bottom of the

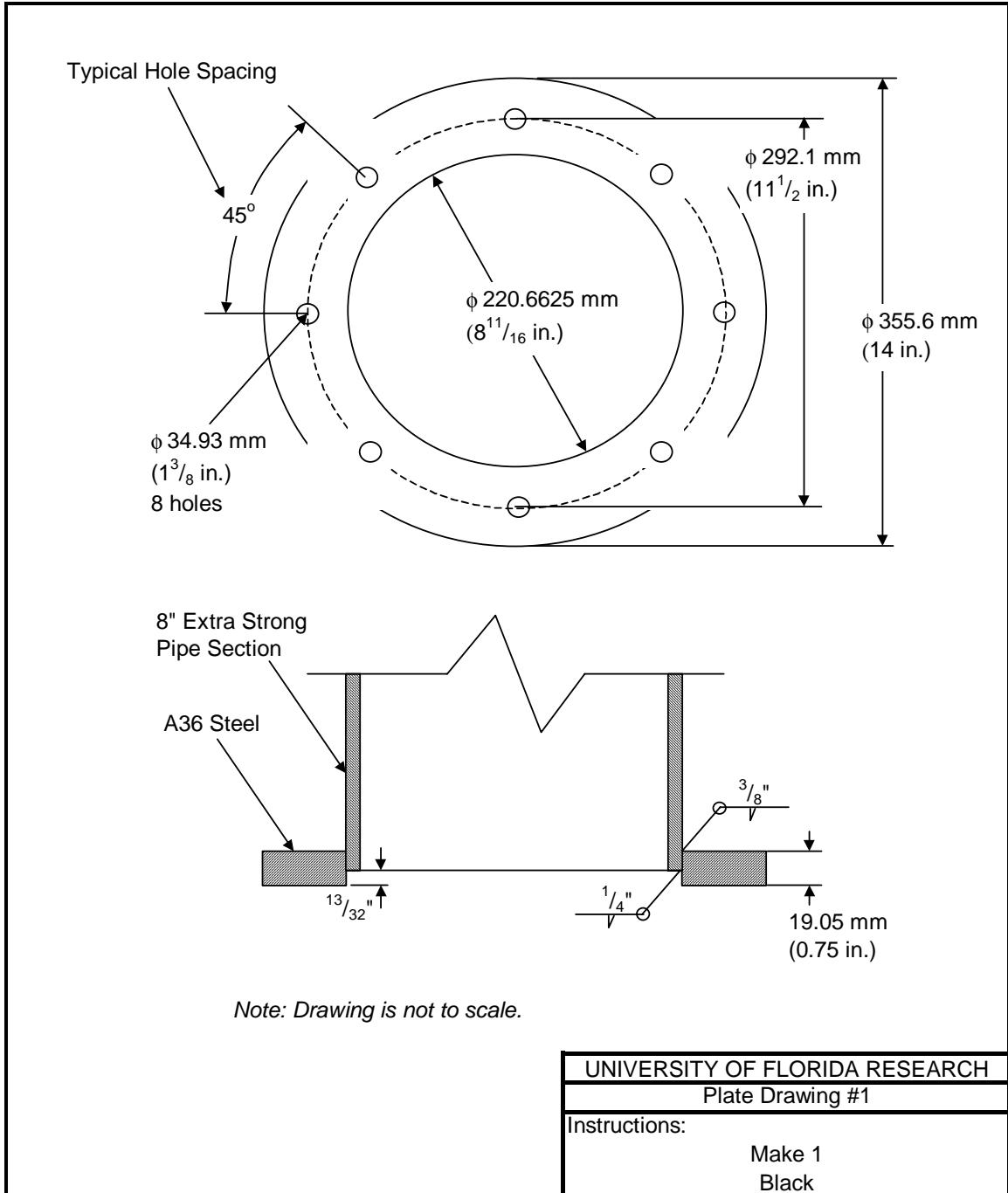
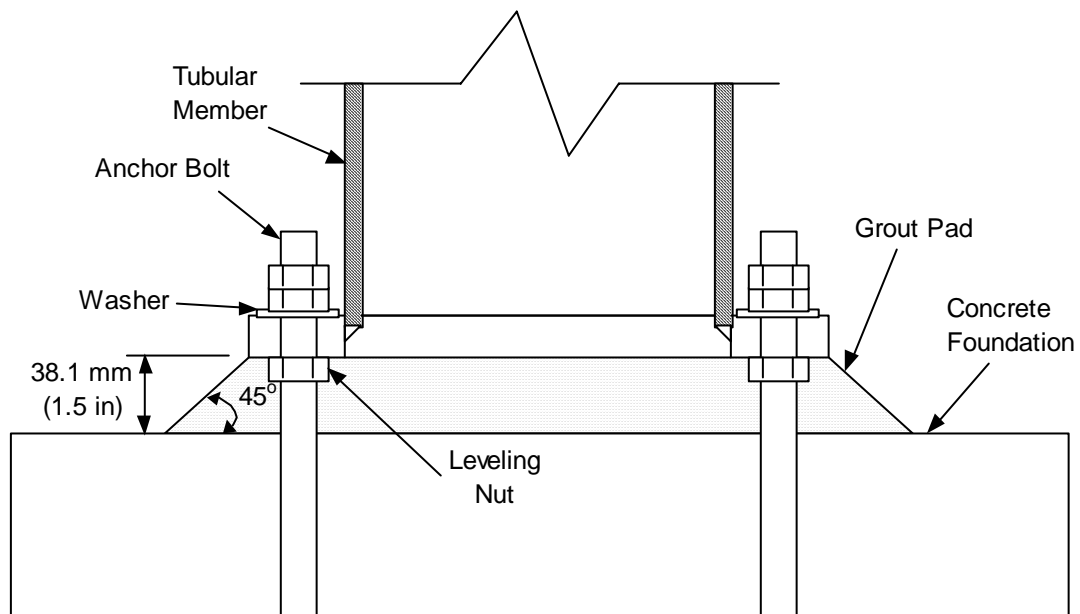


Figure 3.4 Typical shop drawing

base plate. In addition, the grout pad is required to extend away from the plate to the foundation, making a 45 degree angle with the horizontal (see Figure 3.5). Thus, the base

of the grout pad would extend 38.1 mm (1.5 inches) out from the bottom of the base plate. However, for this project the grout pads were constructed flush with the edge of the plate.

Figure 3.5 FDOT grout pad requirement



#### 3.4.2.4 Tubular Members

The member length was determined using a typical length-to-diameter ratio obtained from FDOT drawings for tubular structures. The ratio was taken as 12 for the test program. This ensured that shear was not over represented in the connection. Nominal pipe diameters of 152.4 mm and 203.2 mm (six and eight inches) were chosen to vary the  $r_d/t$  ratios of the base plates enough to model plates with significantly different flexibilities. Using the length-to-diameter ratio calculated above, the pipe was loaded at 1.83 and 2.44 meters (six and eight feet) respectively. The 152.4 mm (six inch) nominal diameter pipes were 2.44 meters (eight feet) long and the 203.2 mm (eight inch) nominal diameter pipes were 3.05 meters (ten feet) long.

### 3.4.2.5 Plate Stiffeners

The plate stiffeners, used for the nominal 152.4 mm (six inch) nominal diameter plates only, were cut into rectangular plates. The rectangles were 152.4 mm (six inches) in length and were made to fit flush against the pipe and the edge of the plate. Figure 3.6 shows a plan view the position of the stiffeners for Specimen's #3 and #4.

### 3.4.3 Test Block Design Basis

As shown in Figure 3.7, the test blocks were 609.6 mm (24 inches) wide by 1219.2 mm (48 inches) long by 1219.2 mm (48 inches) deep, and were reinforced with eight #4 hoops with four perpendicular to the other four to create a cage.

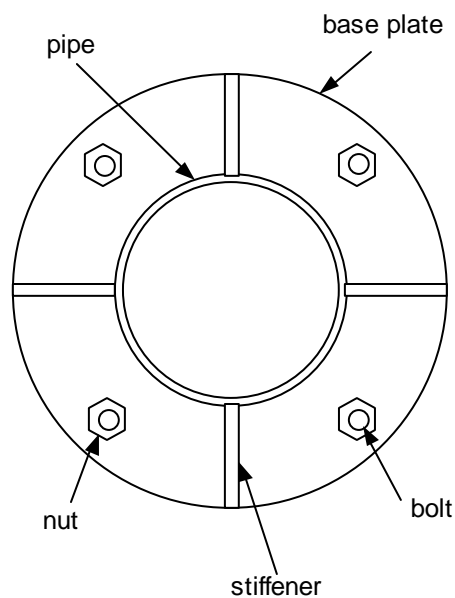


Figure 3.6 Position of plate stiffeners

### 3.5 Development of Test Setup

The test setup was developed to apply bending moments to the base plate-pipe connection through an eccentric shear force applied to the pipe. The test setup is illustrated schematically in Figure 3.8.

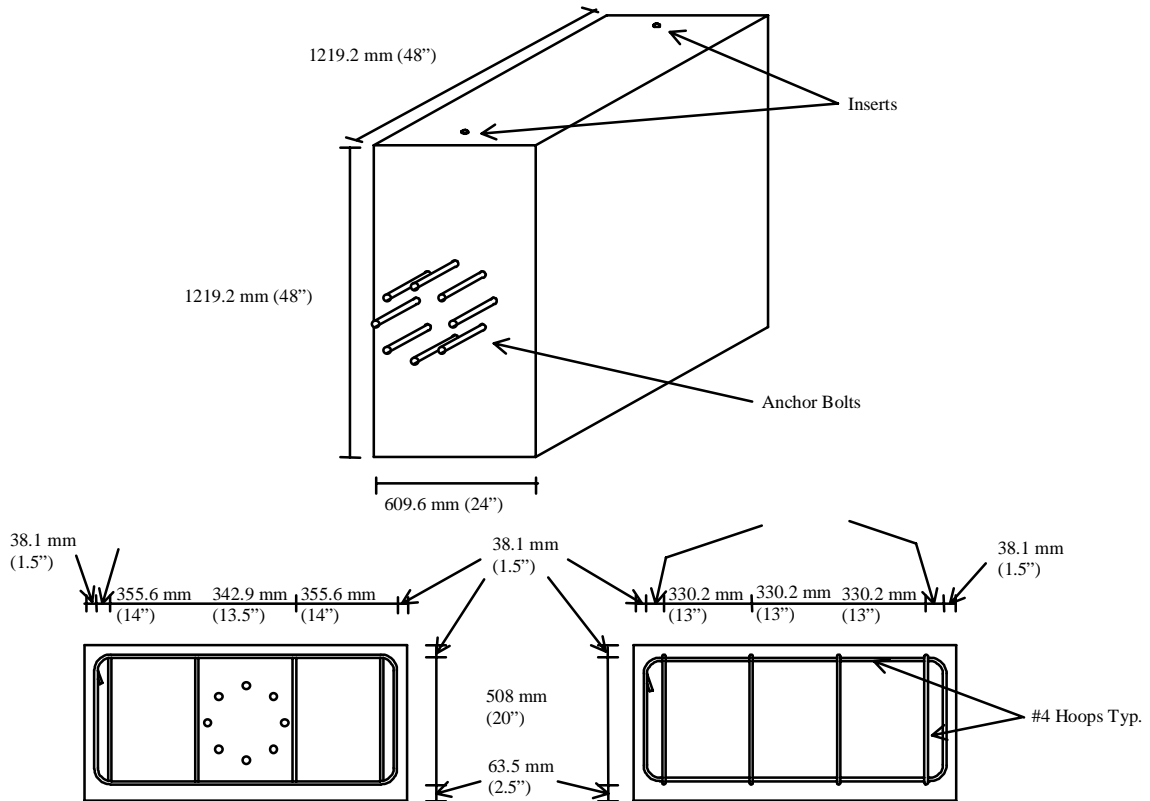


Figure 3.7 Typical test block

The test setup consisted of the following components:

- 1) A large-throat 400-kip universal testing machine which confined the test block during testing.
- 2) The test block.

- 3) A steel pipe that acted as the moment arm for the applied moment at the plate/pipe connection.
- 4) A hydraulic ram at the end of the pipe with a load cell to measure the applied load. Moments were applied to the connection by raising the ram

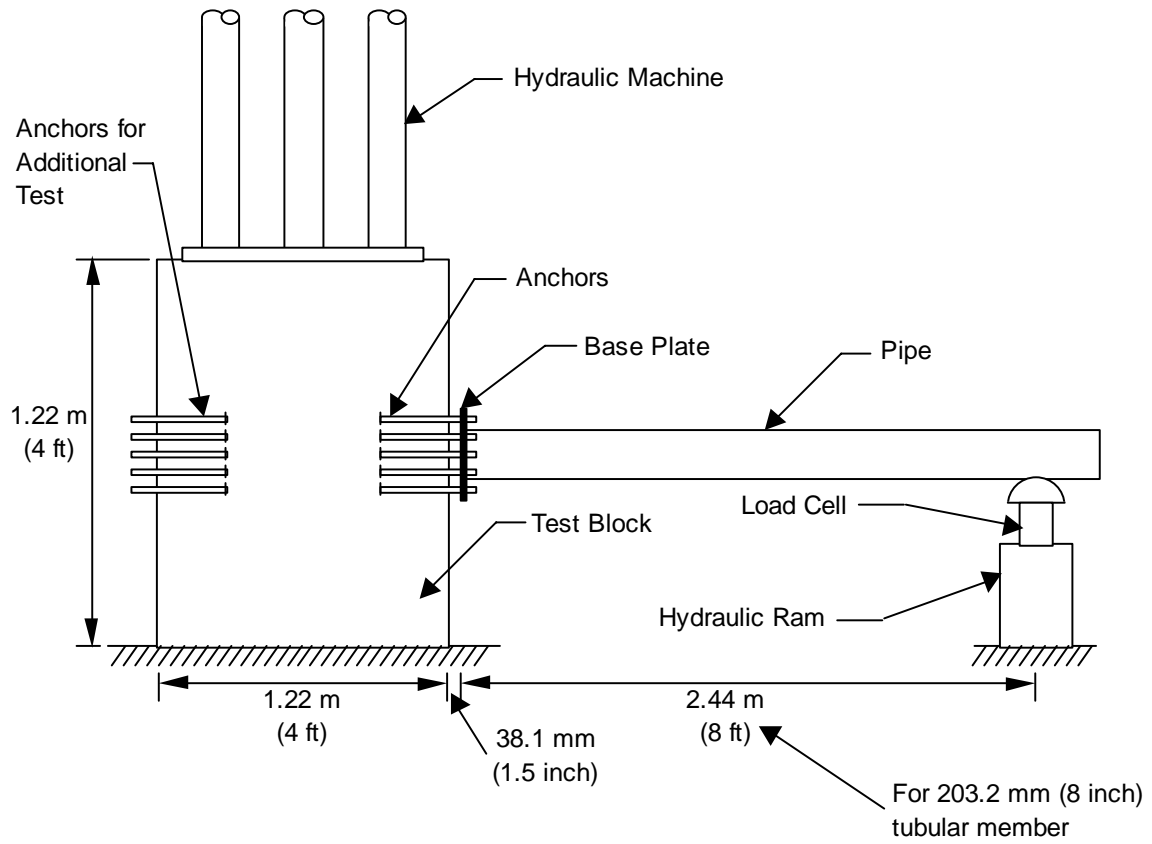


Figure 3.8 Schematic diagram of typical test setup

with a hand pump.

- 5) Load cells were embedded in the grout between the bottom of the base plate and the outer face of the test block to measure the bolt loads. The bolt displacements were recorded by LVDT's located on the outer exposed face of the bolts. LVDT's were located at the extreme top and bottom of

the face of the base plate for all of the tests performed with plates fitted with four bolts.

CHAPTER 4  
IMPLEMENTATION OF EXPERIMENTAL PROGRAM

4.1 Introduction

All tests were conducted in the Structural Engineering Laboratory of at the University of Florida.

4.3.1 Concrete

The compressive strength of the 152.4 mm (six inch) diameter by 304.8 mm (12 inch) cylinders at 28 days are shown in Table 4.1 The compressive strength was also computed on the day of the first test, 141 days after the concrete pour, and is shown in Table 4.2.

Table 4.1 Concrete cylinder strengths at 28 days

Cylinder #	Compressive Strength 28 days MPa (psi)	Compressive Strength 28 days (average) MPa (psi)
1	36.21 (5250)	36.03 (5230)
2	36.00 (5220)	
3	35.89 (5210)	

Table 4.2 Concrete cylinder strengths at 141 days

Cylinder #	Compressive Strength 141 days MPa (psi)	Compressive Strength 141 days (average) MPa (psi)
1	36.84 (5340)	38.75 (5620)
2	40.05 (5810)	
3	39.37 (5710)	

### 4.3.2 Anchor Bolts

The anchor bolt tensile strengths were determined by failing three smooth rods and three threaded rods in tension using a 400-kip universal Tinius Olsen machine. The rods were all made from the same stock used to make the anchor bolts. The results of the tensile strength tests are shown in Table 4.3.

Table 4.3 Anchor bolt tensile strengths

Type of Rod	Sample #	Tensile Strength kN (kips)	Average Tensile Strength kN (kips)
Smooth	1	322.62 (72.53)	311.97 (70.13)
	2	306.50 (68.90)	
	3	306.81 (68.97)	
Threaded	1	253.55 (57.00)	251.06 (56.44)
	2	250.06 (56.21)	
	3	249.57 (56.10)	

### 4.3.3 Grout Mixtures

The compressive strengths of the 5.08 cm (two inch) square grout cubes are shown in Table 4.4. The grout cubes were made at the time of mixing using the standard steel forms.

Table 4.4 Grout cube strengths

Specimen #	Cube #	Compressive Strength 14 days MPa (psi)	Compressive Strength 14 days (average) MPa (psi)
1 (8-3/4-8)	1	42.99 (6235)	39.50 (5730)
	2	36.02 (5225)	
2 (8-3/4-4s)	1	62.78 (9105)	64.18 (9310)
	2	65.58 (9510)	
3 (6-3/4-4s)	1	64.02 (9285)	64.72 (9390)
	2	65.43 (9490)	
4 (6-3/4-4sW)	1	77.14 (11190)	71.55 (10380)
	2	65.97 (9570)	

The grout was initially mixed according to the mixture to water ratio recommended by the manufacturer. The flow of the grout mix was then tested using a flow cone as described by ASTM C 939. A flow time of 20 to 25 seconds was desired. The water to mix ratio was adjusted until the proper flow time was achieved. The final results of the flow cone tests are shown in Table 4.5.

Table 4.5 Flow cone results

Specimen #	Trial #	Flow Time (sec)	Average Flow Time (sec)
1 (8-3/4-8)	1	20	21
	2	21	
2 (8-3/4-4s)	1	25	25
	2	25	
3 (6-3/4-4s)	1	22	22
	2	21	
4 (6-3/4-4sW)	1	22	22
	2	21	

#### 4.3.4 Base Plates

The actual values of the yield stress,  $F_y$ , and the ultimate stress,  $F_u$ , were contained in a mill report provided by the manufacturer. The mill report stated a value of 381 MPa (55.3 ksi) for  $F_y$  and a value of 443 MPa (64.3 ksi) for  $F_u$ .

#### 4.3.5 Pipes

A set of tensile coupons (see Figure 4.1) were fabricated from the pipes to determine the actual strength of the pipes. The results of the tensile strength tests are shown in Table 4.6.



Figure 4.1 Coupons for pipe tensile strength tests

Table 4.6 Pipe tensile strength test results

Coupon #	Yield Stress MPa (ksi)	Average Yield Stress MPa (ksi)	Ultimate Stress MPa (ksi)	Average Ultimate Stress MPa (ksi)
1	316.1 (45.9)	317.0 (46.0)	497.1 (72.1)	498.8 (72.3)
2	315.9 (45.8)		495.2 (71.8)	
3	319.2 (46.3)		504.2 (73.1)	

#### 4.2 Anchor Installation

All anchors were cast-in-place and were installed with templates to hold the bolts in the proper position at the correct embedded length during concrete placement (see Figure 4.2).

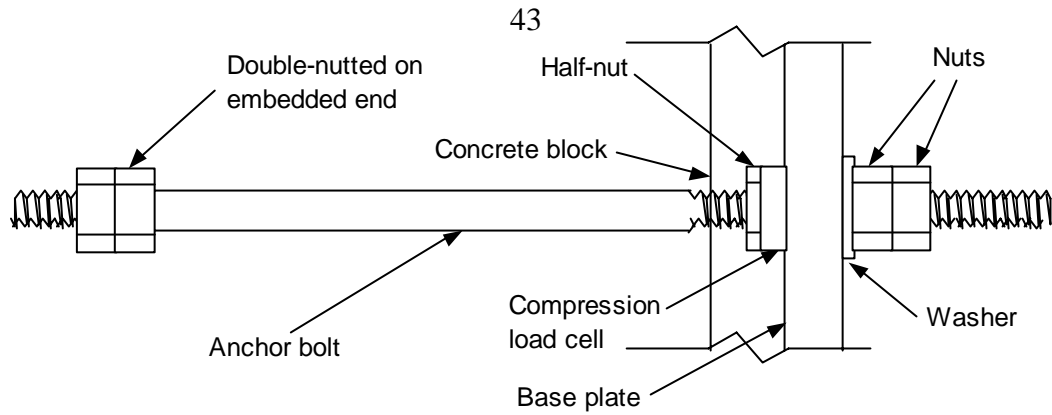


Figure 4.2 Detail for typical compression bolt

#### 4.6 Welding of Stiffeners

Each of the plate specimens attached to a 152.4 mm (six inch) nominal diameter pipe was tested in the elastic range with and without the presence of a grout pad. Then, four stiffeners were welded to the pipe at the base plate connection (see Figure 4.4). Each stiffener was attached perpendicular to the plate halfway between the anchor bolts.

#### 4.7 Test Equipment

The following describes the test setup, hydraulic loading system, load cells, displacement measurement instrumentation, and data acquisition unit used in this experimental program. The test setup for a typical base plate test is shown in Figure 4.5.



Figure 4.5 Typical test setup

#### 4.8 Test Procedure

A typical test involved the following steps:

- 1) Heavy hex leveling nuts were screwed onto the anchors so that the distance between the concrete and the bottom of the plate was 38.1 mm (1.5 inches). The interior nuts on the anchors that would be experiencing pure compression were machined to an overall thickness 12.70 mm (1/2 inch) to adequately accommodate the load cells.

- 2) The base plate was installed on the anchors until the bottom of the plate was flush with the nuts of the tension anchors and load cells of the compression anchors. The base plate was adjusted until the sides of the anchor bolts were touching the sides of the holes. All of the compression anchors were fitted with washers and two heavy hex nuts. The tension bolts were fitted with a washer, a load cell, another washer and a single heavy hex nut. The heavy hex nuts were hand tightened to a snug fit.
- 3) The LVDTs were attached to the base plate, pipe and anchors using the template. The hydraulic ram was set up at the point where the shear load was to be applied. All instruments were connected to the data acquisition unit. All LVDTs and load cells were tested to make sure they were reading and the heavy hex nuts on the anchors with load cells were loosened if they were showing a preload. The load cells showed a preload during the tests with a grout pad due to grout expansion during curing.
- 4) Load was applied by pumping the hydraulic ram at a steady pace.
- 5) Each plate specimen was tested in both the elastic and inelastic stress ranges. For the elastic range tests, a carefully monitored load was applied until the displacements approached the elastic limit. Then, the loading was removed and the pipe could be reused. Loading continued until a structural failure occurred for all tests in the inelastic range.
- 6) The applied shear load was released. Raw data was downloaded to a Microsoft Excel 97 spreadsheet where it could be reduced.
- 7) The pipe and plate system were removed from the anchor bolts and inspected for

failure and any unusual deformations.

## CHAPTER 5 TEST RESULTS

### 5.1 Introduction

This chapter discusses the test observations, a summary of the test results, and typical individual test results. Complete results of all of the tests are provided in the appendices.

### 5.2 Test Observations

The following subsections contain an account of the observations made during testing on all of the specimens.

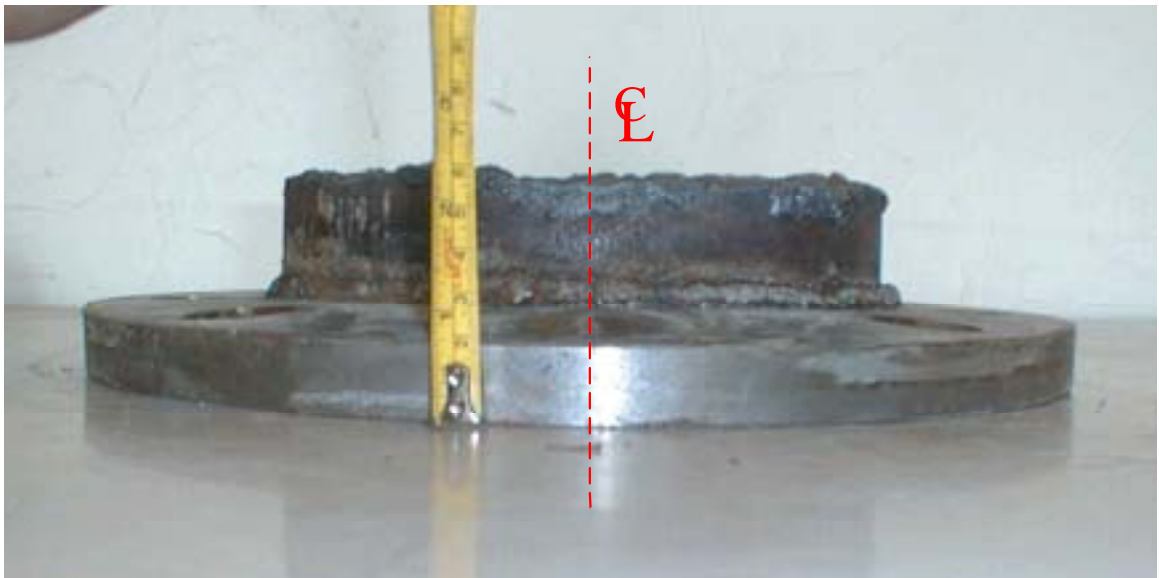


Figure 5.1 Deformed shape at axis of bending of Specimen #1



Figure 5.2 Deformed shape in tension region of Specimen #1

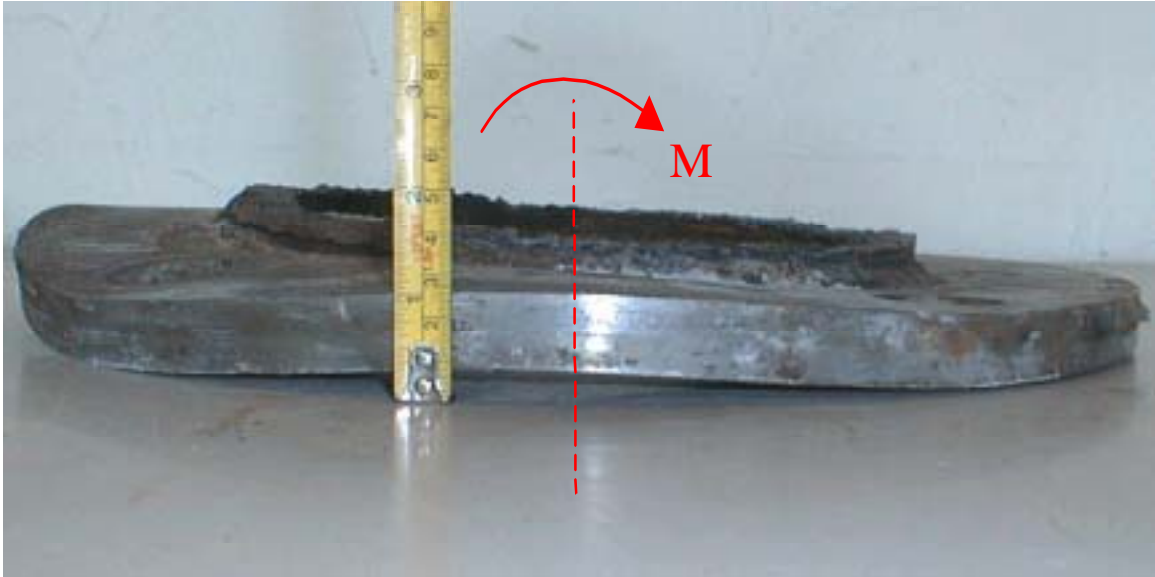


Figure 5.6 Deformed shape at axis of bending of Specimen #2



Figure 5.7 Deformation in tension region of Specimen #2



Figure 5.9 Deformed shape at axis of bending of Specimen #3

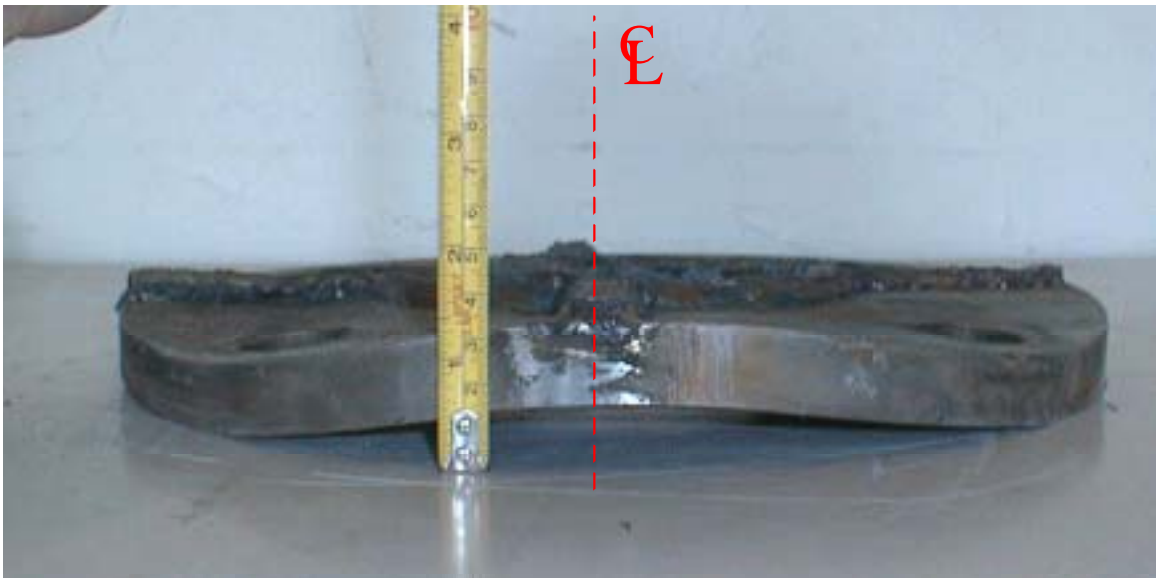


Figure 5.10 Deformed shape in tension region of Specimen #3

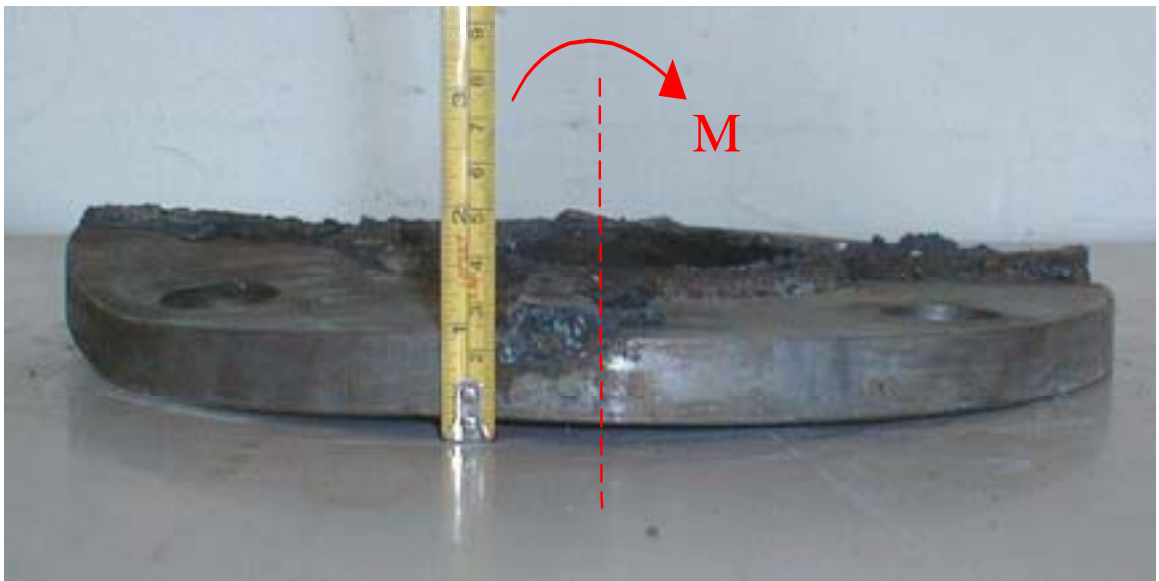


Figure 5.12 Deformed shape at axis of bending of Specimen #4



Figure 5.13 Deformed shape in tension region of Specimen #4

### 5.3 Discussion of Failure Loads

All four specimens were loaded until a system failure occurred. The mode of failure in Specimens #1 and #2 was the combination of the formation of a plastic hinge in the pipe and the failure of the weld between the pipe and the plate. The mode of failure in Specimens #3 and #4 was the formation of a plastic hinge in the tubular member. The equation for calculating the yield moment of a steel section is:

$$M_y = F_y S_x \quad (5-1)$$

where:

$M_y$  = yield moment of the pipe

$F_y$  = yield stress of the pipe

$S_x$  = elastic section modulus of the cross-section

The equation for calculating the moment which will cause a plastic hinge to form in a steel section is:

$$M_p = F_y Z \quad (5-2)$$

where:

$M_p$  = plastic moment capacity of the pipe

$F_y$  = yield stress of the pipe

$Z$  = plastic section modulus

The value for  $F_y$ , 317 MPa (46.0 ksi), was taken from the pipe tensile strength results described in Chapter 4.

Table 5.1 contains the predicted pipe moments which would cause yielding and a plastic hinge formation. Table 5.2 contains a comparison of the predicted plastic moment and the maximum applied moment to the pipe.

Specimen #	Test #	$S_x$ mm <sup>3</sup> (in <sup>3</sup> )	Z mm <sup>3</sup> (in <sup>3</sup> )	Predicted $M_y$ kN-mm (kip-in)	Predicted $M_p$ kN-mm (kip-in)
1	8-3/4-8-G	401,000 (24.5)	541,000 (33.0)	127,000 (1130)	172,000 (1520)
2	8-3/4-4s-G	401,000 (24.5)	541,000 (33.0)	127,000 (1130)	172,000 (1520)
3	6-3/4-4sW-GS	200,000 (12.2)	272,000 (16.6)	63,400 (561)	86,300 (764)
4	6-3/4-4s-GS	200,000 (12.2)	272,000 (16.6)	63,400 (561)	86,300 (764)

Table 5.1 Predicted yield and plastic moments in pipe

Specimen #	Test #	Predicted $M_p$ kN-mm (kip-in)	Maximum $M_{Measured}$ kN-mm (kip-in)	$M_{Measured}/$ Predicted $M_p$
1	8-3/4-8-G	172,000 (1520)	101,000 (891)	0.587
2	8-3/4-4s-G	172,000 (1520)	110,000 (970)	0.639
3	6-3/4-4sW-GS	86,300 (764)	78,000 (690)	0.903
4	6-3/4-4s-GS	86,300 (764)	78,600 (696)	0.911

Table 5.2 Comparison of predicted plastic moment and maximum moment in pipe

The calculated results of Table 5.2 were consistent with the observations made during the ultimate load test performed on each specimen. The maximum moment that could be applied to Specimens #1 and #2 was significantly lower than the predicted plastic moment capacity of the pipe. However, a weld failure was observed on both of these specimens just before the loading was discontinued. The predicted plastic moment capacity for Specimens #3 and #4 was slightly less than the maximum moment applied to the pipe when loading was stopped.

#### 5.4 Summary of Test Results

The load displacement graphs for all tests performed on each of the four specimens are shown in Figures 5.15, 5.16, 5.17, and 5.18. The graphs show loading

only in the elastic range for comparison purposes. The full-scale load displacement graphs are shown in Figures 5.19, 5.20, 5.21, and 5.22.

As indicated by the figures, the pipe displacements were virtually unchanged by the addition of a grout pad for the two more rigid plates, Specimens #1 and #2. The grout pad basically had no effect on increasing the stiffness of the base plate connection for these more rigid plates.

The grout pad did, however, have an impact on the pipe displacement for the two more flexible plates, Specimens #3 and #4. The grout pad, in effect, reduced the portion of the displacement caused by the plate rotation by significantly increasing the rigidity of the plate. Thus the overall displacement was reduced. The pipe displacements were further reduced by the addition of the plate stiffeners.

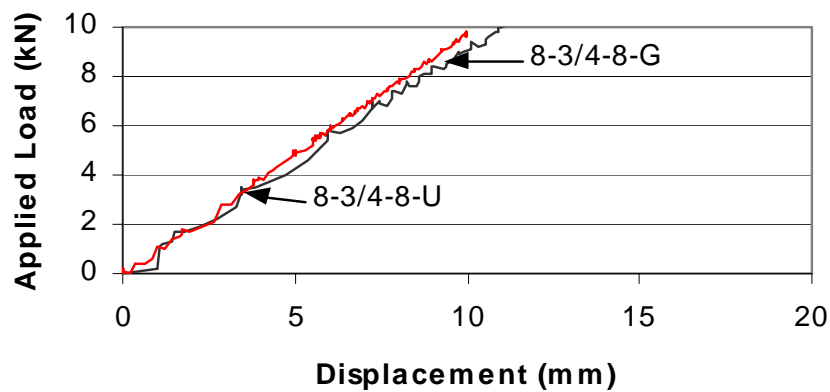


Figure 5.15 Elastic range load-displacement for Specimen #1

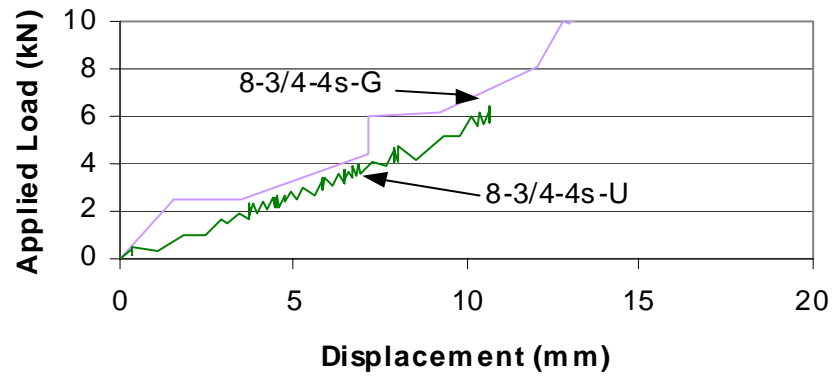


Figure 5.16 Elastic range load-displacement for Specimen #2

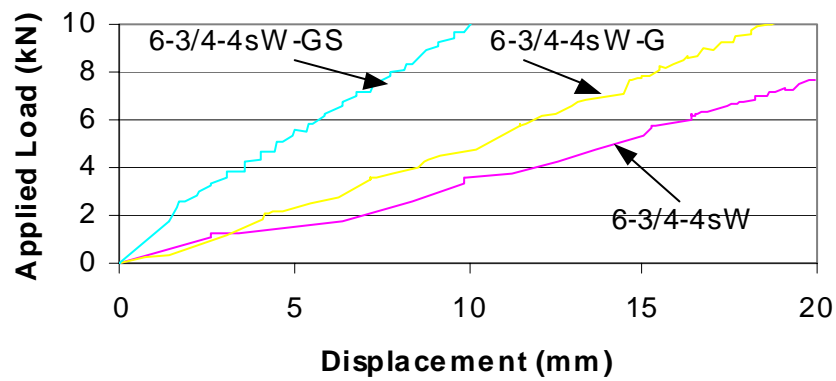


Figure 5.17 Elastic range load-displacement for Specimen #3

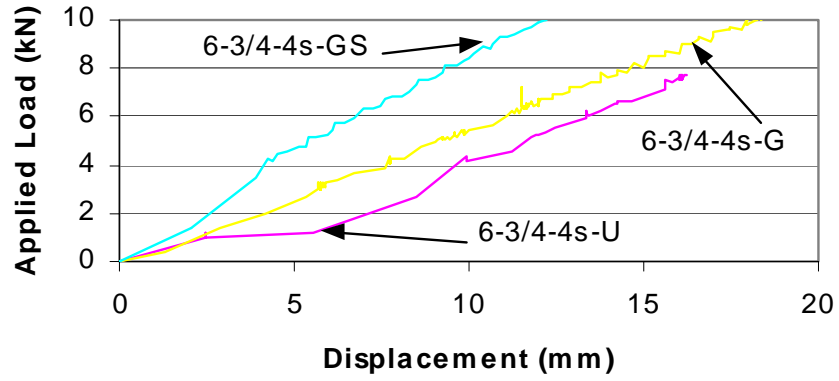


Figure 5.18 Elastic range load-displacement for Specimen #4

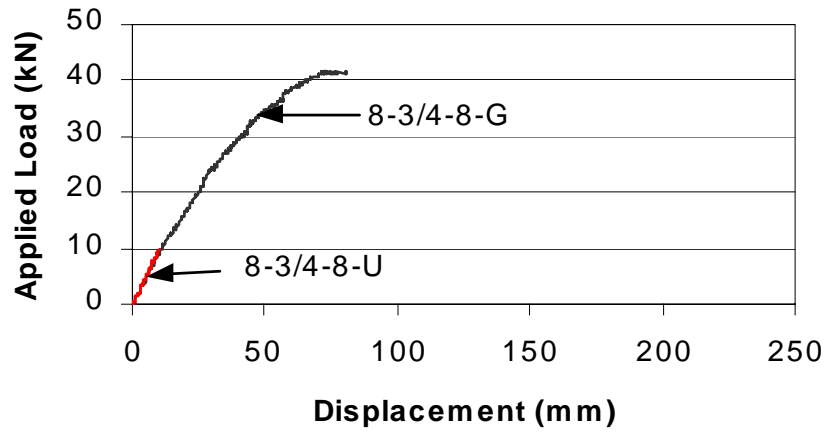


Figure 5.19 Full-scale load-displacement for Specimen #1

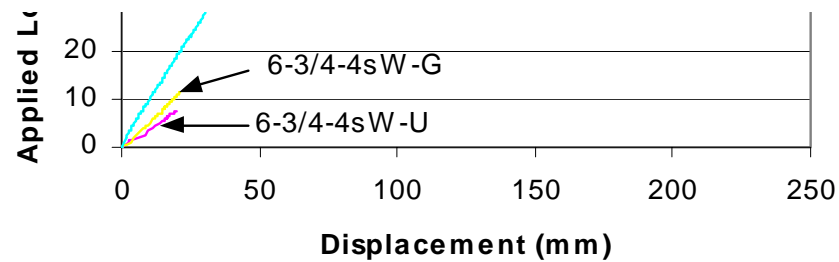
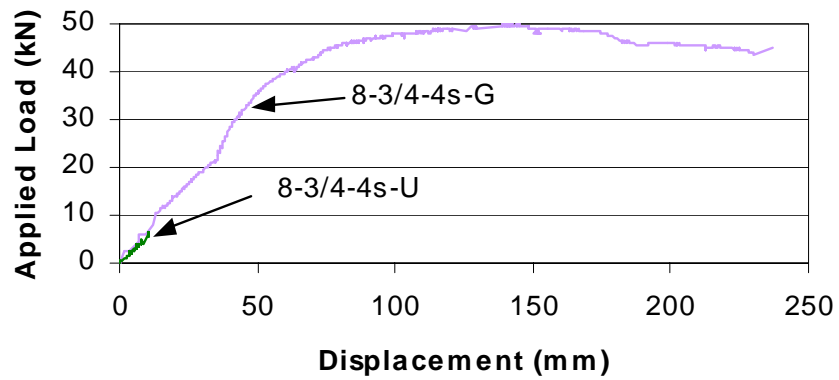


Figure 5.21 Full-scale load-displacement for Specimen #3

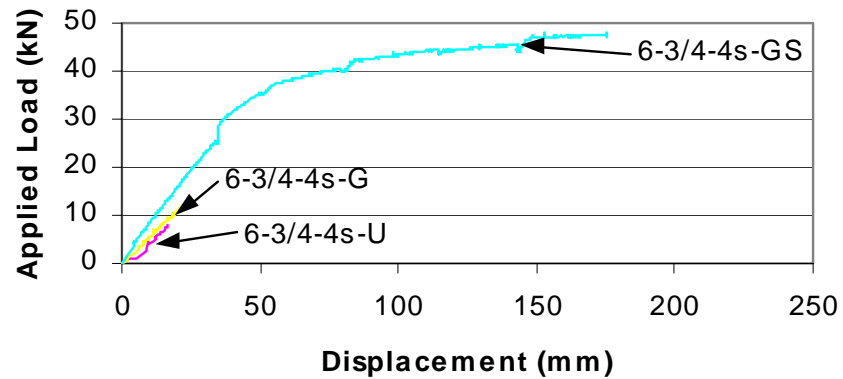


Figure 5.22 Full-scale load-displacement for Specimen #4

Table 5.3 lists the maximum applied moments and the resulting maximum measured compression and tension bolt loads for each test.

Specimen #	Test	Maximum Applied Moment kN-m (kip-in)	Maximum Compression Bolt Load kN (kips)	Maximum Tension Bolt Load kN (kips)
1	8-3/4-8-U	23.7 (209)	43.4 (9.78)	N/A
	8-3/4-8-G	101 (889)	142 (32.0)	N/A
2	8-3/4-4s-U	15.5 (138)	24.7 (5.56)	N/A
	8-3/4-4s-G	110 (970)	36.6 (8.23)	301 (67.6)
3	6-3/4-4sW-U	14.2 (125)	21.5 (4.82)	37.0 (8.32)
	6-3/4-4sW-G	20.9 (185)	20.6 (4.63)	46.1 (10.4)
	6-3/4-4sW-GS	85.1 (753)	12.9 (2.91)	175 (39.5)
4	6-3/4-4s-U	14.2 (126)	41.6 (9.35)	31.2 (7.02)
	6-3/4-4s-G	23.1 (204)	24.8 (5.57)	56.8 (12.8)
	6-3/4-4s-GS	85.8 (756)	23.1 (5.19)	183 (41.2)

Table 5.3 Maximum applied moments and recorded bolt loads

## CHAPTER 6 STRENGTH CONSIDERATIONS

### 6.1 Introduction

The overall performance of the annular base plate connection can be evaluated based on strength and serviceability. Strength considerations are presented in this chapter, while serviceability considerations are discussed in Chapter 7.

Strength considerations are usually related to the yielding of one or more components of a structure. Yielding of any of the components does not necessarily constitute failure of the entire structure. Failure occurs when the structure no longer performs as designed. This may be due to excessive deflections caused by yielding of the tubular member, anchor bolts, base plate, or weld, or a fracture of any portion of the structure.

The following sections contain a discussion of the existing design equations, and the impact of the grout pad on the load transferred to the anchors.

### 6.2 Evaluation of Base Plate Thickness

The results of the four plate thickness design equations are shown in Table 6.1. The strength design factor  $\phi$  was not included in equation (2-17) for comparison to the test results.

Table 6.1 Results of plate thickness design equations

Specimen #	Test #	Max. Applied Moment kN-m (kip-in)	Design Thickness From Eq. (2-17) mm (in)	Design Thickness From Eq. (2-20) mm (in)	Design Thickness From Eq. (2-22) mm (in)	Design Thickness From Eq. (2-28) mm (in)
1	8-3/4-8-G	101 (889)	33.9 (1.33)	48.0 (1.89)	22.1 (0.871)	24.0 (0.943)
2	8-3/4-4s-G	110 (970)	50.1 (1.97)	50.1 (1.97)	26.2 (1.03)	35.4 (1.39)
3	6-3/4-4sW-GS	85.1 (753)	44.3 (1.74)	44.3 (1.74)	32.2 (1.27)	31.2 (1.23)
4	6-3/4-4s-GS	85.8 (756)	44.3 (1.74)	44.3 (1.74)	32.5 (1.28)	31.2 (1.23)

The base plate thickness used for all four specimens in this study was 19.05 mm (0.75 in). As shown in Table 6.1, all four of these equations over-predicted the thickness that was necessary to handle the applied moment. Thus, all four of these equations can be considered satisfactory for determining the required thickness of annular base plates equipped with a grout pad.

The four thickness design equations were also used to evaluate the ungrouted base plates used in the study by Cook et al. (1995). The plate specimens in that study were designated in a manner similar to the designations used for this study. Each specimen was designated by the nominal diameter of the tube, the thickness of the base plate, and the number of anchors in the plate. For example, 10-3/4-6 referred to a 3/4" thick plate with a nominal ten-inch diameter tube and six anchor bolts. Three of the examined specimens had four bolts arranged in a diamond pattern (see Figure 6.1), as opposed to the square pattern used throughout this study for the specimens with four bolts. The diamond pattern was designated by a "d" attached to the bolt number in the test designation. The value used in the calculations for  $F_y$  was 362 MPa (52.5 ksi) for the 25.4 mm (one inch) thick plates and 382 MPa (55.4 ksi) for the 19.1 mm (3/4 inch). These values were experimentally determined by coupon testing. The results of the calculations are shown in Table 6.2.

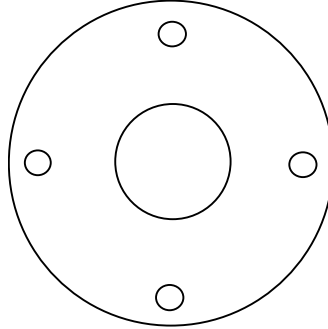


Figure 6.1 Four bolt diamond arrangement

Table 6.2 Design analysis for plates from Cook (1995) study

Test #	Max. Applied Moment kN-m (kip-in)	Design Thickness From Eq. (2-17) mm (in)	Design Thickness From Eq. (2-20) mm (in)	Design Thickness From Eq. (2-22) mm (in)	Design Thickness From Eq. (2-28) mm (in)
6-1-4d	60.5 (534)	38.1 (1.50)	38.1 (1.50)	28.0 (1.10)	27.0 (1.06)
6-1-4s	73.4 (647)	42.0 (1.65)	42.0 (1.65)	30.8 (1.21)	29.7 (1.17)
6-1-6	78.0 (688)	35.3 (1.39)	43.4 (1.70)	30.0 (1.18)	25.0 (0.984)
6-1-8	80.0 (706)	31.0 (1.22)	43.8 (1.73)	21.7 (0.853)	21.9 (0.863)
6-3/4-4d	39.8 (351)	30.1 (1.18)	30.9 (1.22)	22.1 (0.869)	21.3 (0.838)
6-3/4-8	45.9 (405)	22.9 (0.900)	33.2 (1.31)	16.0 (0.629)	16.2 (0.636)
8-3/4-4d	63.7 (562)	38.1 (1.50)	38.1 (1.50)	19.9 (0.783)	26.9 (1.06)
8-3/4-6	97.8 (863)	38.5 (1.52)	47.2 (1.86)	30.6 (1.20)	27.2 (1.07)
8-3/4-8	109 (962)	35.2 (1.39)	49.8 (1.96)	23.0 (0.904)	24.9 (0.980)

These results indicate that most accurate results were generated by equation (2-28). This equation was evaluated for numerous ungrouted base plates. Since the grouted base plates were found to be stiffer, as is discussed in detail in Chapter 7, the equation can be assumed to be satisfactory for the design of base plates with grout pads as well. Thus, if a strength design factor is applied, the final recommended formula for the design of the necessary base plate thickness is equation (6-1).

$$t = \sqrt{\frac{8M}{(\phi F_y) \pi n r_b}} \quad (6-1)$$

where:

$t$  = required base plate thickness

$M$  = applied moment

$\phi$  = strength design factor = 0.90

$F_y$  = yield stress of the base plate

$n$  = number of bolts

$r_b$  = distance from center of plate to center of bolt

### 6.3 Magnitude and Location of the Reaction Acting on the Grout Pad

The magnitude of the force that was transferred to the grout during testing was easily calculated by analyzing the internal equilibrium of the plate. This analysis was performed for Specimens #2, #3, and #4. Specimen #1 did not incorporate tension load cells. The load transferred to the grout for all tests on these specimens performed with grout pads is shown in Table 6.3.

Table 6.3 Load carried by grout pad

Specimen #	Test #	$\Sigma$ Loads on Tension Bolts kN (kips)	$\Sigma$ Loads on Compression Bolts kN (kips)	Load Carried by Grout Pad kN (kips)	% Load Carried by Grout Pad
2	8-3/4-4s-G	601.6 (135.2)	73.3 (16.5)	528.3 (118.8)	88
3	6-3/4-4sW-G	92.1 (20.7)	41.2 (9.3)	50.9 (11.4)	55
	6-3/4-4sW-GS	351.0 (78.9)	36.0 (8.1)	315.0 (70.8)	90
4	6-3/4-4s-G	113.6 (25.5)	49.6 (11.2)	64.0 (14.4)	56
	6-3/4-4s-GS	366.2 (82.3)	46.2 (10.4)	320.0 (71.9)	87

The location of the compressive reaction acting on the grout pad could be found by equating the external applied moment to the sum of the internal moments of the bolt forces and the compressive reaction and solving for the location of the compressive

reaction on the grout. The results of these calculations at the maximum applied moment for each test with a grout pad are shown in Table 6.4.

Table 6.4 Calculated location of compressive reaction acting on the grout pad

Specimen #	Test #	Maximum Applied Moment kN-m (kip-in)	Location of Resultant Compressive Force Relative to Axis of Bending mm (in)
1	8-3/4-8-G	101 (889)	N/A
2	8-3/4-4s-G	110 (970)	75.6 (2.97)
3	6-3/4-4sW-G	20.9 (185)	140.1 (5.52)
	6-3/4-4sW-GS	85.1 (756)	143.7 (5.66)
4	6-3/4-4s-G	23.1 (277)	97.6 (3.84)
	6-3/4-4s-GS	85.8 (756)	135.0 (5.31)

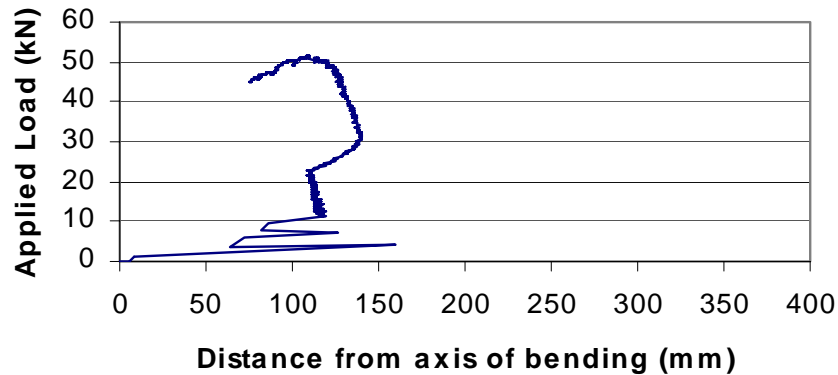


Figure 6.2 Plot of movement of grout reaction resultant during loading for 8-3/4-4s-G

#### 6.4 Analysis of Loads within Anchor Bolts

Equation (2-13) can be used to calculate the maximum anticipated load within the bolts and was used to compute the predicted bolt loads for the base plates in this study.

An applied moment of 14,000 kN-mm (124 kip-in) was selected for all of the calculations for comparison purposes. This applied loading was known to be in the elastic range for

all four specimens. Table 6.5 shows the results of these comparisons. Table 6.6 shows a comparison of the bolt loads predicted by equation (2-13) and the bolt forces measured at the ultimate level for each specimen.

As shown in Table 6.5, equation (2-13) slightly over-predicted the expected bolt forces in the elastic range for all four specimens tested. This was most likely due to the

Table 6.5 Comparison of predicted and measured bolt loads at service load level

Specimen #	Test #	Measured $P_{bolt}$ kN (kips)	Predicted $P_{bolt}$ kN (kips)	Measured $P_{bolt}$ / Predicted $P_{bolt}$
1	8-3/4-8-U	23.7 (5.32)	24.0 (5.39)	0.99
	8-3/4-8-G	N/A	24.0 (5.39)	N/A
2	8-3/4-4s-U	33.3 (8.07)	33.9 (7.62)	0.98
	8-3/4-4s-G	39.6 (7.48)	33.9 (7.62)	1.17
3	6-3/4-4sW-U	31.2 (7.02)	33.9 (7.62)	0.92
	6-3/4-4sW-G	37.2 (8.35)	33.9 (7.62)	1.10
	6-3/4-4sW-GS	23.8 (5.34)	33.9 (7.62)	0.70
4	6-3/4-4s-U	30.8 (6.93)	33.9 (7.62)	0.91
	6-3/4-4s-G	33.6 (7.55)	33.9 (7.62)	0.99
	6-3/4-4s-GS	29.6 (6.65)	33.9 (7.62)	0.87
Mean:				0.96
COV:				0.14

Table 6.6 Comparison of predicted to measured bolt forces at ultimate load level

Specimen #	Test #	Maximum Applied Moment kN-m (kip-in)	Measured $P_{bolt}$ kN (kips)	Predicted $P_{bolt}$ kN (kips)	Measured $P_{bolt}$ / Predicted $P_{bolt}$
1	8-3/4-8-G	101 (889)	N/A	172 (38.7)	N/A
2	8-3/4-4s-G	110 (970)	301 (67.6)	265 (59.6)	1.13
3	6-3/4-4sW-GS	85.1 (753)	176 (39.5)	206 (46.3)	0.85
4	6-3/4-4s-GS	85.8 (756)	183 (41.2)	207 (46.5)	0.89
Mean:					0.96

plate flexibility which may have influenced the assumed elastic distribution of the loads within the bolts. As shown in Table 6.6, the equation also slightly over-predicted the bolt loads measured at the ultimate load for the specimens. Thus, based on these results, equation (2-13) can be used to derive a design equation for the necessary bolt diameter

$$d_b = \sqrt{\frac{32M}{3\pi(\phi F_y)nr_b}} \quad (6-6)$$

The results in Table 6.5 indicated that the expected bolt loads were amplified by the addition of the grout pad. This was most likely due to the flexibility of the base plate and the location of the resultant compressive force between the compression and tension anchors, as was discussed in Chapter 2. The results in Table 6.5 also showed that the addition of plate stiffeners brought the bolt loads back down to levels slightly below the magnitudes measured before the grout pads were added.

The bolt loads predicted by equation (2-13) were very close to the actual bolt loads measured for the specimens at their ultimate loads. In fact, the equation slightly under-predicted the actual load for Specimen #2, the grouted plate at ultimate load. The equation was satisfactory for determining bolt loads at ultimate load levels for Specimen #3 and #4, the two specimens with grout pads and plate stiffeners. The bolt loads for these specimens were only almost 90% of the predicted bolt loads.

### 6.5 Grout Bearing Strength Considerations

Another one of the concerns of placing a grout pad beneath a base plate is that the bearing capacity of the grout pad may be exceeded as the applied bending moment becomes large. ACI 318-95 states that bearing on concrete supports shall not

exceed the design level of  $\phi(0.85f'_cA_1)$ , where  $A_1$  is the loaded area directly beneath the bearing plate. The results of the bearing evaluation are shown in Table 6.7.

Table 6.7 Grout bearing stress evaluation

Specimen #	$f'_c$ grout MPa (psi)	Maximum Applied Bearing Load kN (kips)	Calculated Grout Design Bearing Capacity kN (kips)	Applied Bearing/ Bearing Capacity
1	39.50 (5730)	N/A	N/A	N/A
2	64.18 (9310)	528 (119)	2352 (529)	0.225
3	64.72 (9390)	315 (70.8)	512 (115)	0.616
4	71.55 (10380)	320 (71.9)	784 (177)	0.406

### 6.6 Conclusions – Strength Considerations

The existing strength design equations for annular base plates were found to be conservative from the experimental results of this study. The equations over-predicted the results that were actually observed. It is recommended that equation (6-1), for its simplicity and relatively conservative results, be used to design the required thickness of both ungrouted and grouted base plates. The results of the study found that the anchor bolts should be designed by equation (6-6). This equation also proved to be largely conservative when compared to the observations from the tests.

The designer can expect that the grouted plate will behave as a rigid body in lower load levels. As loading reaches higher levels, the plate will start to experience local yielding, and a larger area of the plate will be in contact with the grout pad. However, bearing on the grout pad is not a serious design concern. For these specimens, the localized yielding was also not a strength concern, as a plastic hinge failure occurred in the tubular member before the plate.

## CHAPTER 7 SERVICEABILITY CONSIDERATIONS

### 7.1 Introduction

Serviceability is the other primary concern when designing base plates for sign and lighting structures. Serviceability considerations are related to overall deflection of the sign or lighting structure.

This chapter compares test data to previously derived equations for quantifying rotations of tubular members attached to annular base plates and exposed to bending moments. A design equation for predicting rotations is suggested. Modifications to this equation for the addition of a grout pad and for the addition of a grout pad and plate stiffeners are also recommended.

### 7.2 Stiffness Evaluation

The results of the stiffness calculations are shown in Table 7.1.

Specimen #	Test	Total Stiffness kN/mm (kip/in)	Pipe Stiffness kN/mm (kip/in)	Connection Stiffness kN/mm (kip/in)	Total Stiffness/ Connection Stiffness
1	8-3/4-8-U	0.909 (5.19)	1.83 (10.4)	1.81 (10.3)	0.502
	8-3/4-8-G	0.901 (5.15)	1.83 (10.4)	1.78 (10.2)	0.506
2	8-3/4-4s-U	.0585 (3.34)	1.83 (10.4)	0.861 (4.91)	0.680
	8-3/4-4s-G	0.637 (3.64)	1.83 (10.4)	0.980 (5.59)	0.651
3	6-3/4-4sW-U	0.500 (2.86)	1.65 (9.44)	0.719 (4.10)	0.697
	6-3/4-4sW-G	0.542 (3.10)	1.65 (9.44)	0.808 (4.62)	0.672
	6-3/4-4sW-GS	0.716 (4.09)	1.65 (9.44)	1.26 (7.21)	0.567
4	6-3/4-4s-U	0.434 (2.48)	1.65 (9.44)	0.589 (3.36)	0.737
	6-3/4-4s-G	0.576 (3.29)	1.65 (9.44)	0.884 (5.05)	0.651
	6-3/4-4s-GS	0.892 (5.10)	1.65 (9.44)	1.94 (11.1)	0.460

Table 7.1 Connection stiffnesses

The results in Table 7.1 show that the stiffnesses of the base plate connections were only moderately improved by the addition of a grout pad. However, the connection stiffnesses were significantly enhanced by the addition of both a grout pad and plate stiffeners.

### 7.3 Analysis of Connection Rotation

Calculating the connection stiffness could further be used to quantify the portion of the rotation that comes from the plate and bolts within the elastic loading range. As discussed earlier, the stiffness of the connection can be determined from knowing the stiffness of the tubular member and the overall stiffness. Rearranging the terms yielded the final equation for calculating the rotation of the connection based on stiffness:

$$\theta_{\text{predicted}} = \frac{P}{LK_{\text{connection}}} \quad (7-6)$$

Equation (7-6) was used to evaluate all four specimens at the same applied moment of 14,000 kN-mm (124 kip-in). This was the equivalent of an applied shear load of 5.74 kN (1.29 kips) and 7.66 kN (1.72 kips) for Specimens #1 and #2, and Specimens #3 and #4, respectively. This applied loading was known to be in the elastic range for all four specimens.

Equation (2-31) was derived based on a finite element analysis of the rotation of the plate and the rotation of the bolts.

$$\theta_{\text{total}} = \theta_{\text{plate}} + \theta_{\text{bolt}} \quad (7-7)$$

Specimen #	Test	Connection Stiffness kN/mm (kip/in)	Load for $\theta$ Calculations kN (kips)	$\theta_{\text{measured}}$	$\theta_{\text{calculated}}$ by equation (2-31)	$\theta_{\text{measured}} / \theta_{\text{calculated}}$
1	8-3/4-8-U	1.81 (10.3)	5.74 (1.29)	0.00130	0.00342	0.381
2	8-3/4-4s-U	0.861 (4.91)	5.74 (1.29)	0.00274	0.00394	0.695
3	6-3/4-4sW-U	0.719 (4.10)	7.66 (1.72)	0.00583	0.00566	1.03
4	6-3/4-4s-U	0.589 (3.36)	7.66 (1.72)	0.00711	0.00566	1.26

Table 7.2 Comparison of predicted connection rotations

The contribution to the rotation from the bolts was found by:

$$\theta_{\text{bolt}} = \frac{1.5ML_b}{s_g A_b E_b r_b} \quad (7-11)$$

The individual contributions of flexure, shear, and bolt rotation terms to the overall calculated rotation found by Equation (2-20) are shown in Table 7.3.

The largest contribution to the calculated rotation from equation (2-31) comes from the shear component. The flexure contribution, when compared to the shear

Table 7.3 Components of calculated connection rotation using equation (2-31)

Specimen #	Test	$\theta_{\text{flexure}}$	$\theta_{\text{shear}}$	$\theta_{\text{bolt}}$	$\theta_{\text{total}}$
1	8-3/4-8-U	0.000359	0.00179	0.00127	0.00342
2	8-3/4-4s-U	0.000359	0.00179	0.00179	0.00394
3	6-3/4-4sW-U	0.00142	0.00246	0.00179	0.00566
4	6-3/4-4s-U	0.00142	0.00246	0.00179	0.00566

contribution, is very small. These results indicate that for design purposes the plate rotation can be assumed to be dominated by the shear term.

#### 7.4.1 Deflection from Bolts

A portion of the connection rotation was known to come from the anchor bolts. When the system was loaded, the compression bolts shortened, while the tension bolts

elongated. A rigid body rotation of the plate occurred as a result of this event, as shown in Figure 7.2

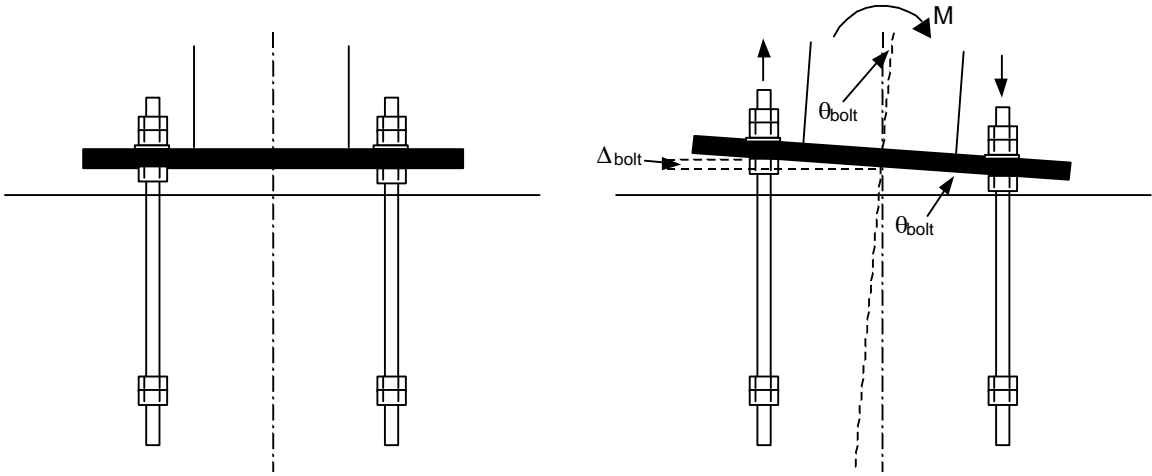


Figure 7.2 Rotation of system due to bolts

$$\theta_{\text{bolt}} = \frac{2ML_b}{nr_b^2 A_b E_b} \quad (7-15)$$

where:

$M$  = applied bending moment

$L_b$  = length of bolt under tension or compression

$n$  = number of bolts

$r_b$  = distance from the center of the plate to the center of the bolts

$A_b$  = cross-sectional area of bolt

$E_b$  = modulus of elasticity of bolt

The formula for the bolt rotation that was mentioned in equation (7-11) was multiplied by an adjustment factor of 1.5. That factor was not included for equation (7-

15) because, as is shown in Table 7.4, the formula already over-predicted the value of the bolt rotation that was measured.

Table 7.4 Evaluation of predicted bolt rotation

Specimen #	Test #	$\theta_{\text{measured}}$	$\theta_{\text{predicted}}$ by equation (7-15)	$\theta_{\text{measured}}/\theta_{\text{predicted}}$
1	8-3/4-8-U	0.0873	0.197	0.442
2	8-3/4-4s-U	0.260	0.395	0.658
4	6-3/4-4s-U	0.278	0.395	0.703
Mean:				0.601
COV:				0.232

#### 7.4.2 Deflection from Plate Rotation

Once the total connection rotation and the rotation from the bolts were known, the remaining rotation was assumed to be from the plate. The plate rotation was determined by modifying equation (7-10). The results in Table 7.3 indicated that the majority of the rotation from the plate comes from shear. Thus, the flexure term was disregarded and the plate rotations were quantified entirely by the shear contribution. Thus, by making modifications to equation (7-10), a final form of the plate rotation term was derived. The results of the comparisons are shown in Table 7.5.

Table 7.5 Comparison of prediction equation to FEM predictions and test values

Test Designation	Eq. (7-10)	Prediction		Eq. (7-10)/
		FEM	Test	Prediction
10-3/4-6	0.3129	0.4500		0.6953
10-1-6	0.2347	0.2620		0.8957
10-1.75-6	0.1877	0.1730		1.0852
25-2-8	0.0188	0.0258		0.7270
25-2.375-8	0.0158	0.0186		0.8492
25-3-8	0.0125	0.0112		1.1165
24-1.75-12	0.0233	0.0337		0.6924
24-1.75-12	0.0181	0.0207		0.8772
24-1.75-12	0.0148	0.0129		1.1475
6-1-4d	0.4314		0.7738	0.5574
6-1-4s	0.4314		0.7907	0.5456
6-1-6	0.4314		0.7110	0.6067
6-1-8	0.4314		0.6813	0.6332
6-3/4-4d	0.5752		1.2878	0.4466
6-3/4-8	0.5752		1.0767	0.5342
8-3/4-4d	0.4192		0.7238	0.5791
8-3/4-6	0.4192		0.5681	0.7378
8-3/4-8	0.4192		0.2243	1.8691
8-3/4-4s	0.4192		0.4693	0.8932
6-3/4-4s	0.5752		1.5567	0.3695

The final form of the shear term and thus the overall plate rotation term for the connection rotations was:

$$\theta_{\text{shear}} = \frac{45M}{Er_b^2 b} \left( \frac{r_{\Delta}}{t_{\text{plate}}} \right)^{1.83} \quad (7-17)$$

The results obtained by equation (7-17) were compared to the results measured for the three ungrouted specimens for this study in which bolt rotations were measured. The measured bolt rotations were necessary for determining the measured rotations from the plate. The results were calculated for an applied moment of 14,000 kN-mm (124 kip-in) and are shown in Table 7.7.

Table 7.6 Comparison of predicted plate rotations to  $r_{\Delta}/t_{\text{plate}}$  ratio

Test Designation	Eq. (7-17)	Prediction		Eq. (7-17)/ Prediction	$r_{\Delta}/t$
		FEM	Test		
10-3/4-6	0.3912	0.4500		0.8693	1.67
10-1-6	0.2311	0.2620		0.8819	1.25
10-1.75-6	0.1536	0.1730		0.8879	1.00
25-2-8	0.0273	0.0258		1.0574	2.00
25-2.375-8	0.0199	0.0186		1.0710	1.68
25-3-8	0.0130	0.0112		1.1599	1.33
24-1.75-12	0.0339	0.0337		1.0071	2.00
24-1.75-12	0.0214	0.0207		1.0356	1.56
24-1.75-12	0.0148	0.0129		1.1470	1.27
6-1-4d	0.7394		0.7738	0.9555	2.44
6-1-4s	0.7394		0.7907	0.9351	2.44
6-1-6	0.7394		0.7110	1.0399	2.44
6-1-8	0.7394		0.6813	1.0852	2.44
6-3/4-4d	1.2517		1.2878	0.9720	3.25
6-3/4-8	1.2517		1.0767	1.1626	3.25
8-3/4-4d	0.5885		0.7238	0.8131	1.92
8-3/4-6	0.5885		0.5681	1.0359	1.92
8-3/4-8	0.2599		0.2243	1.1591	1.92
8-3/4-4s	0.5885		0.4693	1.2541	1.92
6-3/4-4s	1.2517		1.5567	0.8040	3.25

Table 7.7 Evaluation of predicted plate rotation

Specimen #	Test #	$\theta_{\text{measured}}$	$\theta_{\text{predicted}}$	$\theta_{\text{measured}}/\theta_{\text{predicted}}$
1	8-3/4-8-U	0.000958	0.00251	0.381
2	8-3/4-4s-U	0.00200	0.00251	0.797
4	6-3/4-4s-U	0.0066478	0.00535	1.244

### 7.4.3 Final Rotation Formula

The equations derived above were combined to derive a final formula for finding the connection rotation of a tubular member attached to an annular base plate. The connection rotation was quantified as the summation of the rotation from the bolts and the plate:

$$\theta_{\text{bolt+plate}} = \theta_{\text{bolt}} + \theta_{\text{plate}} \quad (7-18)$$

Thus, the connection rotation could be found by equation (7-18).

$$\theta_{\text{bolt+plate}} = \frac{2ML_b}{nr_b^2 A_b E} + \frac{45M}{Er_b^2 b} \left( \frac{r_b - r_p}{t} \right)^{1.83} \quad (7-19)$$

Table 7.8 contains a comparison of the results predicted by this equation and the measured experimental rotations.

Table 7.8 Comparison of measured to predicted rotations

Specimen #	Test #	$\theta_{\text{measured}}$	$\theta_{\text{predicted}}$	$\theta_{\text{measured}}/\theta_{\text{predicted}}$
1	8-3/4-8-U	0.00130	0.00336	0.388
2	8-3/4-4s-U	0.00274	0.00420	0.651
3	6-3/4-4sW-U	0.00583	0.00704	0.828
4	6-3/4-4s-U	0.00711	0.00704	1.01

### 7.5 Adjustments to Design Equation for Addition of Grout Pad

Equation (7-19) was derived based on the experimental results of the specimens when they were tested without grout pads. The earlier calculations of the connection stiffnesses revealed that, as expected, the connections were made stiffer by the addition of a grout pad. The results of this analysis are shown in Table 7.9.

Table 7.9 Evaluation of predicted plate rotation for three specimens with grout pads

Specimen #	Test #	$\theta_{\text{measured}}$	$\theta_{\text{predicted}}$	$\theta_{\text{measured}}/\theta_{\text{predicted}}$
2	8-3/4-4s-G	0.00240	0.00420	0.572
3	6-3/4-4sW-G	0.00517	0.00704	0.735
4	6-3/4-4s-G	0.00473	0.00704	0.672
			Mean:	0.660
			COV:	0.125

The measured connection rotations were, on average, about 66% of the predicted rotations in the second analysis. Thus, the original formula, equation (7-19) was modified by an adjustment factor of 0.66, to yield equation (7-20).

$$\theta_{\text{grouted plate+bolt}} = 0.66\theta_{\text{plate+bolt}} \quad (7-20)$$

This form of the equation was compared to the results obtained during experimentation (see Table 7.10).

Table 7.10 Evaluation of serviceability design equation for base plates with grout pads

Specimen #	Test #	$\theta_{\text{measured}}$	$\theta_{\text{predicted}}$	$\theta_{\text{measured}}/\theta_{\text{predicted}}$
1	8-3/4-8-G	0.00132	0.00222	0.594
2	8-3/4-4s-G	0.00240	0.00277	0.867
3	6-3/4-4sW-G	0.00517	0.00464	1.11
4	6-3/4-4s-G	0.00473	0.00464	1.02

#### 7.6 Adjustments to Design Equation for Addition of Grout Pads and Plate stiffeners

It was observed during the experimental determination of the connection stiffnesses that the use of both a grout pad and plate stiffeners significantly increased the connection stiffness of the base plates. The results are shown in Table 7.11.

Table 7.11 Evaluation of design equation for base plates with grout pads and stiffeners

Specimen #	Test #	$\theta_{\text{measured}}$	$\theta_{\text{predicted}}$	$\theta_{\text{measured}}/\theta_{\text{predicted}}$
3	6-3/4-4sW-GS	0.00331	0.00704	0.471
4	6-3/4-4s-GS	0.00215	0.00704	0.306
			Mean:	0.388

Table 7.11 shows that the original serviceability equation yields a significant over-prediction of the measured connection rotation. The measured values were an average of about 39% of the predicted values. Thus, an adjustment factor of 0.39 was applied to the original form of equation (7-19). The result was equation (7-21).

$$\theta_{\text{stiffened plate+bolt}} = 0.39\theta_{\text{plate+bolt}} \quad (7-21)$$

Equation (7-21) was compared to the actual results measured for an applied moment of 14,000 kN-mm (124 kip-in) for the two plates tested with grout pads and plate stiffeners. The results are shown in Table 7.12.

Table 7.12 Evaluation of final rotation equation for plates with grout pads and stiffeners

Specimen #	Test #	$\theta_{\text{measured}}$	$\theta_{\text{predicted}}$	$\theta_{\text{measured}}/\theta_{\text{predicted}}$
3	6-3/4-4sW-GS	0.00331	0.00274	1.21
4	6-3/4-4s-GS	0.00215	0.00274	0.784

### 7.7 Conclusions – Serviceability Considerations

Understanding serviceability considerations is vital to the design of annular base plate connections. A large portion of the rotation of tubular members attached to base plates can be modeled by assuming the member has a fixed end support. However, this does not account for the total rotation.

The recommended formula to account for the additional rotation for ungrouted annular base plates was equation (7-19).

$$\theta_{\text{plate+bolt}} = \frac{2ML_b}{nr_b^2 A_b E_b} + \frac{45M}{Er_b^2 b} \left( \frac{r_b - r_p}{t} \right)^{1.83} \quad (7-19)$$

where:

$M$  = applied moment

$L_b$  = length of bolt in tension or compression

$n$  = number of anchor bolts

$A_b$  = cross-sectional area of anchor bolt

$E_b$  = modulus of elasticity of bolt

$E$  = modulus of elasticity of plate

$r_b$  = distance from center of plate to center of bolt

$r_p$  = radius of pipe

$t$  = thickness of base plate

$$b = 2\sqrt{r_b^2 - r_p^2}$$

An adjustment factor was applied to this equation for base plates constructed with grout pads beneath them. The recommended serviceability design equation for grouted base plates was:

$$\theta_{\text{grouted plate+bolt}} = 0.66\theta_{\text{plate+bolt}} \quad (7-20)$$

Finally, the original suggested serviceability design equation was adjusted for base plates constructed with both grout pads and plate stiffeners. This suggested design equation was:

$$\theta_{\text{stiffened plate+bolt}} = 0.39\theta_{\text{plate+bolt}} \quad (7-21)$$

## CHAPTER 8 SUMMARY, CONCLUSIONS, AND RECOMMENDATIONS

### 8.1 Summary

The purpose of this research study was to examine the behavior of annular base plates constructed with grout pads beneath them. The base plates evaluated here were to model those used for Florida Department of Transportation (FDOT) sign and lighting structures. The loading on those base plates is dominated by bending moment, as were the base plates tested here. The final goal was to recommend strength and serviceability criteria for the design of these structural elements.

The placement of a grout pad was found to very slightly increase the stiffness of the connection and therefore decrease the total rotation of the pipe. The grout pad also served to reduce the magnitude of the load transferred to the anchors on the compression side of the plate by carrying some of the load itself. However, the loads in the tension bolts were magnified when the grout pad was added since the location of the compressive reaction moved from the compressive bolts inward (i.e. the internal moment arm was reduced).

The plate stiffeners were found to considerably enhance the stiffness of the plate connection, and consequently further reduce the pipe rotation. They also relieved the stresses in the compression bolts by absorbing much of the applied load. The loads in the tension bolts were found to be lower than the bolt loads that were experienced when the plates were loaded without grout pads or stiffeners.

The research resulted in the derivation of design criteria for strength and serviceability considerations. It was observed throughout this research that the strength design of the base plate with a grout pad is not the primary concern for these structures. The primary design concern for these structural elements, however, is the serviceability considerations. The pipe rotations experienced at service loads were greater than those found by assuming that the tubular member has a fixed-end or cantilevered support. The source of the additional deflection was found to be from local yielding and rotation of the base plate and rotation due to deformations in the anchor bolts.

## 8.2 Conclusions

Based on the results of this research, the following conclusions were made:

- The use of a grout pad with unstiffened annular base plates was not found to provide significant enhancement to the stiffness of the base plate connection. In fact, the additional stiffness provided was found to be offset by the amplification of the loads carried by the tension bolts. .
- The connection stiffnesses of the base plate specimens tested with grout pads and plate stiffeners were, however, notably improved by the combination of these two components. As a result, the pipe rotations were sufficiently reduced in the working load range. In addition, the loads within the tension bolts of the base plates fitted with both grout pads and stiffeners were lower than the loads within the tension bolts of the plain base plates.
- The use of a grout pad provided additional support to the compression side of the plate, as a large percentage of the compressive reaction was carried by the grout

compared to the bolts. However, the tension side did not benefit as much from the grout pad.

- Design criteria were recommended for the strength design of base plates, including thickness (equation 6-1) and the size of the anchor bolts (equation 6-6). The experimental observations found that bearing from the plates on the grout pads was not a primary concern for the design of these elements.
- Design criteria was recommended for the serviceability of these structures (equation 7-19) for when they are constructed without grout pads. This equation was modified (equation 7-20) for the design of base plates fitted with grout pads. One final modification to the original equation was performed to yield a design equation for base plates constructed with both grout pads and plate stiffeners (equation 7-21).
- The use of a grout pad alone with these annular base plate specimens was not found to provide a significant structural enhancement to the connections. The true structural improvements were observed when the grout pads were combined with plate stiffeners.

### 8.3 Recommendations for Future Research

Recommendations for topics of future research include the following:

- None of the grout pads failed during testing of these plates. An analysis of the bearing on the grout pad led to the conclusion that bearing should be of little concern to the base plate designer. However, the effect on the plate deformation and the stresses in the compression bolts would be of interest in the unlikely event

that a grout pad was to fail. Although strength was found to not be a major concern when designing these structures, the behavior may be unpredictable if large load was suddenly transferred from the grout pad to the anchor bolts if the grout pad did fail. In addition, the plate rotation, and its effect on serviceability, should be examined with a grout pad failure.

- The grout selected for this study was found to have a high compressive strength. It is suggested that other FDOT approved grouts, and perhaps some that are not approved, be tested to further understand the expected behavior variations from one grout product to the next. In addition, to mimic mistakes that may inevitably occur in the field, it is suggested that the water to grout mixture ratio be combined in such a way that ASTM C 939, the Flow Cone Test, is not satisfied, but the grout is used anyway.
- No plates with six bolt arrangements or variations in the positions of the anchors in the four bolt arrangement were tested. Since the difference between the observed results for four and eight bolts arrangements for base plates with grout pads was so large, it may be of interest to study such arrangements, with grout pads and grout pads and plate stiffeners.

## LIST OF REFERENCES

- Adihardjo, R., and Soltis, L., "Combined Shear and Tension on Grouted Base Details," *Engineering Journal*, American Institute of Steel Construction, First Quarter, 1979, pp. 23-26.
- AISC Manual of Steel Construction Load & Resistance Factor Design, Second Edition, American Institute of Steel Construction, Inc., USA, 1995.
- Building Code Requirements for Structural Concrete (ACI 318-95) and Commentary (ACI 318R-95), American Concrete Institute, Farmington Hills, MI, 1995.
- Cannon, R. W., "Flexible Baseplates: Effect of Plate Flexibility and Preload on Anchor Loading and Capacity," *ACI Structural Journal*, American Concrete Institute, V. 89, No. 3, May-June 1992, pp. 315-324.
- Cook, R. A., Ellifritt, D. S., Schmid, S. E., Adediran A., and Beese, W., "Design Procedure for Annular Base Plates," Research Report No. 95-4, Engineering and Industrial Experiment Station, University of Florida, Gainesville, Florida, 1995.
- Cook, R. A., Hoit, M. I., and Nieporent, S. B., "Deflection Calculation Model for Structures with Annular Base Plates," Research Report No. 98-1, Engineering and Industrial Experiment Station, University of Florida, Gainesville, Florida, 1998.
- Cook, R.A., and Klingner, R.E., "Behavior and Design of Ductile Multiple-Anchor Steel-to-Concrete Connections," *Research Report No. 1126-3*, Center for Transportation Research, University of Texas at Austin, Austin, Texas, 1989, pp. 16-26, 111-112.
- Cook, R. A. and Klingner, R. E., "Ductile Multiple-Anchor Steel-to-Concrete Connections," *Journal of Structural Engineering*, American Society of Civil Engineers, V. 118, No. 6, June, 1992, pp. 1645-1665.
- DeWolf, J. T., Design of Column Base Plates, American Institute of Steel Construction, Chicago, Illinois, 1991, pp. 2-3, 18-24.
- DeWolf, J. T. and Sarisley, A., "Column Base Plates with Axial Loads and Moments," *Journal of the Structural Division*, American Society of Civil Engineers, V. 106, No. ST11, November, 1980, pp. 2167-2184.

Florida DOT Structures Design Office, "Mast Arm Program, v3.03," 16 July 1997, <<http://www.dot.state.fl.us/Structures/>> (November 16, 1998).

Segui, William T., "LRFD Steel Design", PWS Publishing Company, Boston, 1994, pp.9-10, 127-133.

Specifications for Cantilever Signal Structures, Florida Department of Transportation Structures Design Office, Tallahassee, 1996.

Standard Specifications for Structural Supports for Highway Signs, Luminaries, and Traffic Signals (draft), AASHTO, Birmingham, Alabama, 1997

Targowski, R., Lamblin, D., and Guerlement, G., "Baseplate Column Connection under Bending: Experimental and Numerical Study." *Journal of Constructional Steel Research*, Elsevier Science Publishers Ltd., V. 27, 1993, pp. 37-54.

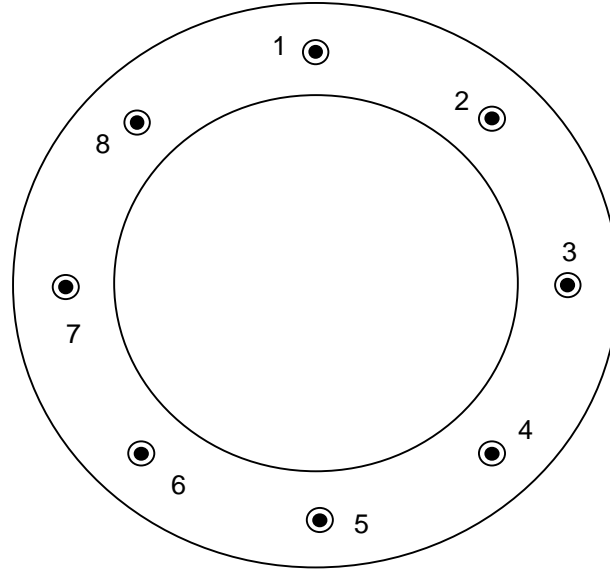
Thambiratman, D. P., and Paramasivam, P., "Base Plates Under Axial Loads and Moments," *Journal of Structural Engineering*, American Society of Civil Engineers, V. 112, No. 5, May, 1986, pp. 1166-1181.

Westergaard, H. M., "Computation of Stresses in Bridge Slabs due to Wheel Loads," U.S. Bureau of Public Roads, V. 11, No. 1, March, 1930, pp. 1-23.

## APPENDIX A: INSTRUMENTATION NUMBERING AND ORIENTATION

**8-3/4-8-U**

LVDT Placement



*Note: LVDT 9 is located over load point on pipe.*

Load Cell Placement

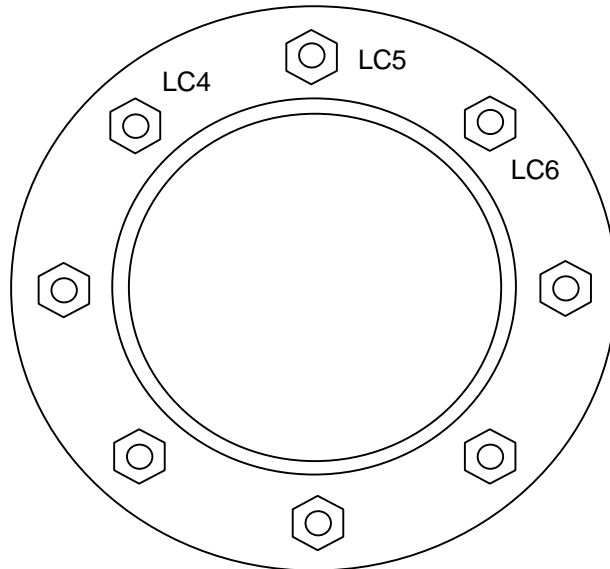
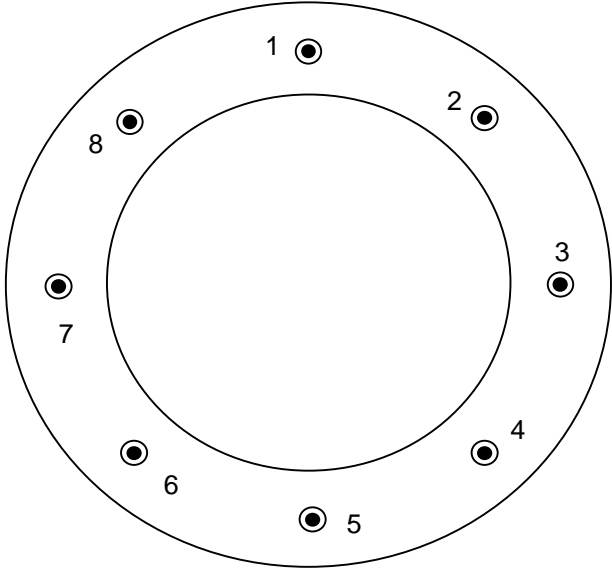


Figure A1.1 Instrumentation placement for Specimen #1, Test 8-3/4-8-U

**8-3/4-8-G**

LVDT Placement



*Note: LVDT 9 is located over load point on pipe.*

Load Cell Placement

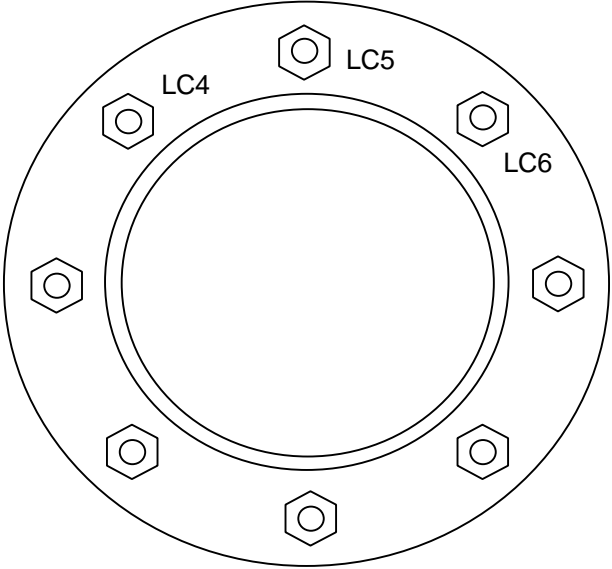
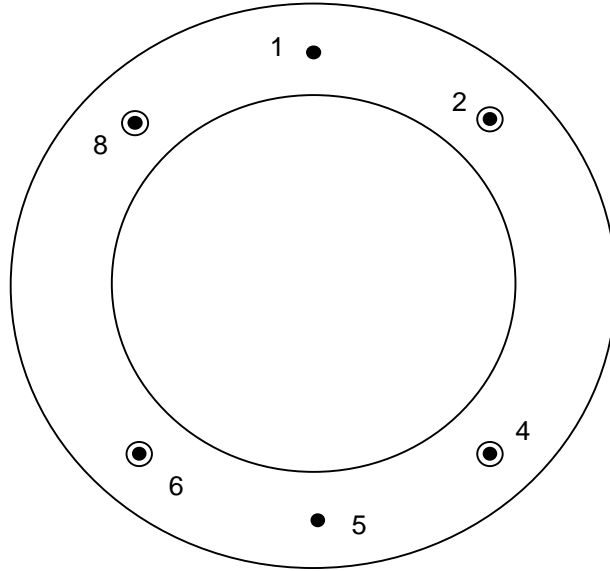


Figure A1.2 Instrumentation placement for Specimen #1, Test 8-3/4-8-G

**8-3/4-4s-U**

LVDT Placement



*Note: LVDT 9 is located over load point on pipe.*

Load Cell Placement

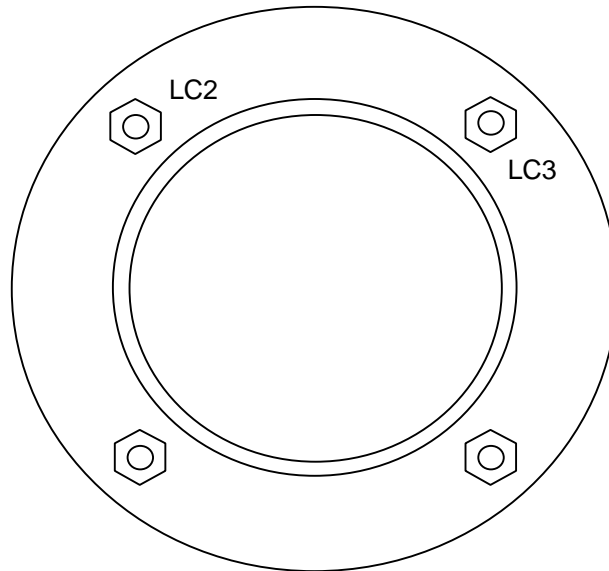
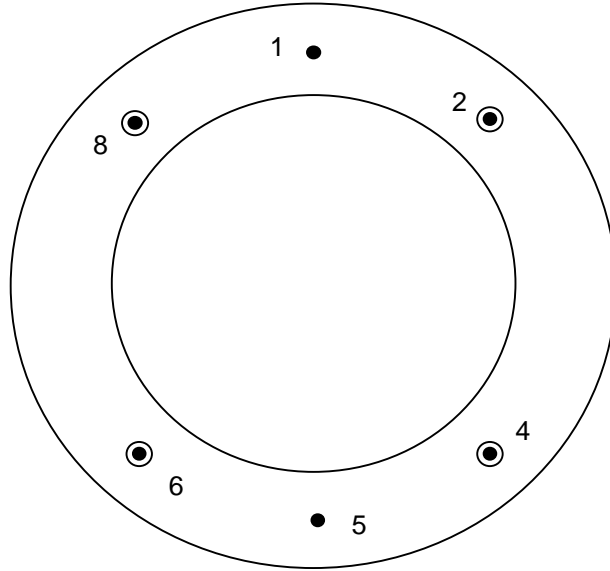


Figure A1.3 Instrumentation placement for Specimen #2, Test 8-3/4-4s-U

**8-3/4-4s-G**

LVDT Placement



*Note: LVDT 9 is located over load point on pipe.*

Load Cell Placement

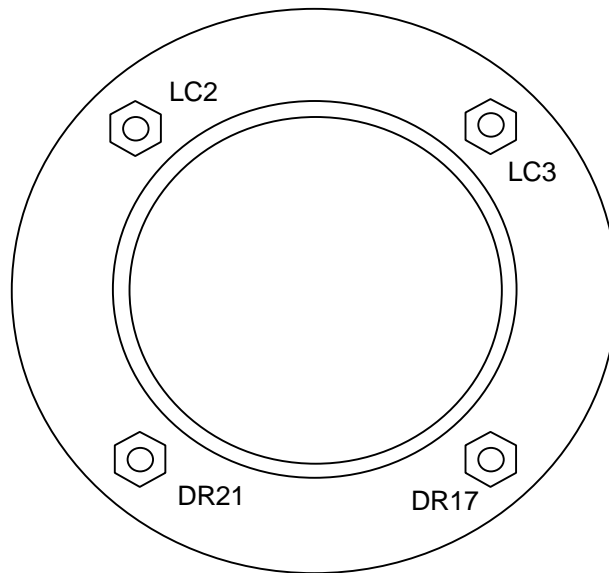
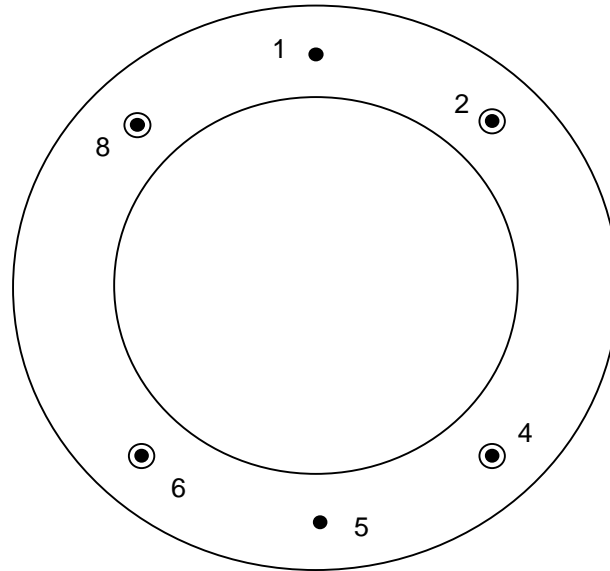


Figure A1.4 Instrumentation placement for Specimen #2, Test 8-3/4-4s-G

**6-3/4-4sW-U**

LVDT Placement



*Note: LVDT 9 is located over load point on pipe.*

Load Cell Placement

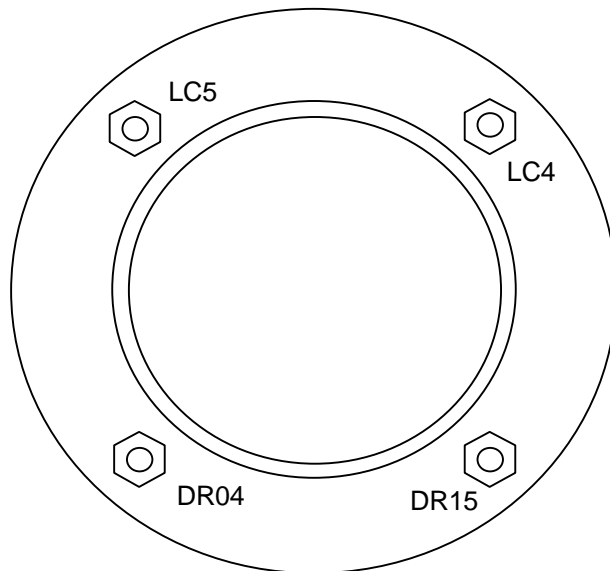
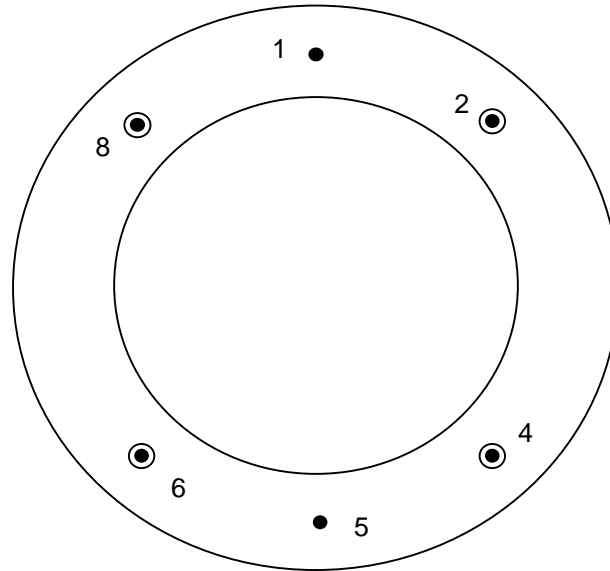


Figure A1.5 Instrumentation placement for Specimen #3, Test 6-3/4-4sW-U

**6-3/4-4sW-G**

LVDT Placement



*Note: LVDT 9 is located over load point on pipe.*

Load Cell Placement

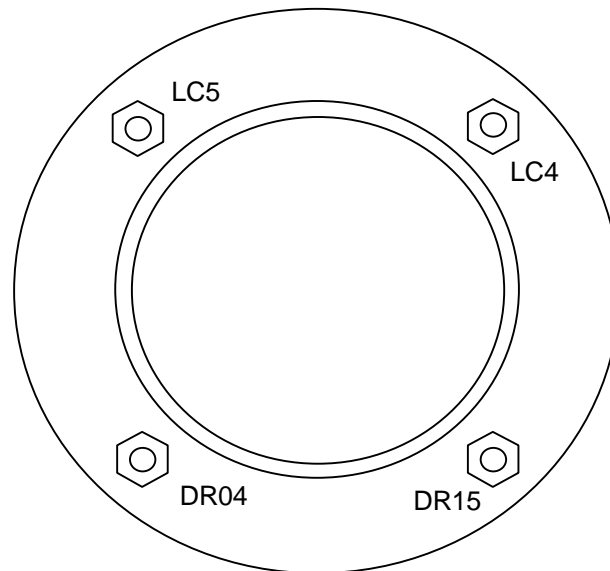
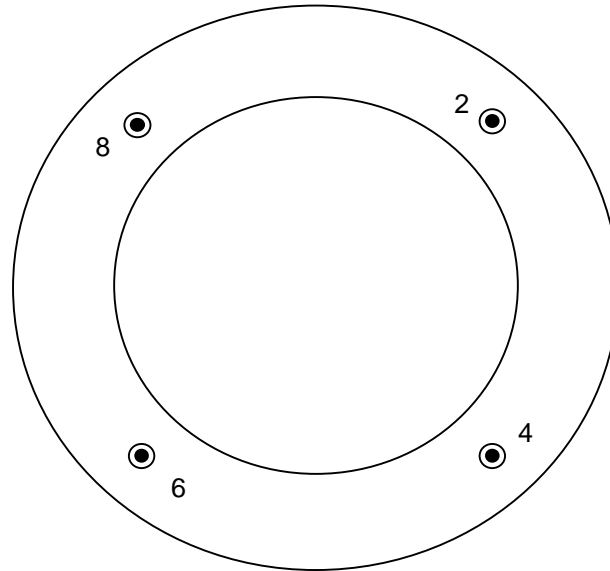


Figure A1.6 Instrumentation placement for Specimen #3, Test 6-3/4-4sW-G

**6-3/4-4sW-GS**

LVDT Placement



*Note: LVDT 9 is located over load point on pipe.*

Load Cell Placement

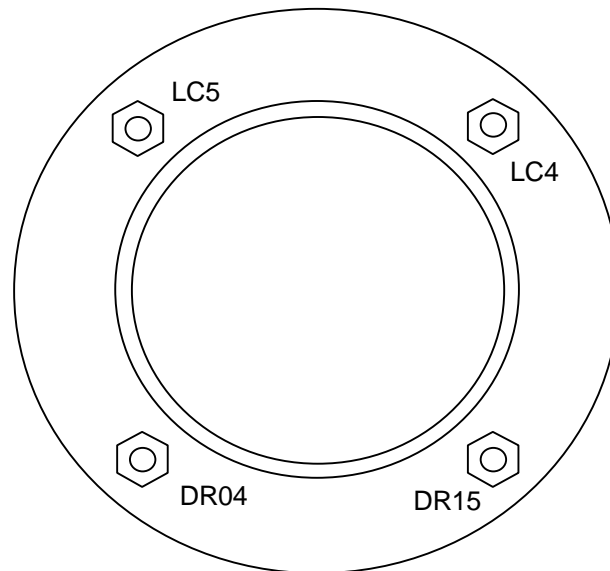
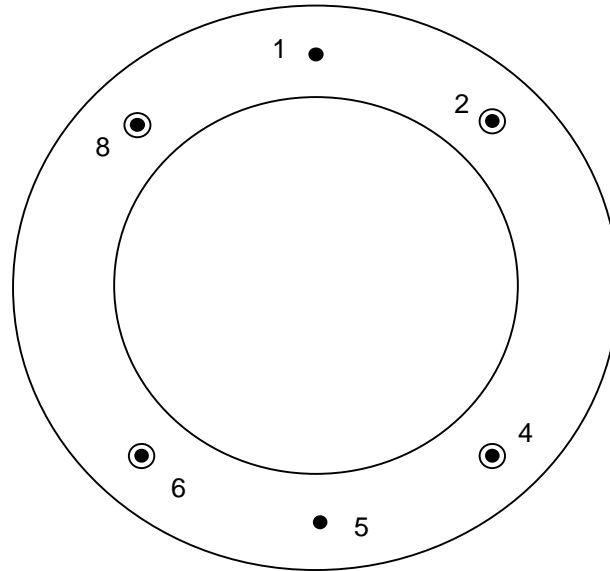


Figure A1.7 Instrumentation placement for Specimen #3, Test 6-3/4-4sW-GS

**6-3/4-4s-U**

LVDT Placement



*Note: LVDT 9 is located over load point on pipe.*

Load Cell Placement

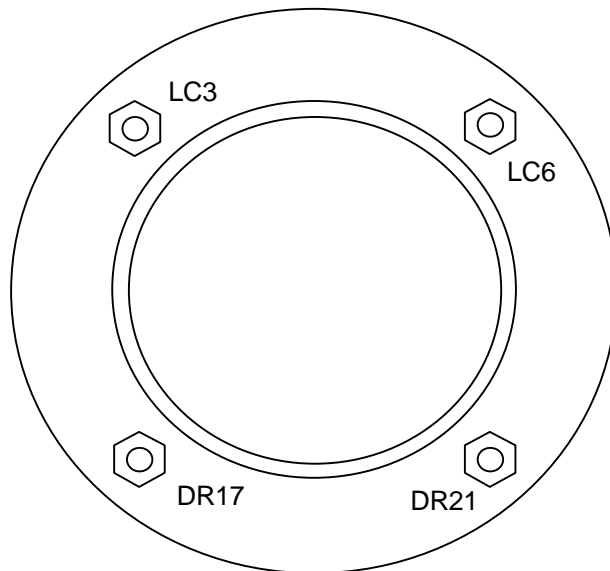
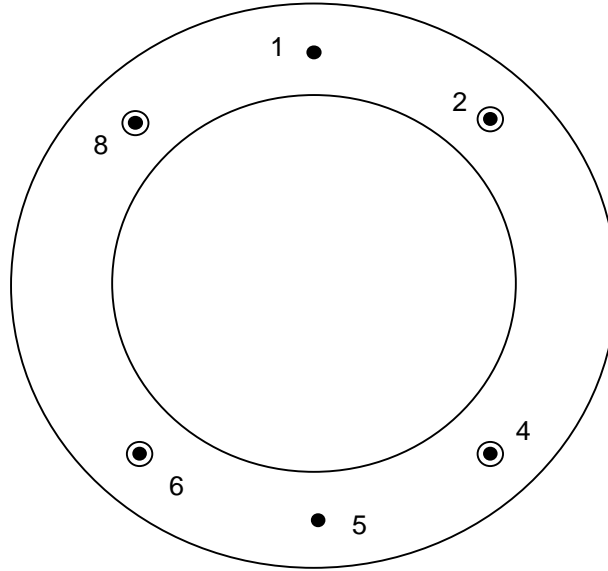


Figure A1.8 Instrumentation placement for Specimen #4, Test 6-3/4-4s-U

**6-3/4-4s-G**

LVDT Placement



*Note: LVDT 9 is located over load point on pipe.*

Load Cell Placement

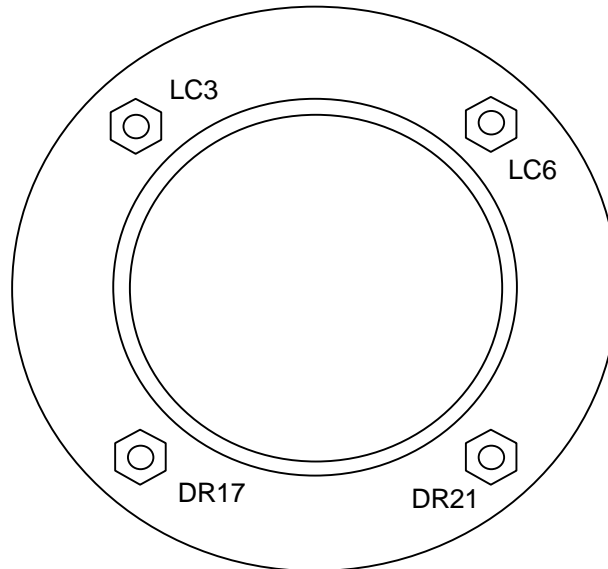
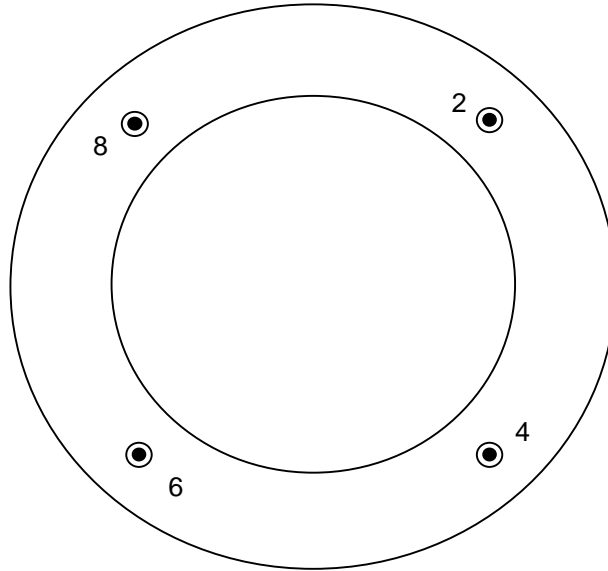


Figure A1.9 Instrumentation placement for Specimen #4, Test 6-3/4-4s-G

**6-3/4-4s-GS**

LVDT Placement



*Note: LVDT 9 is located over load point on pipe.*

Load Cell Placement

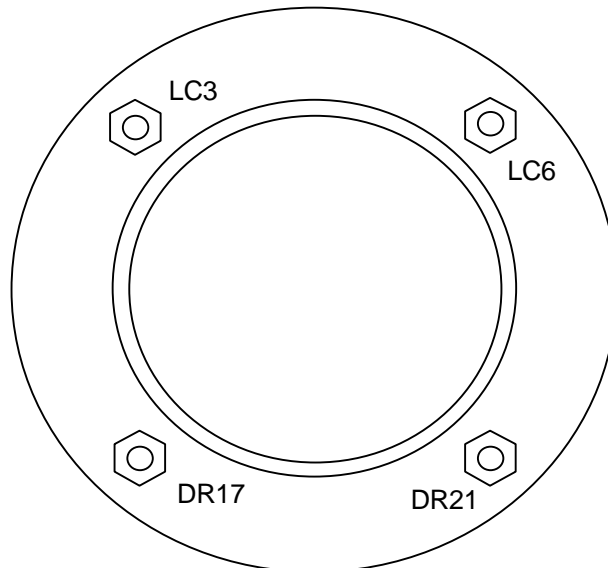


Figure A1.10 Instrumentation placement for Specimen #4, Test 6-3/4-4s-GS

APPENDIX B: LVDT DATA

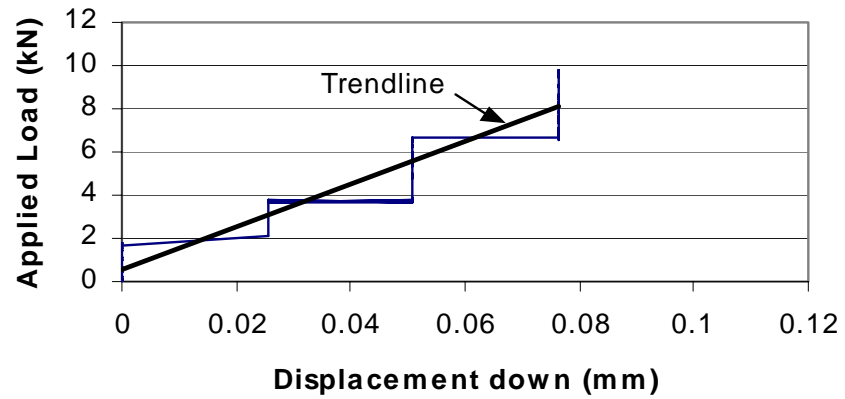


Figure B1.1 Applied Load vs. LVDT 1 (Test 8-3/4-8-U)

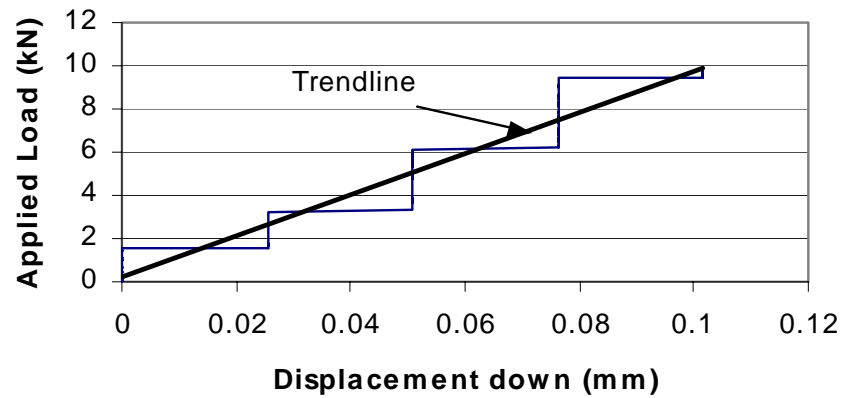


Figure B1.2 Applied Load vs. LVDT 2 (Test 8-3/4-8-U)

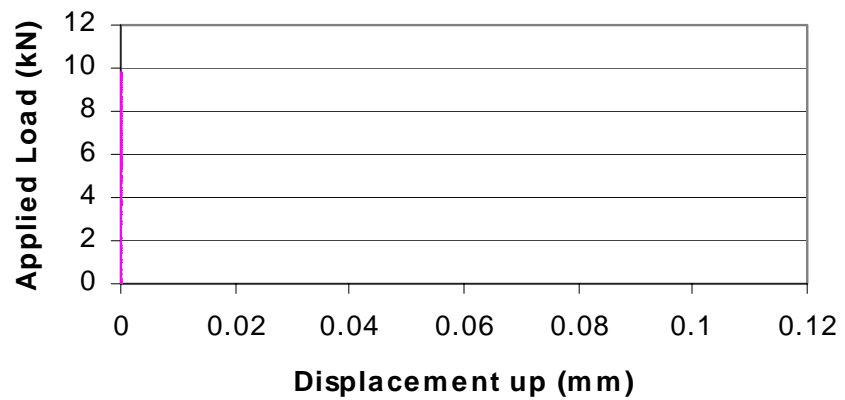


Figure B1.3 Applied Load vs. LVDT 3 (Test 8-3/4-8-U)

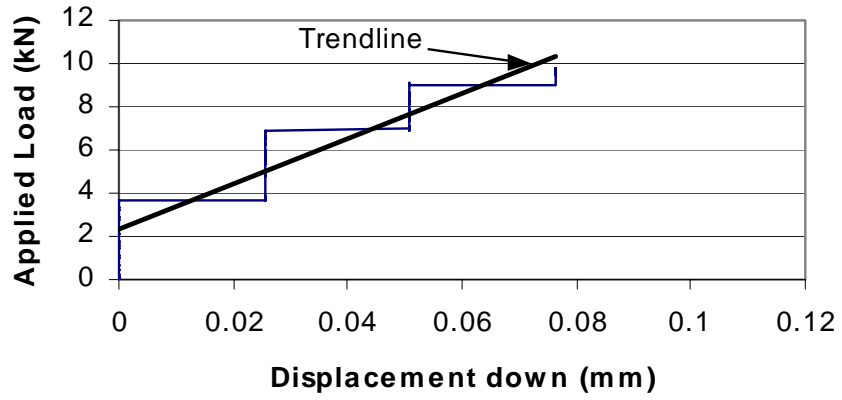


Figure B1.4 Applied Load vs. LVDT 4 (Test 8-3/4-8-U)

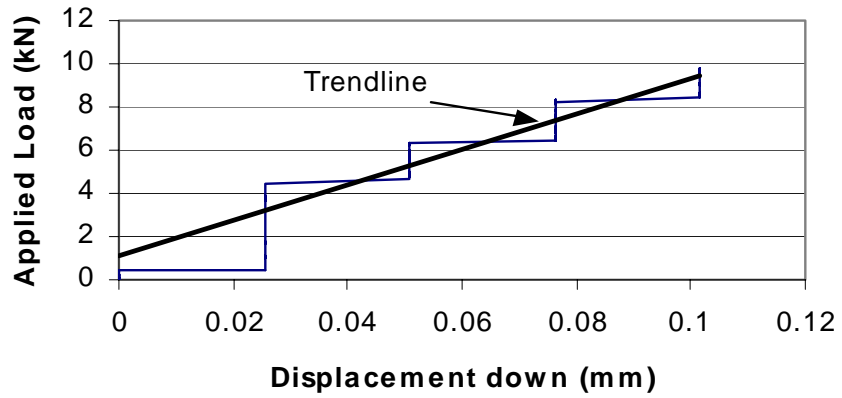


Figure B1.5 Applied Load vs. LVDT 5 (Test 8-3/4-8-U)

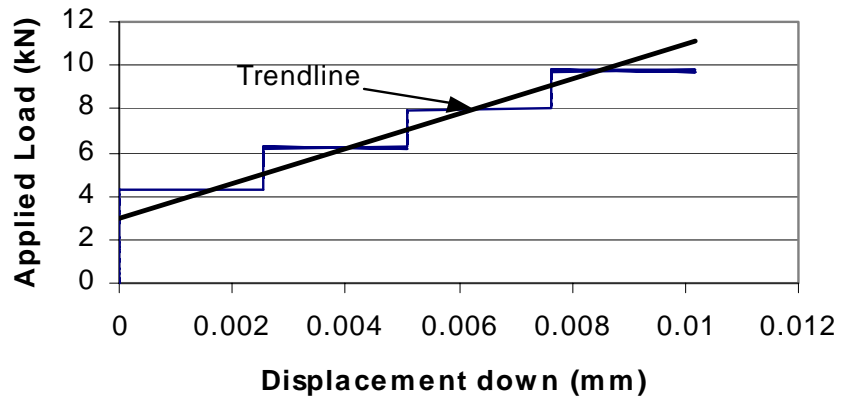


Figure B1.6 Applied Load vs. LVDT 6 (Test 8-3/4-8-U)

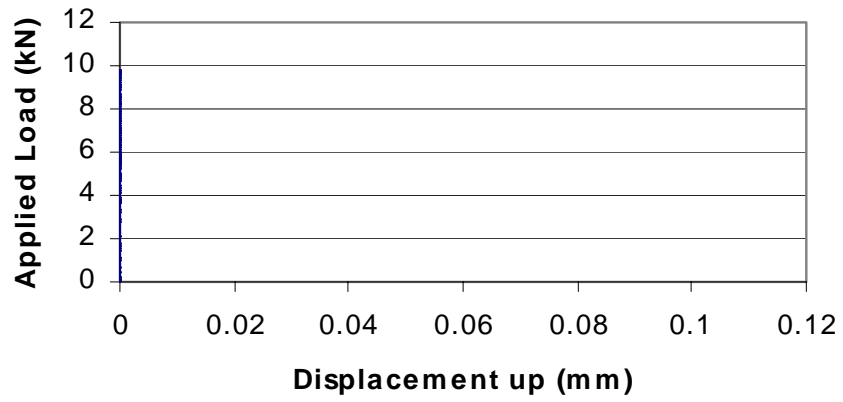


Figure B1.7 Applied Load vs. LVDT 7 (Test 8-3/4-8-U)

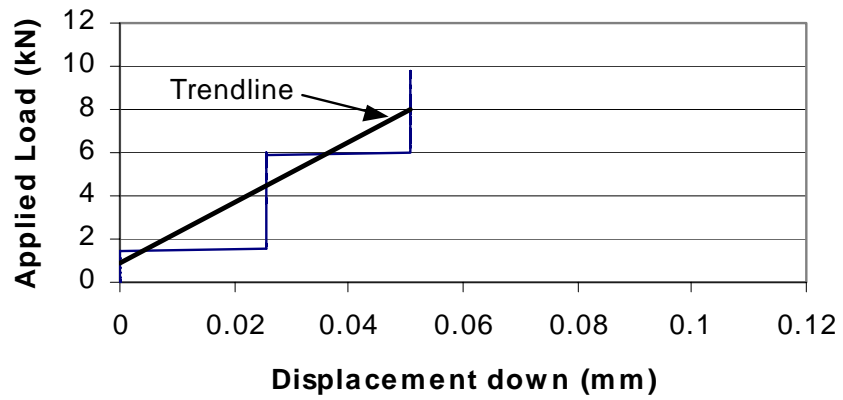


Figure B1.8 Applied Load vs. LVDT 8 (Test 8-3/4-8-U)

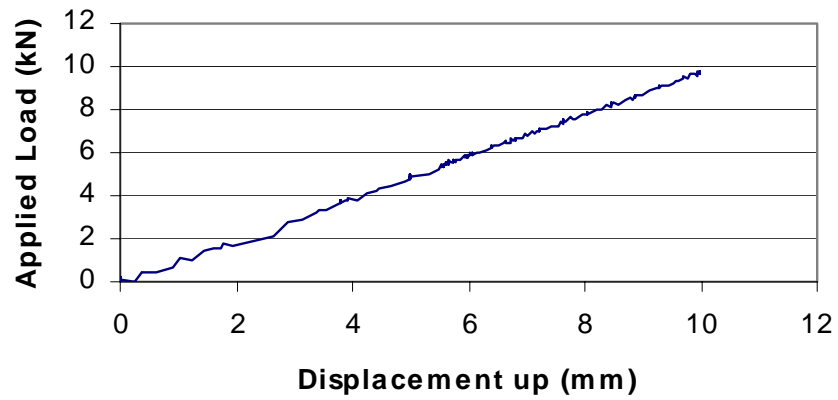


Figure B1.9 Applied Load vs. LVDT 9 (Test 8-3/4-8-U)

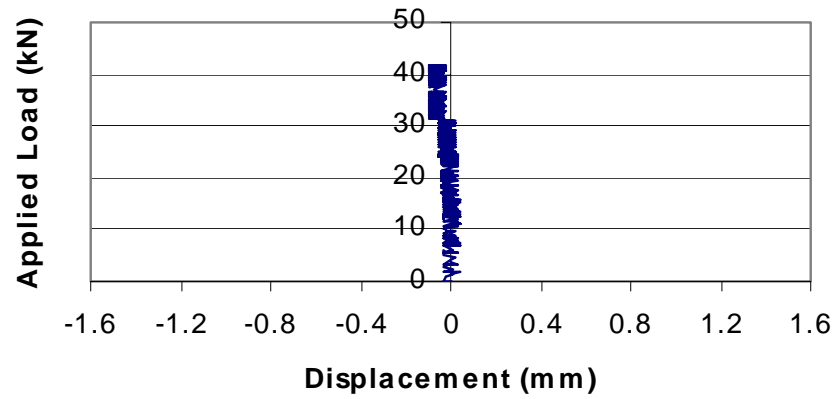


Figure B2.1 Applied Load vs. LVDT 1 (Test 8-3/4-8-G)

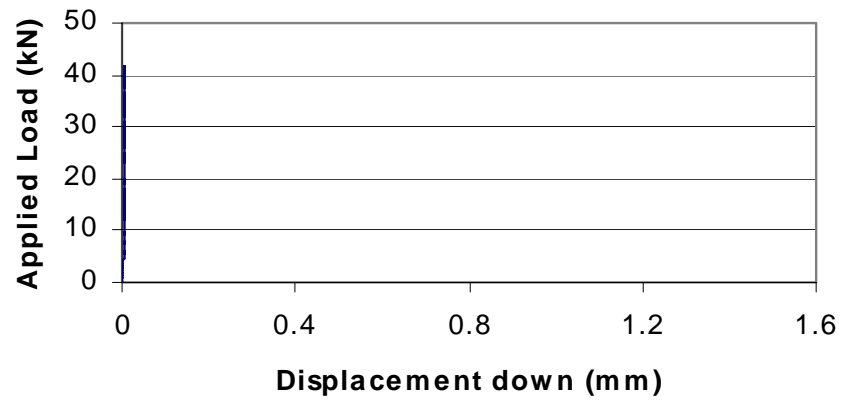


Figure B2.2 Applied Load vs. LVDT 2 (Test 8-3/4-8-G)

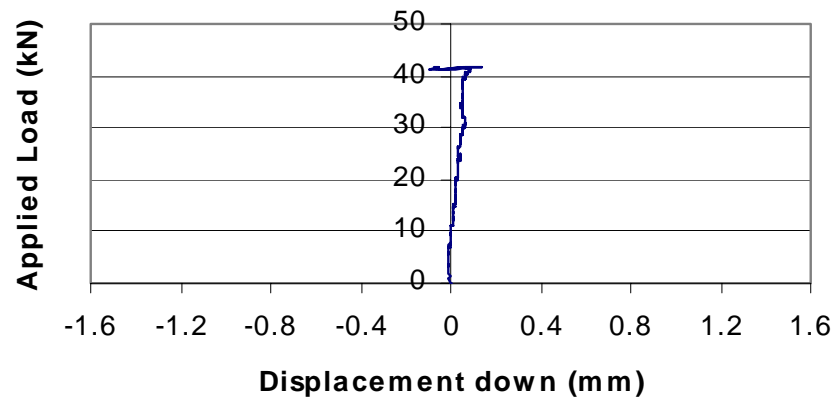


Figure B2.3 Applied Load vs. LVDT 3 (Test 8-3/4-8-G)

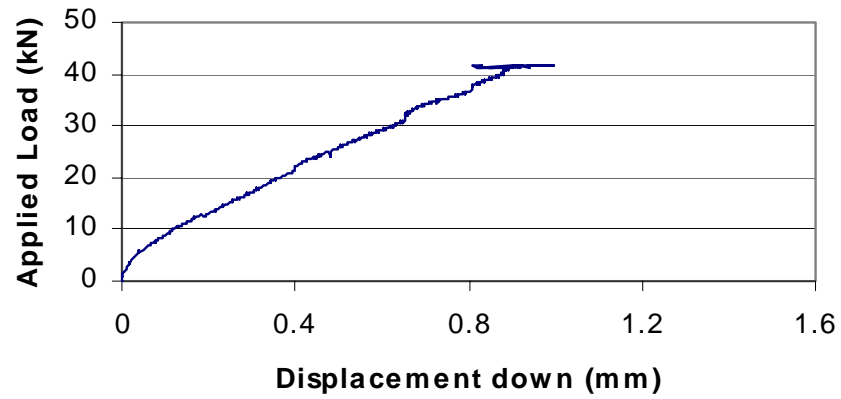


Figure B2.4 Applied Load vs. LVDT 4 (Test 8-3/4-8-G)

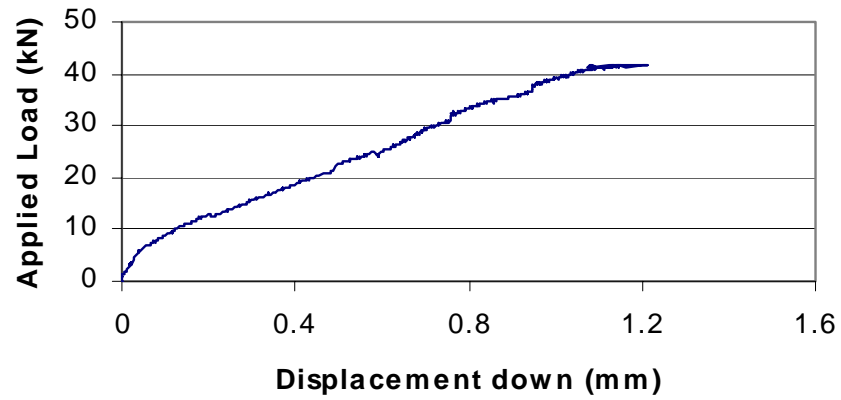


Figure B2.5 Applied Load vs. LVDT 5 (Test 8-3/4-8-G)

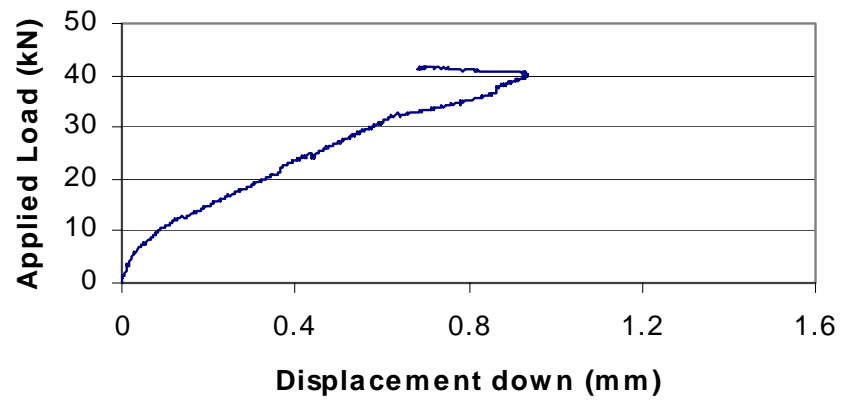


Figure B2.6 Applied Load vs. LVDT 6 (Test 8-3/4-8-G)

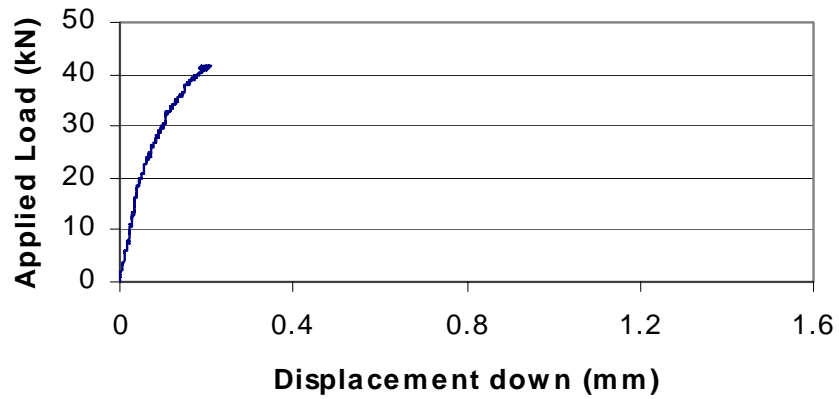


Figure B2.7 Applied Load vs. LVDT 7 (Test 8-3/4-8-G)

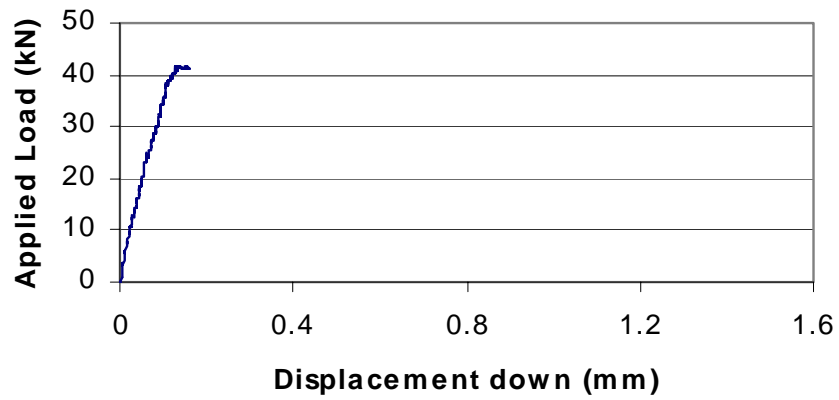


Figure B2.8 Applied Load vs. LVDT 8 (Test 8-3/4-8-G)

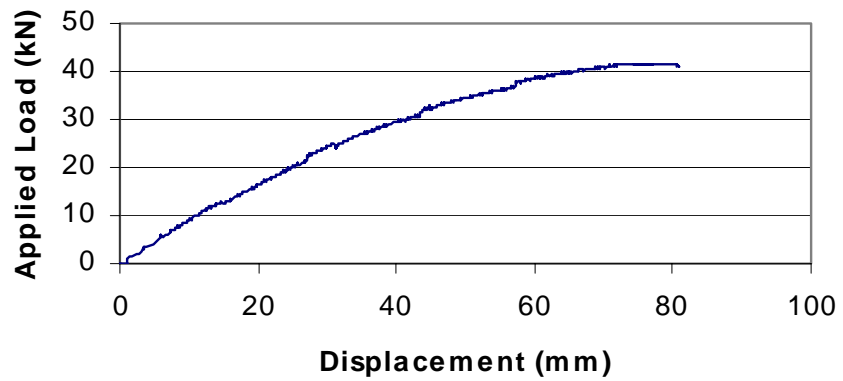


Figure B2.9 Applied Load vs. LVDT 9 (Test 8-3/4-8-G)

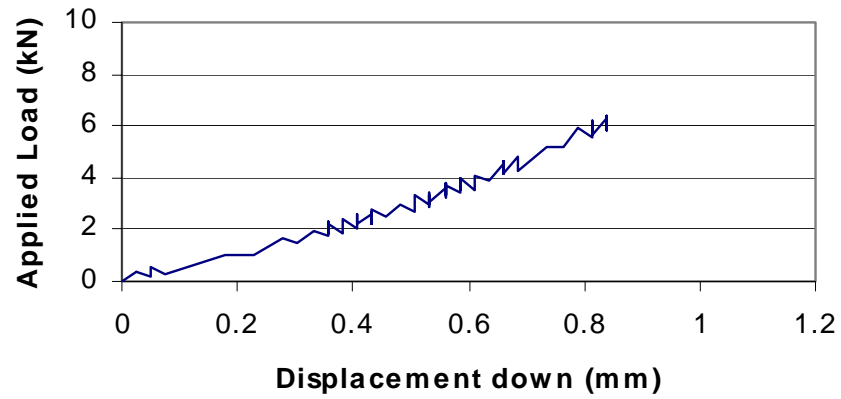


Figure B3.1 Applied Load vs. LVDT 1 (Test 8-3/4-4s-U)

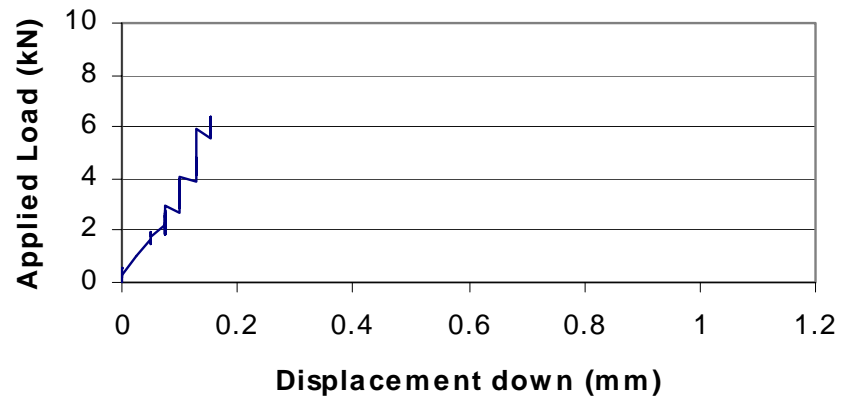


Figure B3.2 Applied Load vs. LVDT 2 (Test 8-3/4-4s-U)

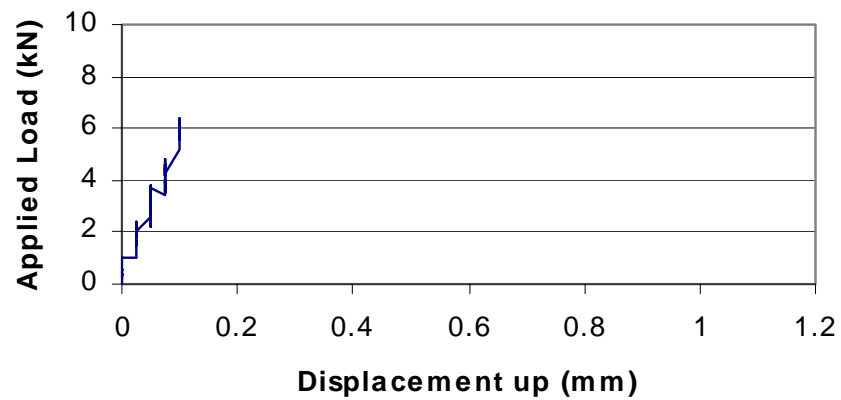


Figure B3.3 Applied Load vs. LVDT 4 (Test 8-3/4-4s-U)

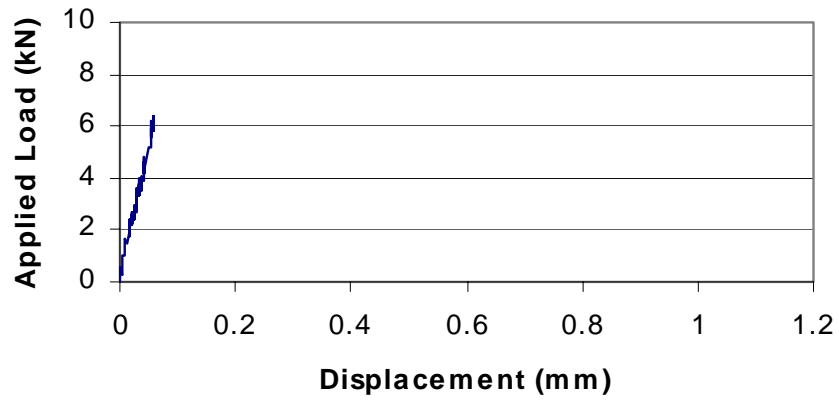


Figure B3.4 Applied Load vs. LVDT 5 (Test 8-3/4-4s-U)

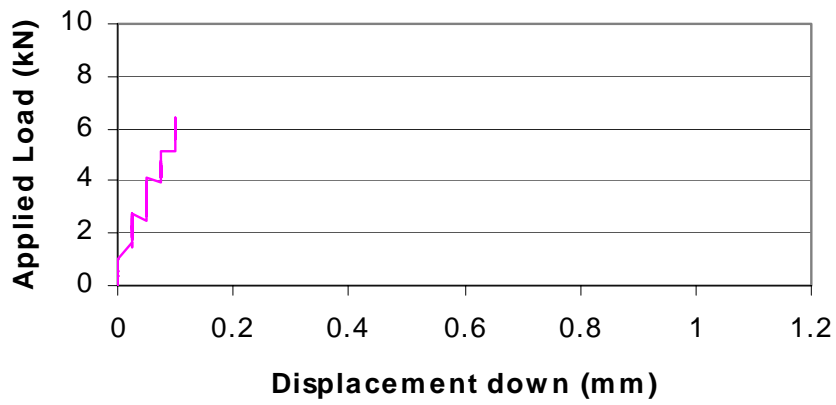


Figure B3.5 Applied Load vs. LVDT 6 (Test 8-3/4-4s-U)

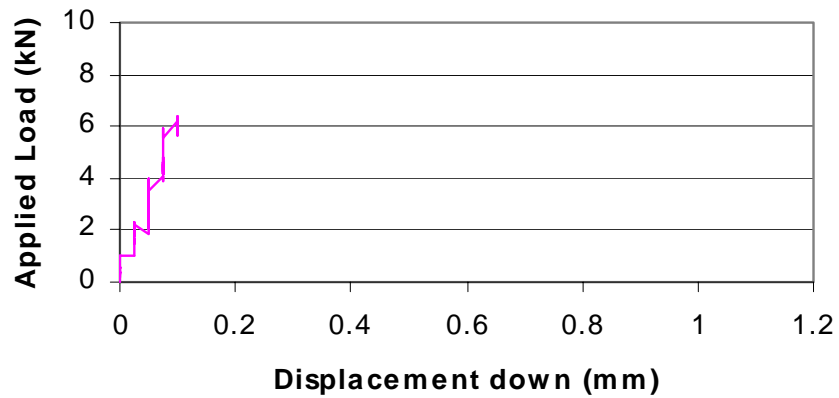


Figure B3.6 Applied Load vs. LVDT 8 (Test 8-3/4-4s-U)

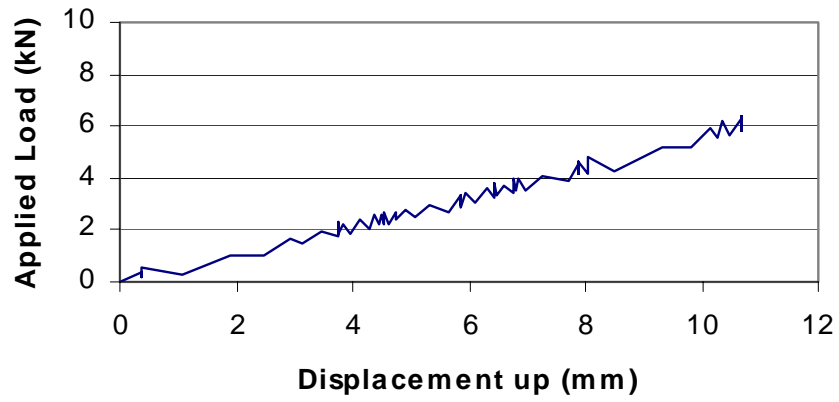


Figure B3.7 Applied Load vs. LVDT 9 (Test 8-3/4-4s-U)

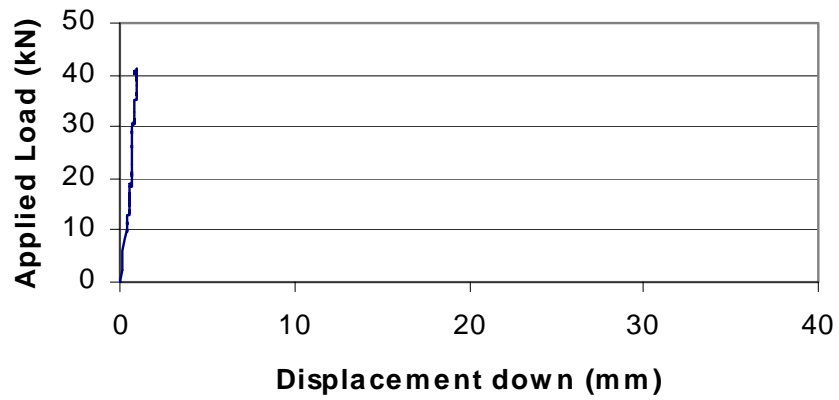


Figure B4.1 Applied Load vs. LVDT 1 (Test 8-3/4-4s-G)

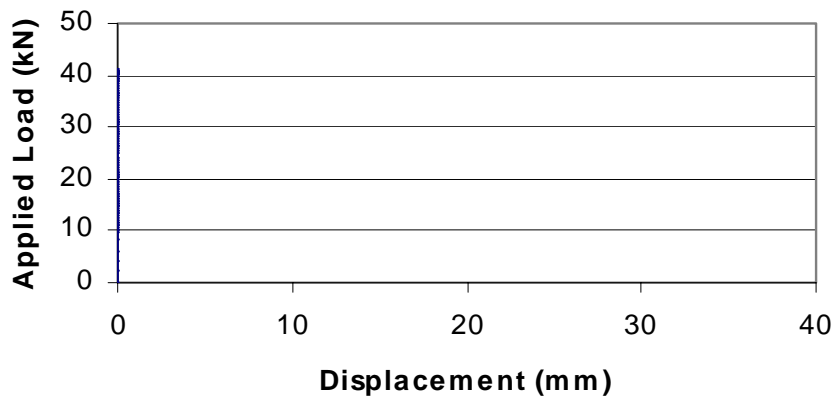


Figure B4.2 Applied Load vs. LVDT 2 (Test 8-3/4-4s-G)

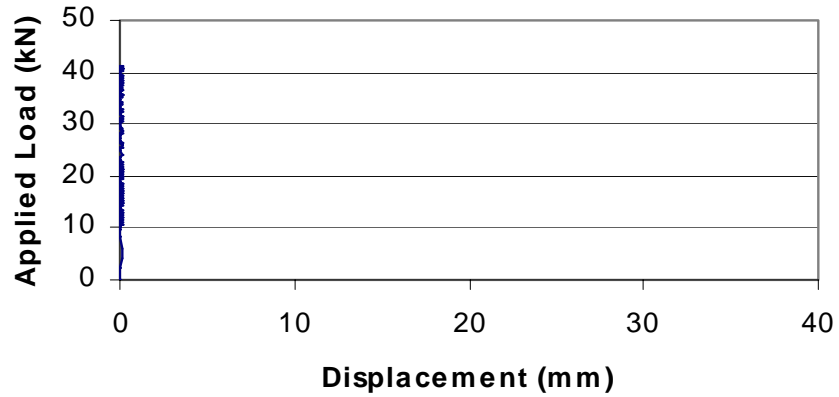


Figure B4.3 Applied Load vs. LVDT 4 (Test 8-3/4-4s-G)

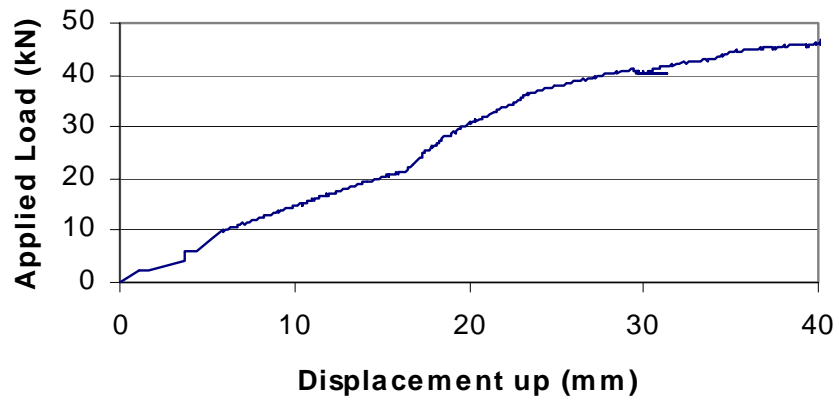


Figure B4.4 Applied Load vs. LVDT 5 (Test 8-3/4-4s-G)

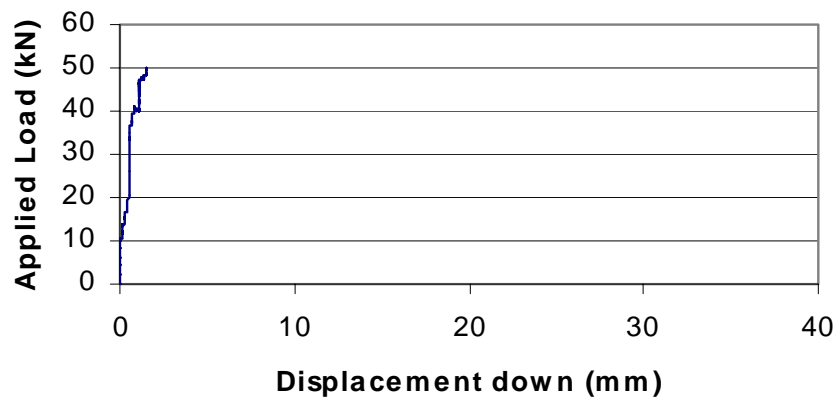


Figure B4.5 Applied Load vs. LVDT 6 (Test 8-3/4-4s-G)



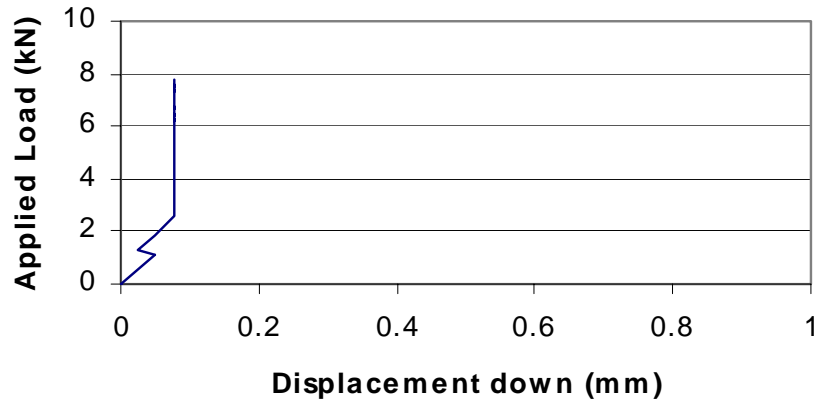


Figure B5.2 Applied Load vs. LVDT 2 (Test 6-3/4-4sW-U)

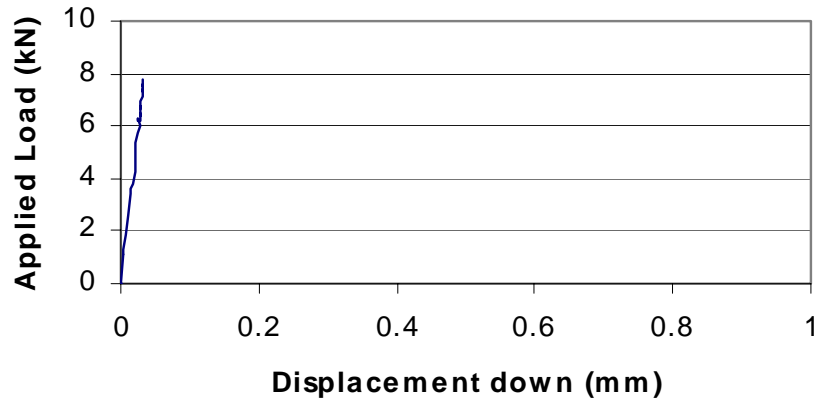


Figure B5.3 Applied Load vs. LVDT 4 (Test 6-3/4-4sW-U)

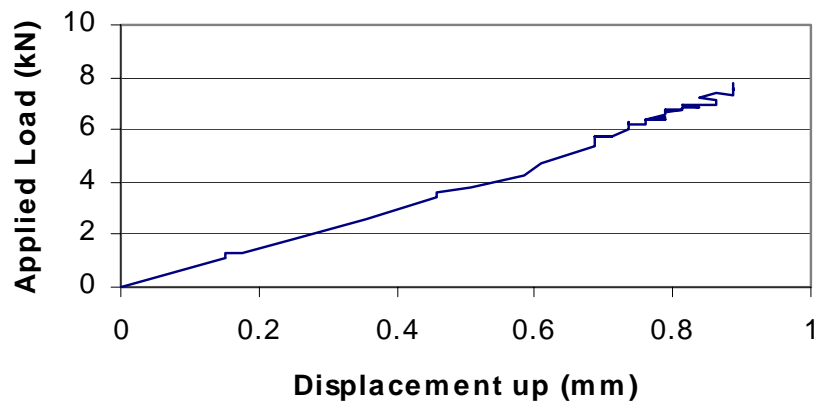


Figure B5.4 Applied Load vs. LVDT 5 (Test 6-3/4-4sW-U)

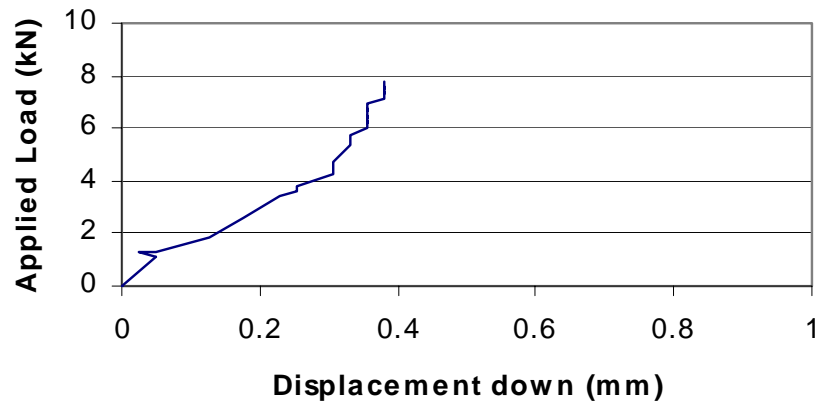


Figure B5.5 Applied Load vs. LVDT 6 (Test 6-3/4-4sW-U)

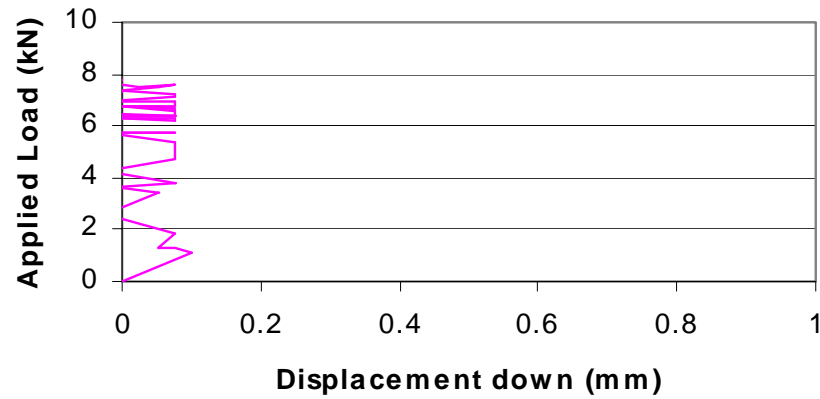


Figure B5.6 Applied Load vs. LVDT 8 (Test 6-3/4-4sW-U)

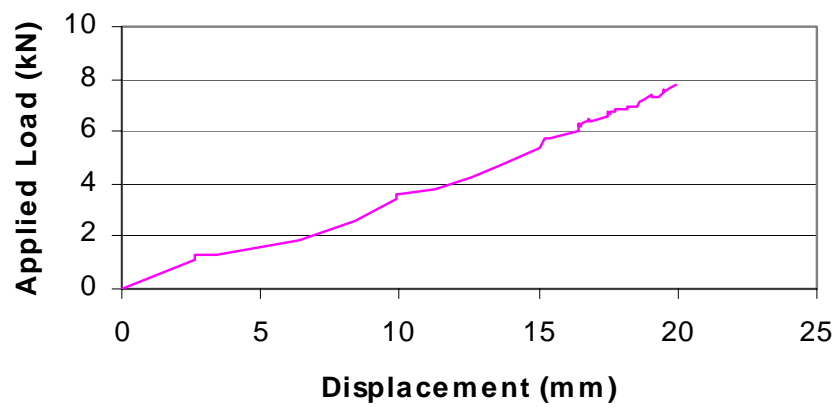


Figure B5.7 Applied Load vs. LVDT 9 (Test 6-3/4-4sW-U)

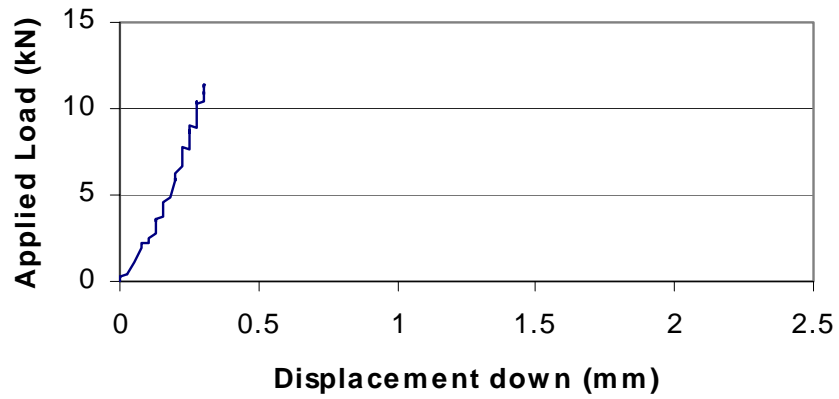


Figure B6.1 Applied Load vs. LVDT 1 (Test 6-3/4-4sW-G)

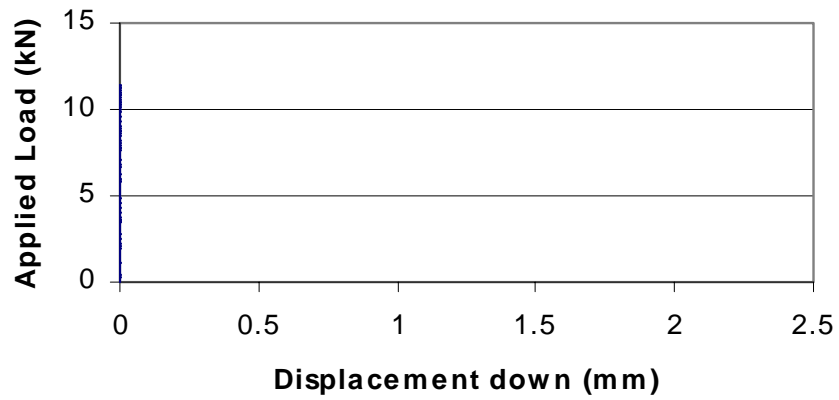


Figure B6.2 Applied Load vs. LVDT 2 (Test 6-3/4-4sW-G)

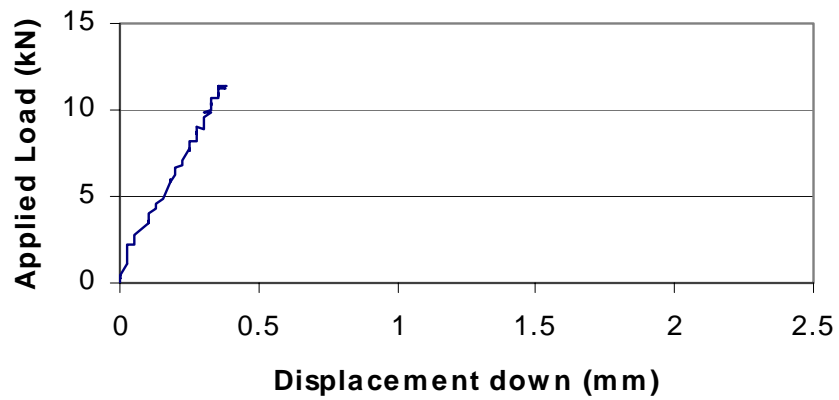


Figure B6.3 Applied Load vs. LVDT 4 (Test 6-3/4-4sW-G)

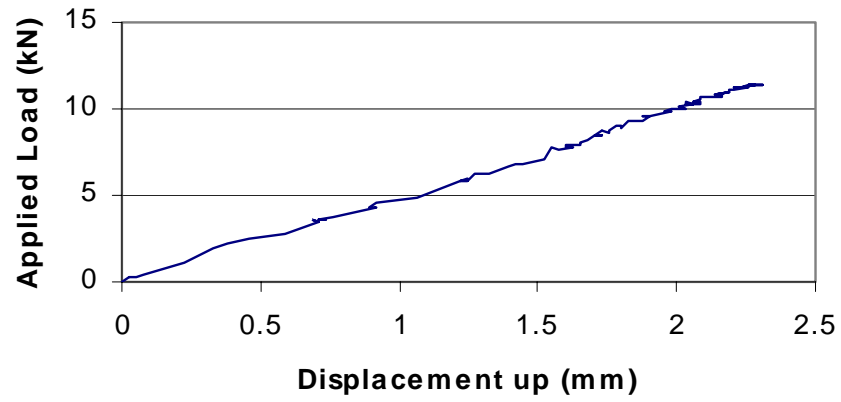


Figure B6.4 Applied Load vs. LVDT 5 (Test 6-3/4-4sW-G)

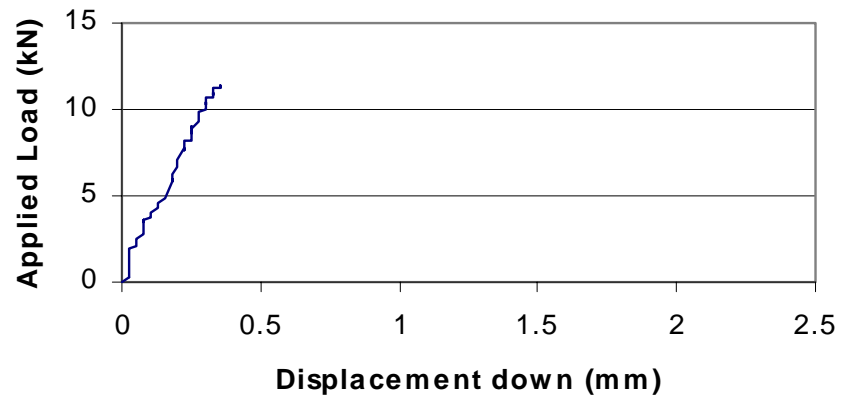


Figure B6.5 Applied Load vs. LVDT 6 (Test 6-3/4-4sW-G)

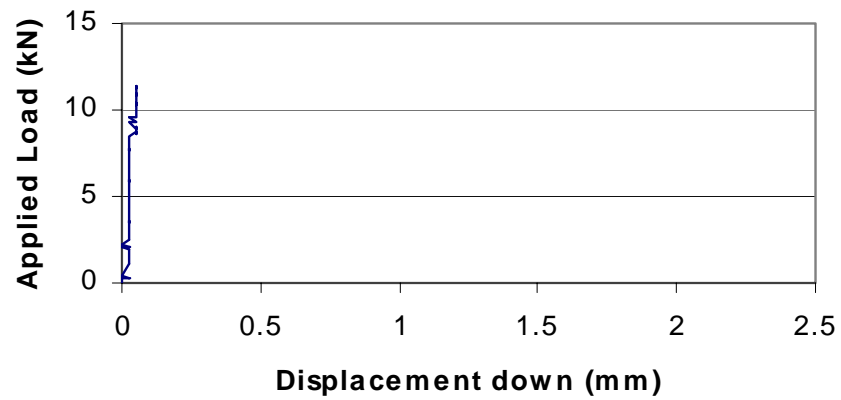


Figure B6.6 Applied Load vs. LVDT 8 (Test 6-3/4-4sW-G)

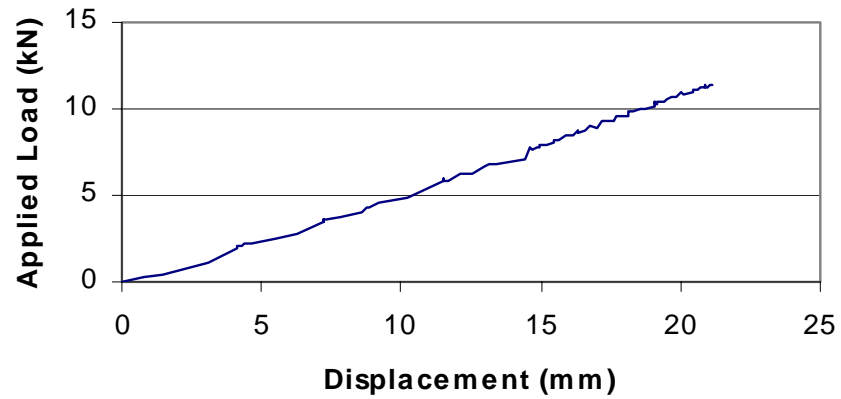


Figure B6.7 Applied Load vs. LVDT 9 (Test 6-3/4-4sW-G)

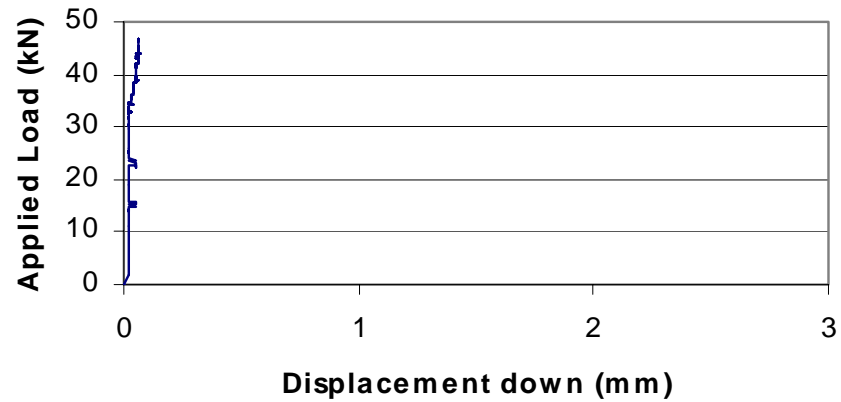


Figure B7.1 Applied Load vs. LVDT 2 (Test 6-3/4-4sW-GS)

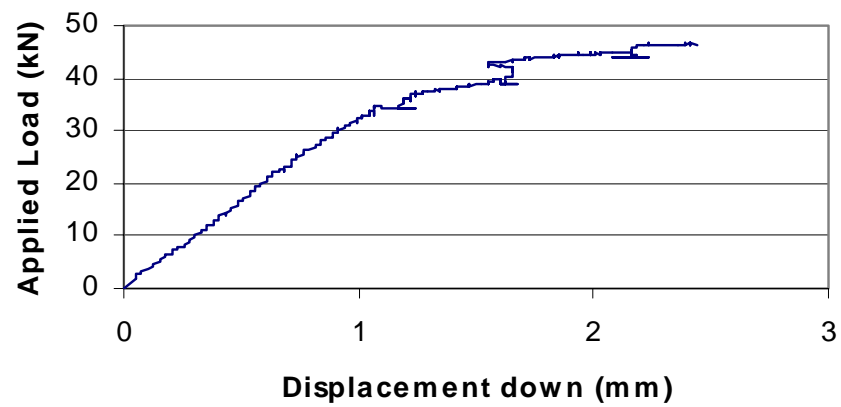


Figure B7.2 Applied Load vs. LVDT 4 (Test 6-3/4-4sW-GS)

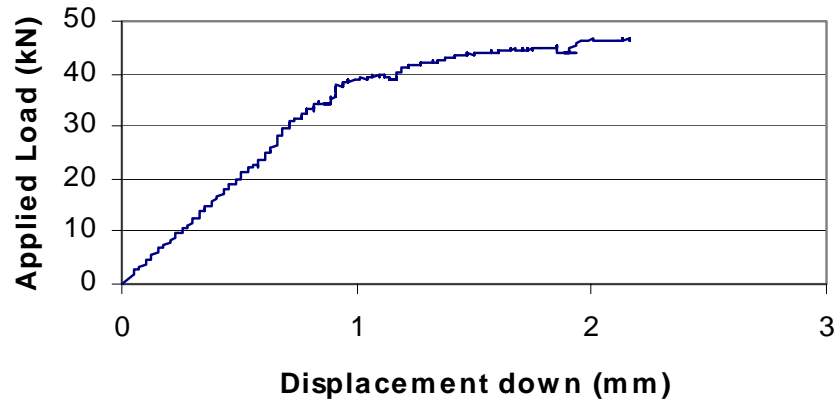


Figure B7.3 Applied Load vs. LVDT 6 (Test 6-3/4-4sW-GS)

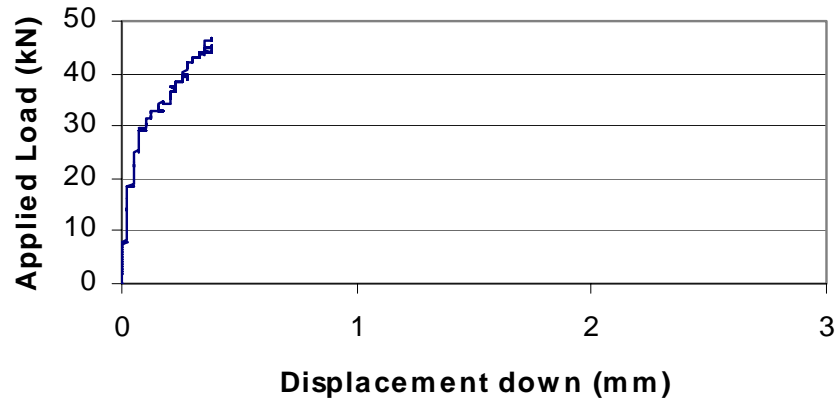


Figure B7.4 Applied Load vs. LVDT 8 (Test 6-3/4-4sW-GS)

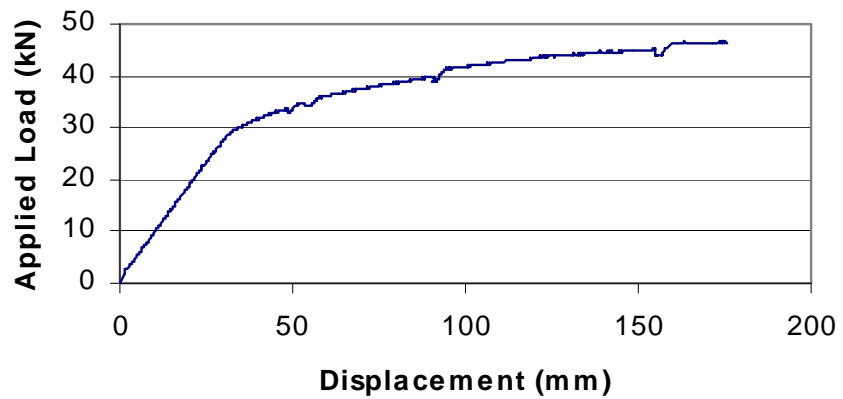


Figure B7.5 Applied Load vs. LVDT 9 (Test 6-3/4-4sW-GS)

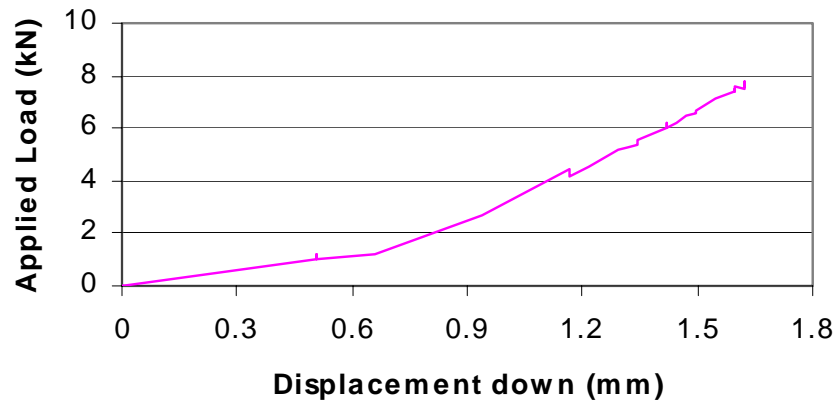


Figure B8.1 Applied Load vs. LVDT 1 (Test 6-3/4-4s-U)

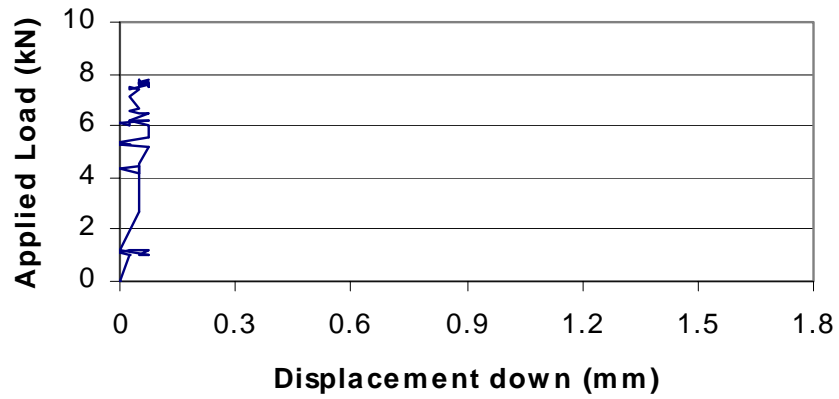


Figure B8.2 Applied Load vs. LVDT 2 (Test 6-3/4-4s-U)

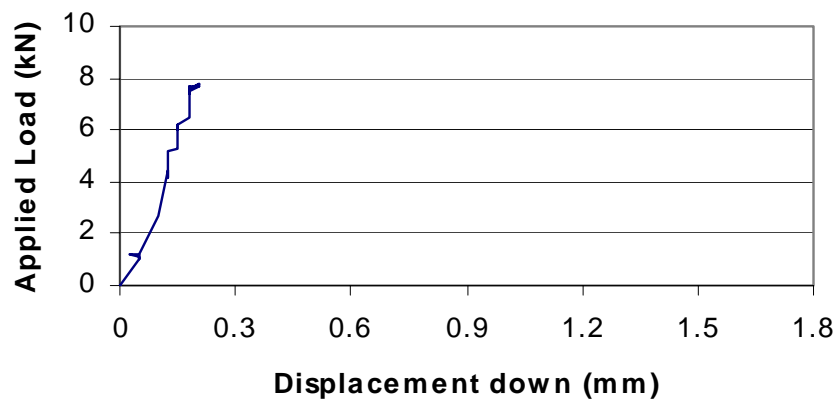


Figure B8.3 Applied Load vs. LVDT 4 (Test 6-3/4-4s-U)

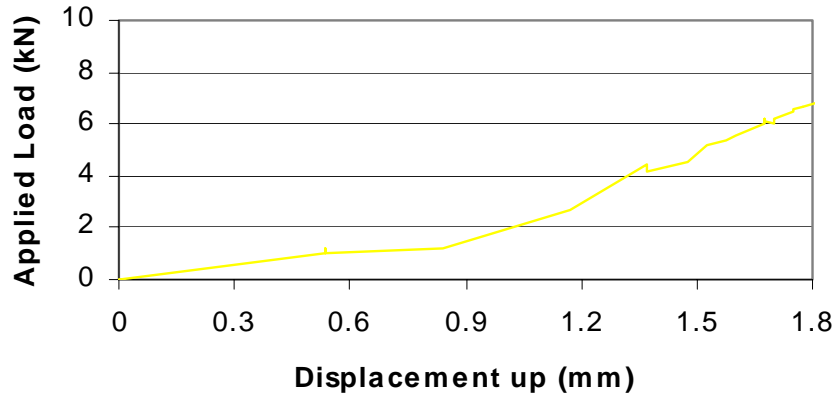


Figure B8.4 Applied Load vs. LVDT 5 (Test 6-3/4-4s-U)

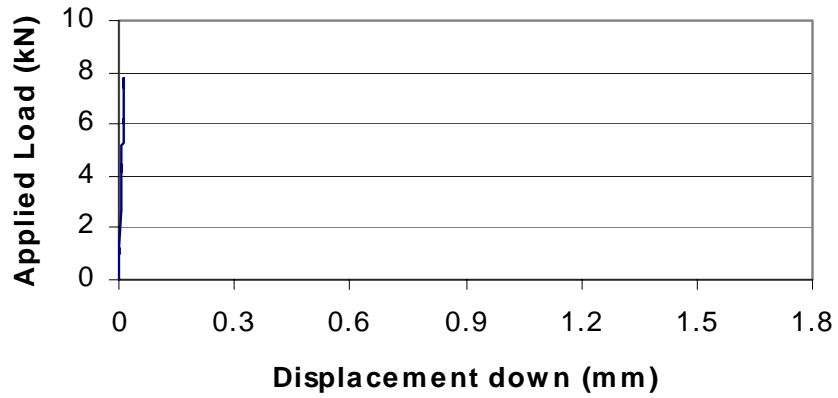


Figure B8.5 Applied Load vs. LVDT 6 (Test 6-3/4-4s-U)

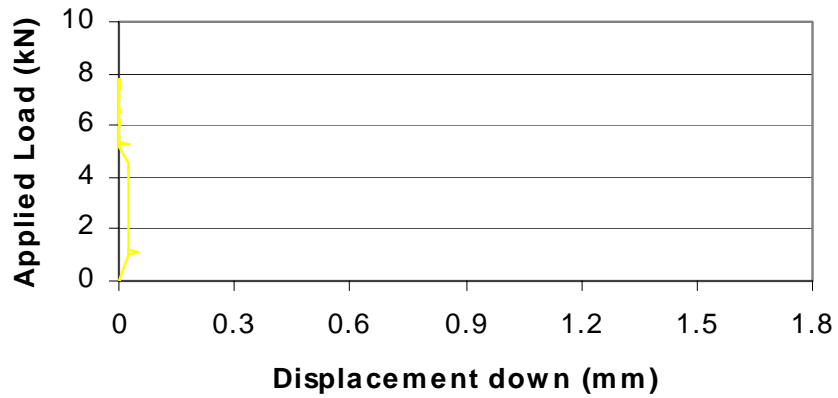


Figure B8.6 Applied Load vs. LVDT 8 (Test 6-3/4-4s-U)

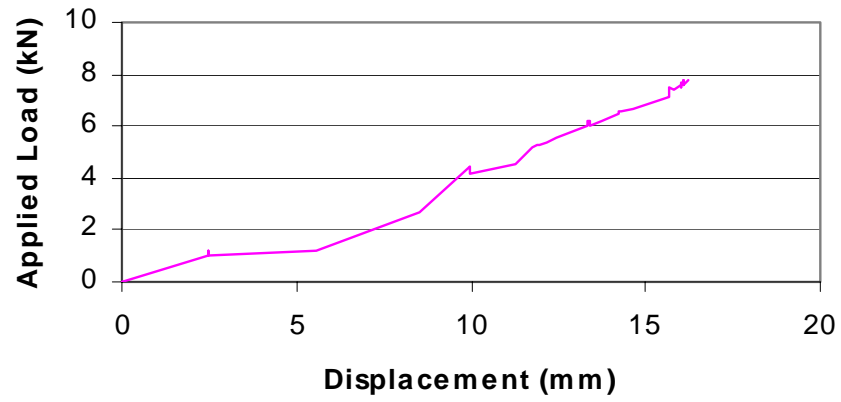


Figure B8.7 Applied Load vs. LVDT 9 (Test 6-3/4-4s-U)

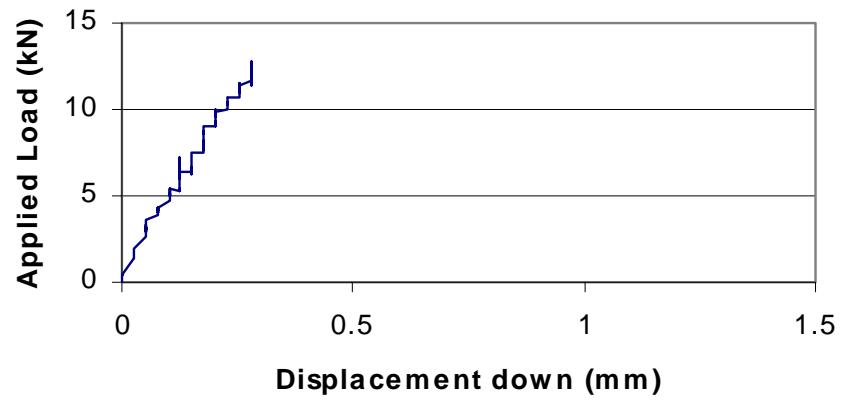


Figure B9.1 Applied Load vs. LVDT 1 (Test 6-3/4-4s-G)

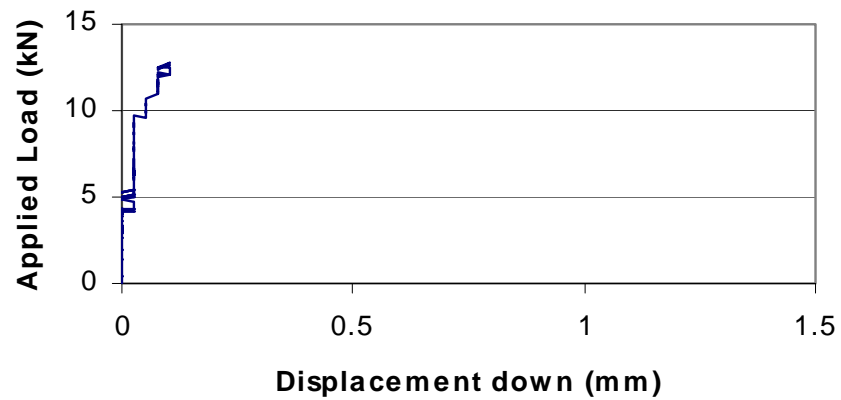


Figure B9.2 Applied Load vs. LVDT 2 (Test 6-3/4-4s-G)

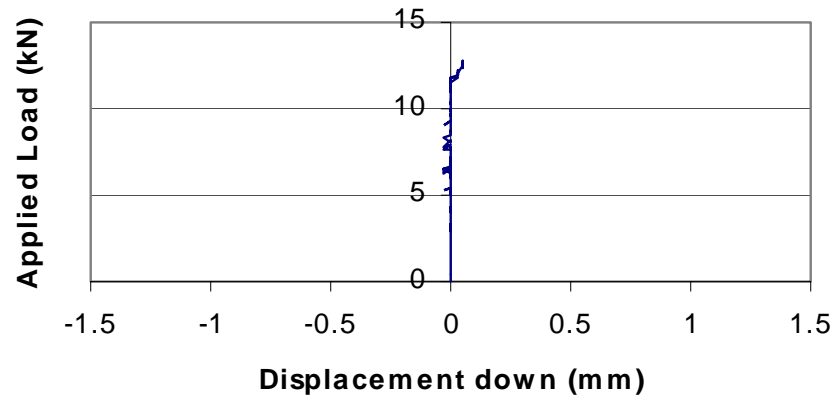


Figure B9.3 Applied Load vs. LVDT 4 (Test 6-3/4-4s-G)

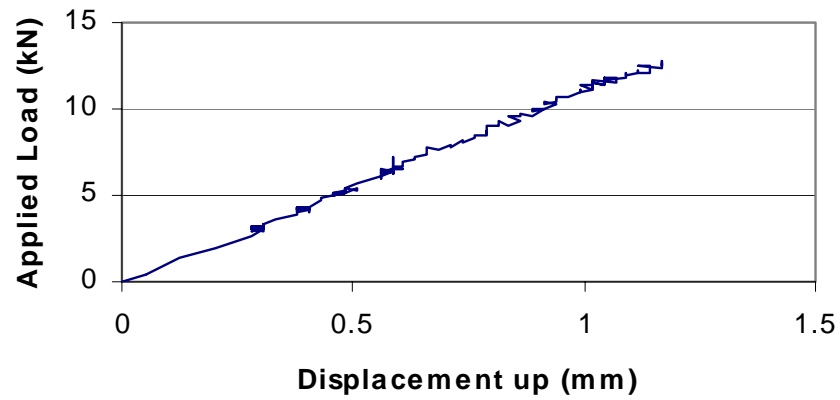


Figure B9.4 Applied Load vs. LVDT 5 (Test 6-3/4-4s-G)

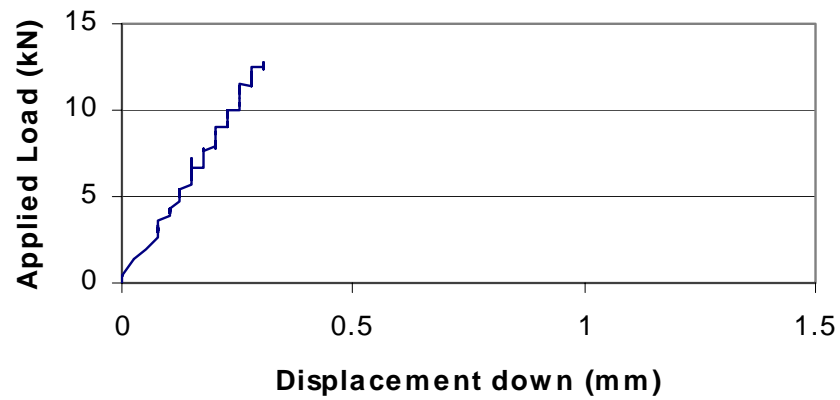


Figure B9.5 Applied Load vs. LVDT 6 (Test 6-3/4-4s-G)

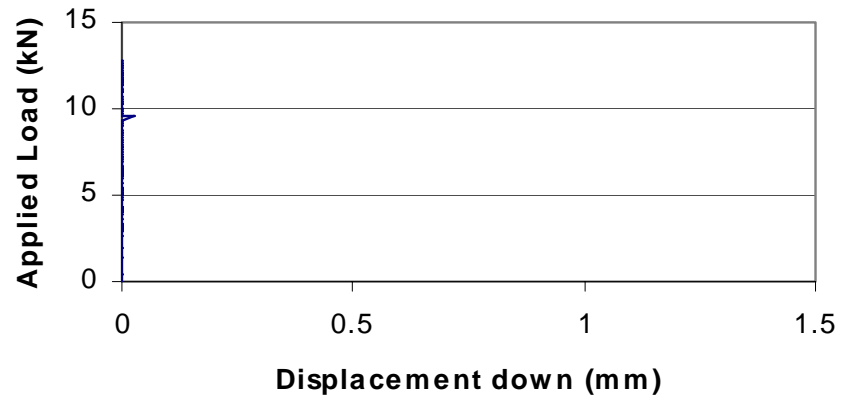


Figure B9.6 Applied Load vs. LVDT 8 (Test 6-3/4-4s-G)

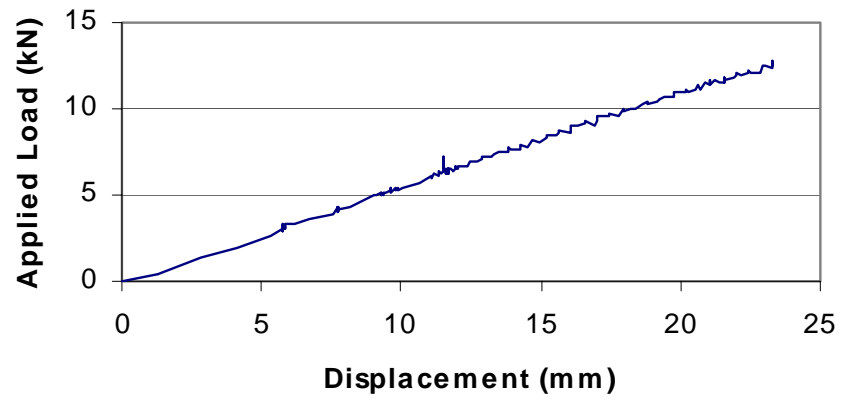


Figure B9.7 Applied Load vs. LVDT 9 (Test 6-3/4-4s-G)

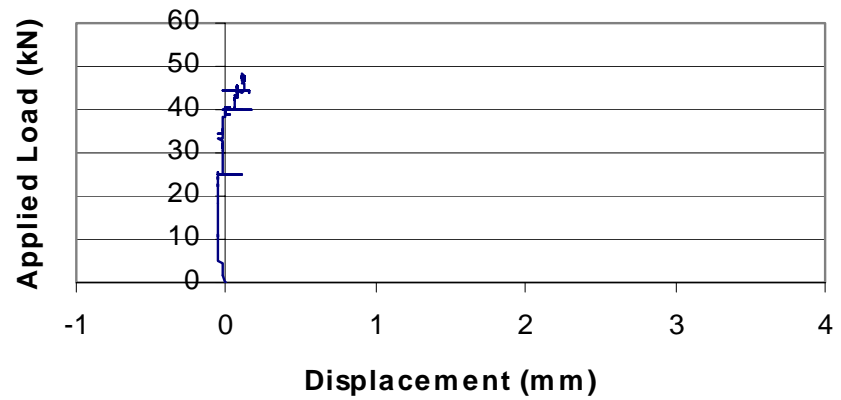


Figure B10.1 Applied Load vs. LVDT 2 (Test 6-3/4-4s-GS)

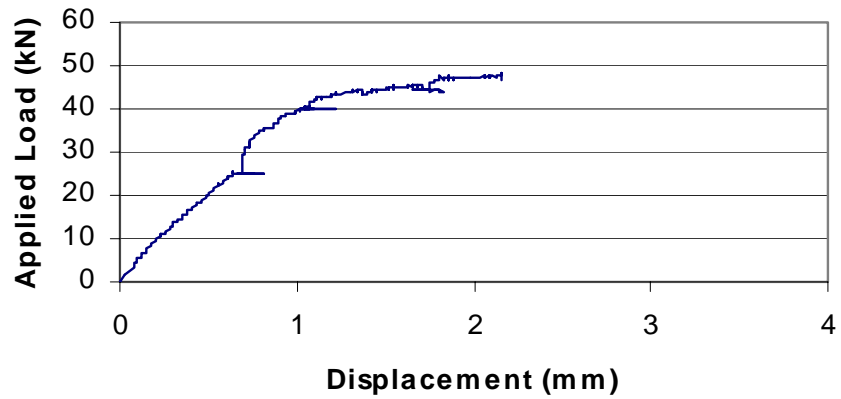


Figure B10.2 Applied Load vs. LVDT 4 (Test 6-3/4-4s-GS)

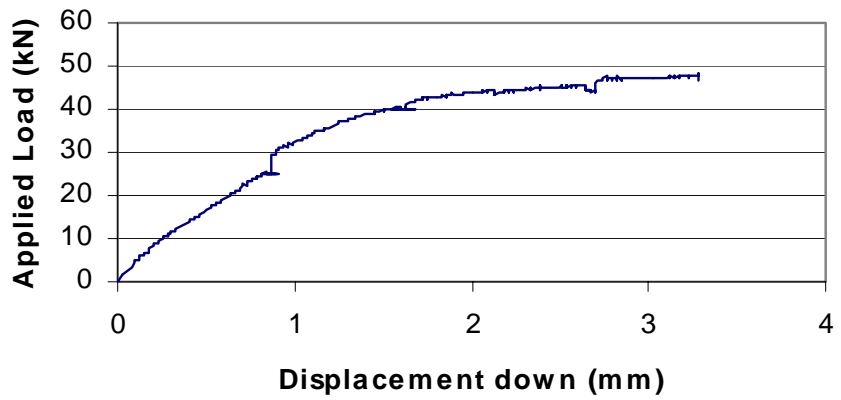


Figure B10.3 Applied Load vs. LVDT 6 (Test 6-3/4-4s-GS)

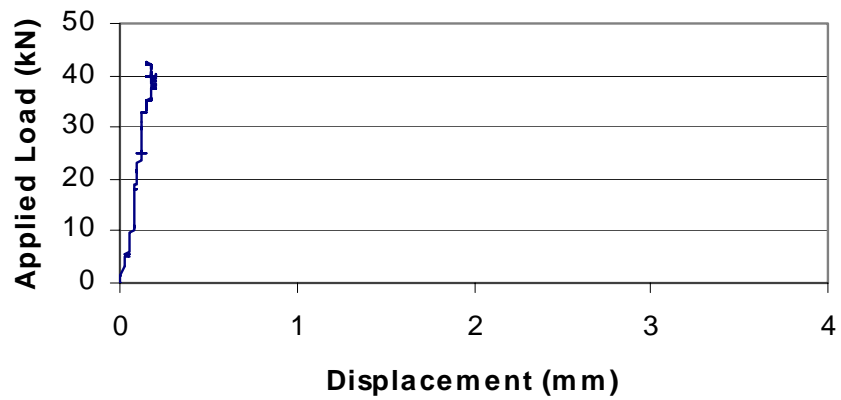


Figure B10.4 Applied Load vs. LVDT 8 (Test 6-3/4-4s-GS)

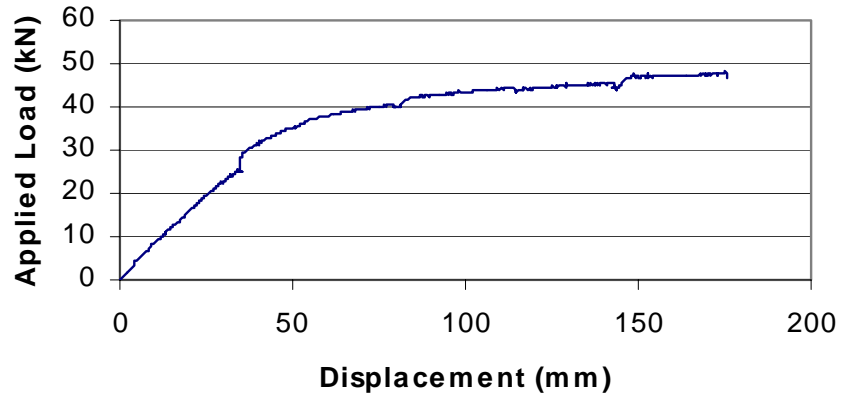


Figure B10.5 Applied Load vs. LVDT 9 (Test 6-3/4-4s-GS)

## APPENDIX C: LOAD CELL DATA

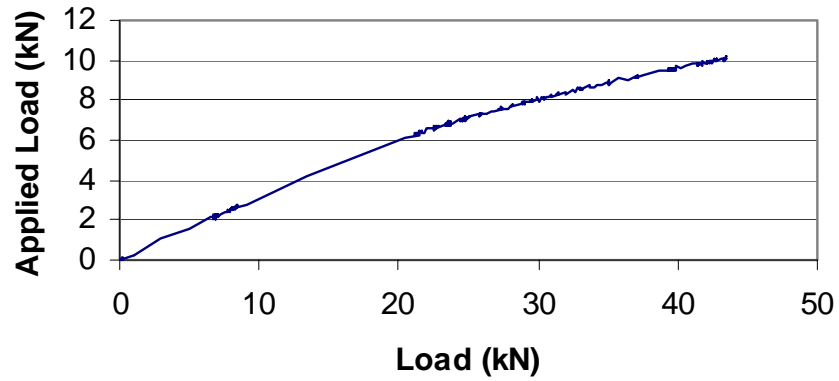


Figure C1.1 Applied Load vs. Load Cell LC4 (Test 8-3/4-8-U)

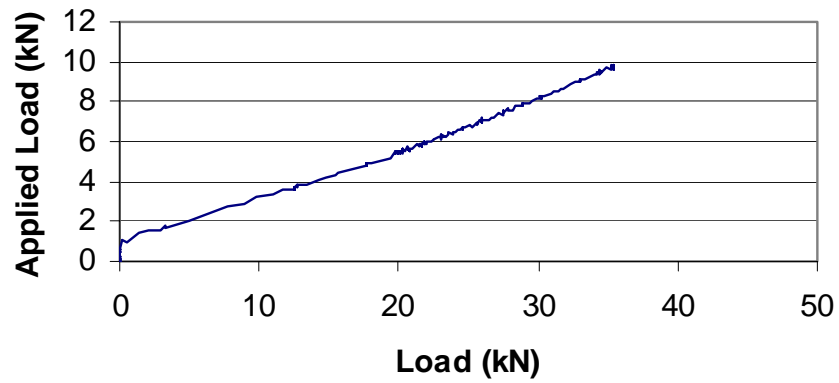


Figure C1.2 Applied Load vs. Load Cell LC5 (Test 8-3/4-8-U)

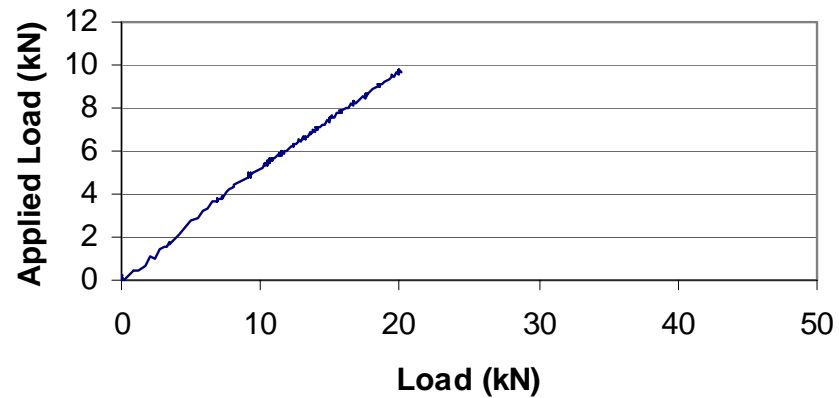


Figure C1.3 Applied Load vs. Load Cell LC6 (Test 8-3/4-8-U)

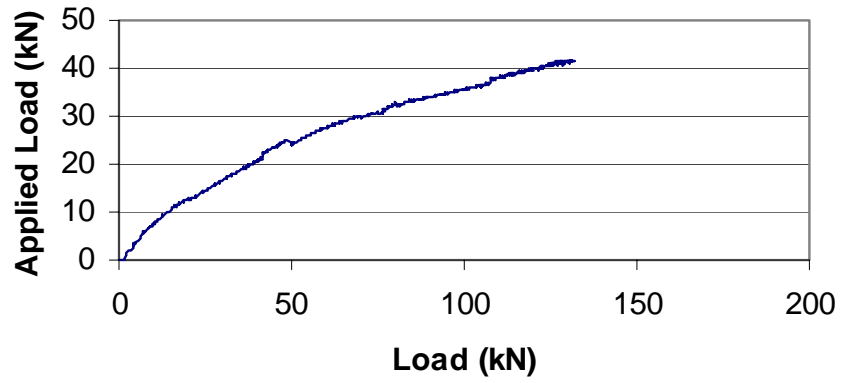


Figure C2.1 Applied Load vs. Load Cell LC4 (Test 8-3/4-8-G)

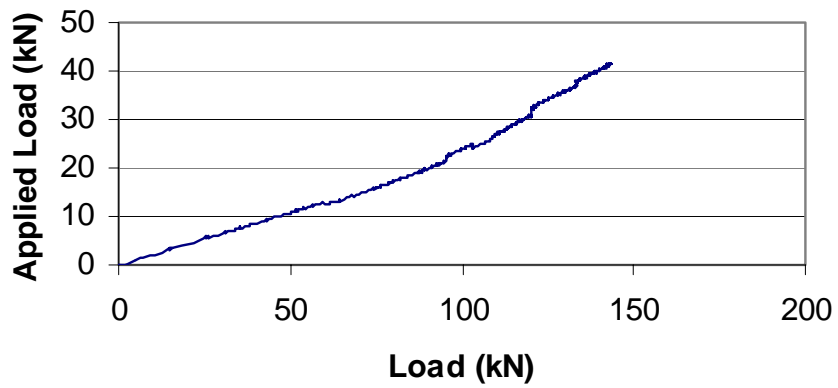


Figure C2.2 Applied Load vs. Load Cell LC5 (Test 8-3/4-8-G)

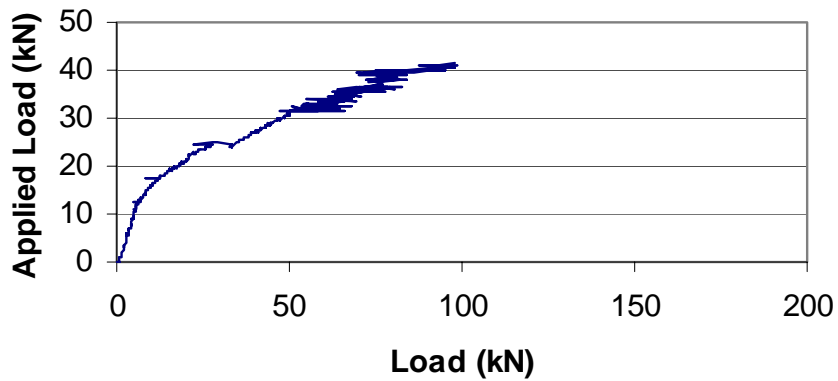


Figure C2.3 Applied Load vs. Load Cell LC6 (Test 8-3/4-8-G)

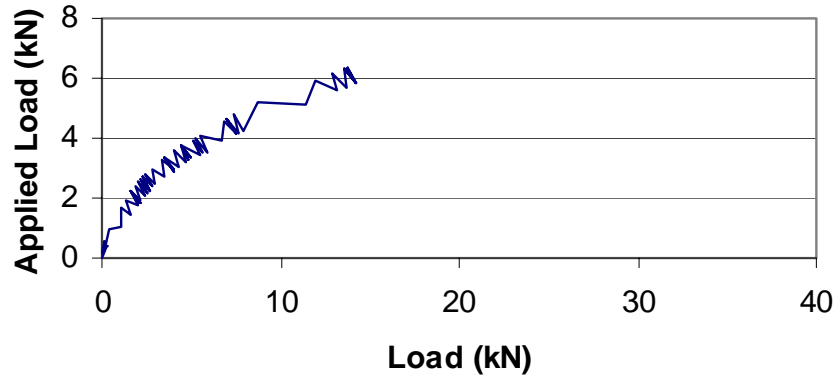


Figure C3.1 Applied Load vs. Load Cell LC2 (Test 8-3/4-4s-U)

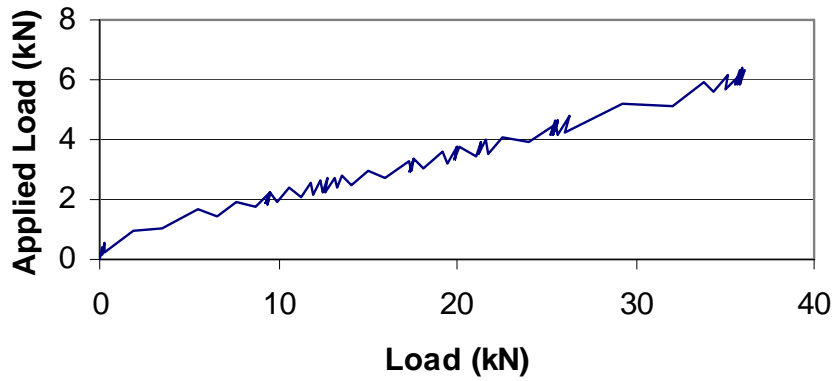


Figure C3.2 Applied Load vs. Load Cell LC3 (Test 8-3/4-4s-U)

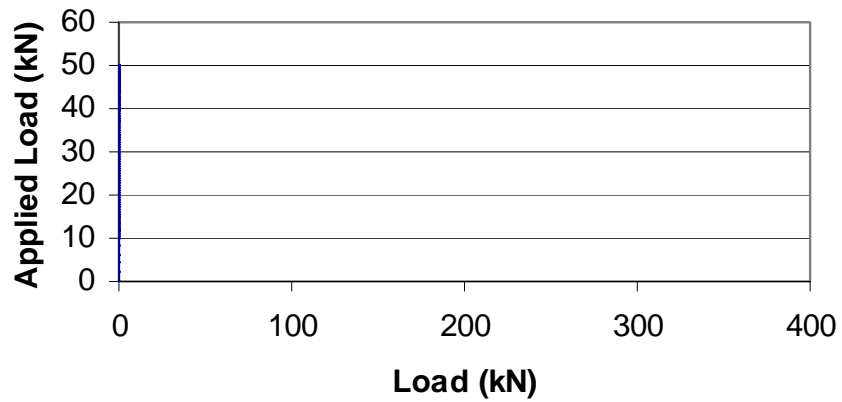


Figure C4.1 Applied Load vs. Load Cell LC2 (Test 8-3/4-4s-G)

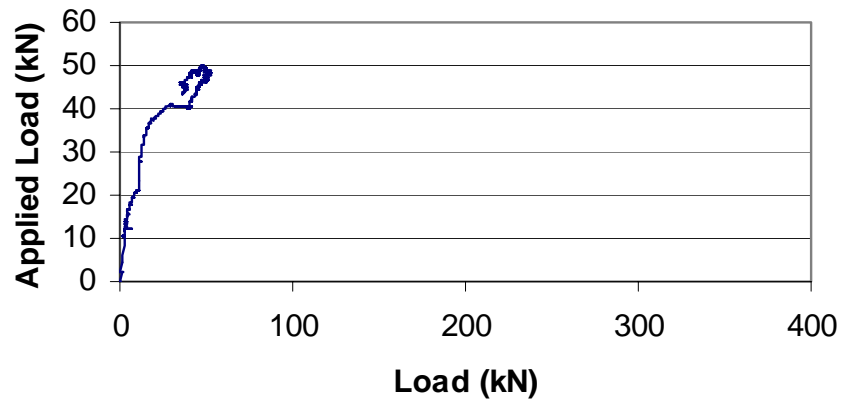


Figure C4.2 Applied Load vs. Load Cell LC3 (Test 8-3/4-4s-G)

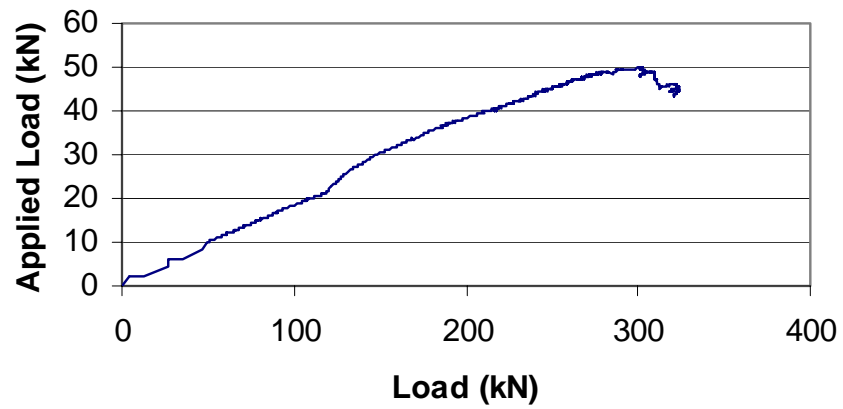


Figure C4.3 Applied Load vs. Load Cell DR21 (Test 8-3/4-4s-G)

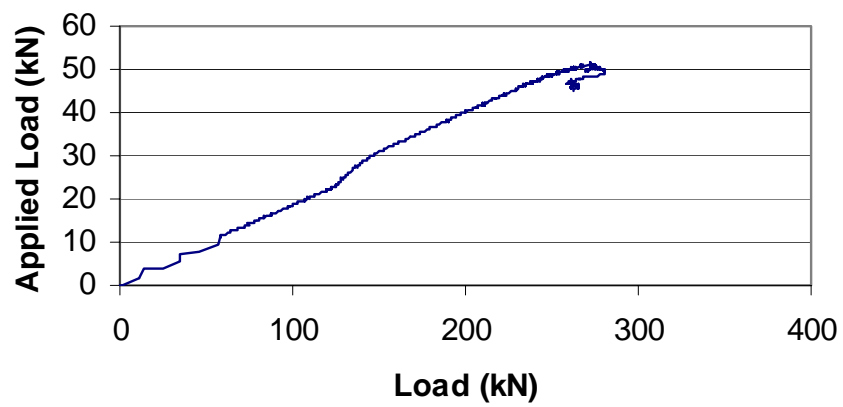


Figure C4.4 Applied Load vs. Load Cell DR17 (Test 8-3/4-4s-G)

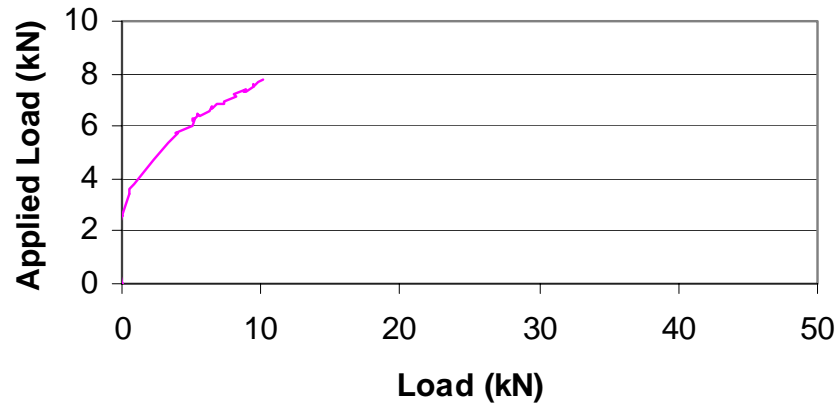


Figure C5.1 Applied Load vs. Load Cell LC5 (Test 6-3/4-4sW-U)

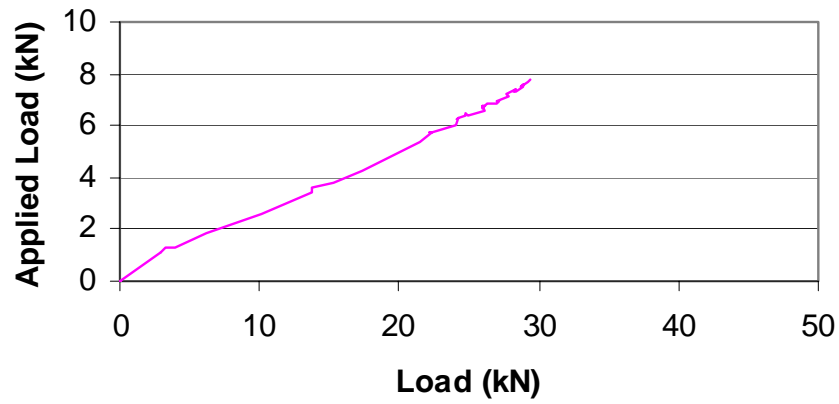


Figure C5.2 Applied Load vs. Load Cell LC4 (Test 6-3/4-4sW-U)

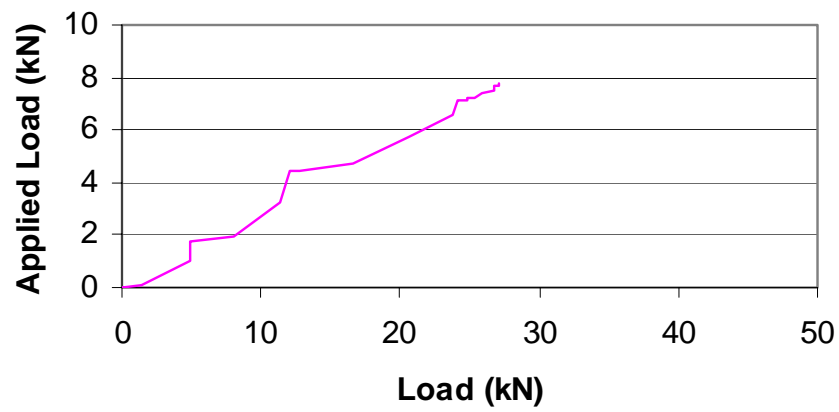


Figure C5.3 Applied Load vs. Load Cell DR04 (Test 6-3/4-4sW-U)

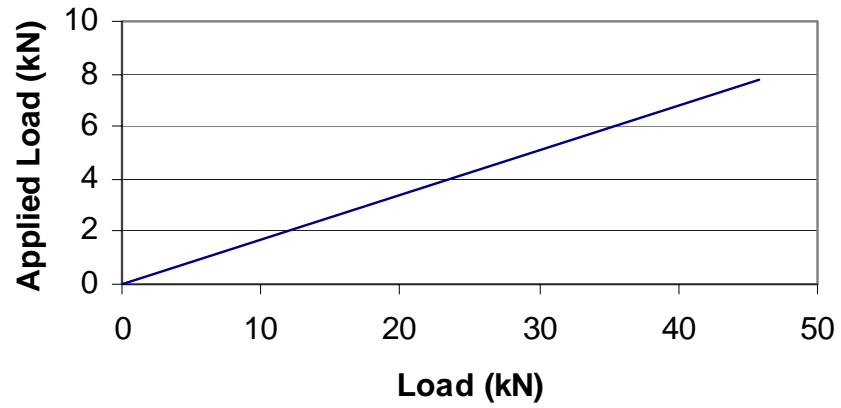


Figure C5.4 Applied Load vs. Load Cell DR15 (Test 6-3/4-4sW-U)

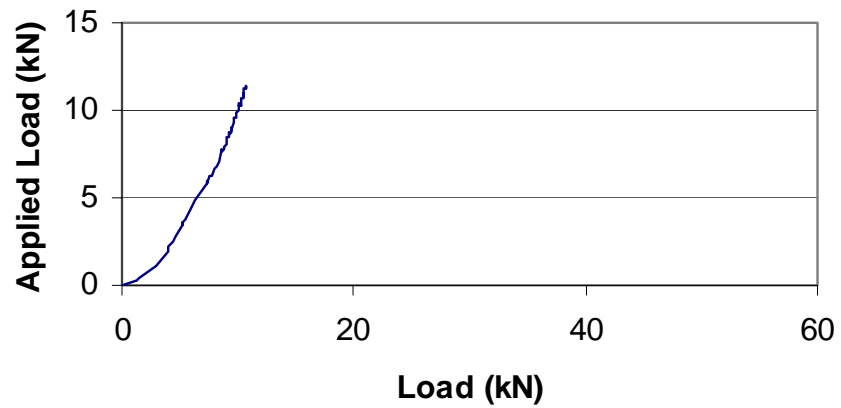


Figure C6.1 Applied Load vs. Load Cell LC5 (Test 6-3/4-4sW-G)

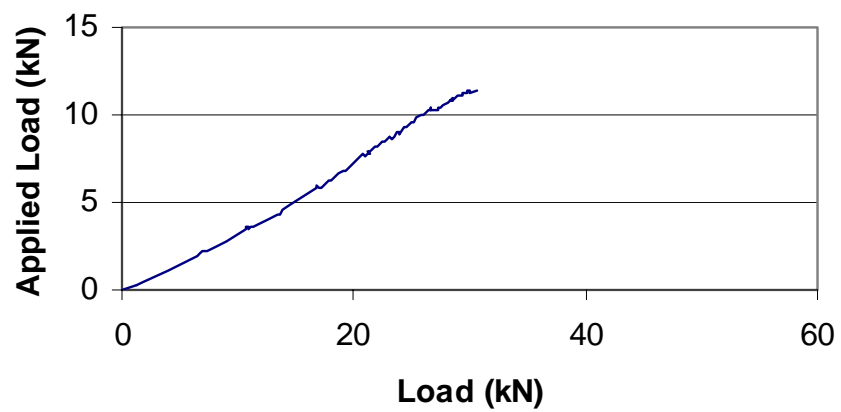


Figure C6.2 Applied Load vs. Load Cell LC4 (Test 6-3/4-4sW-G)

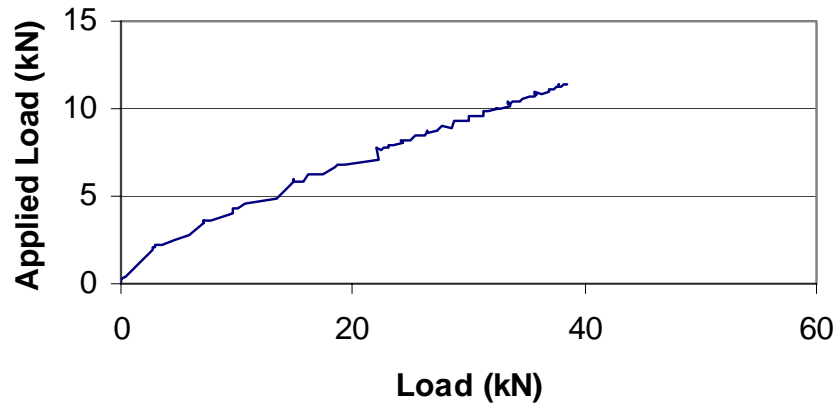


Figure C6.3 Applied Load vs. Load Cell DR04 (Test 6-3/4-4sW-G)

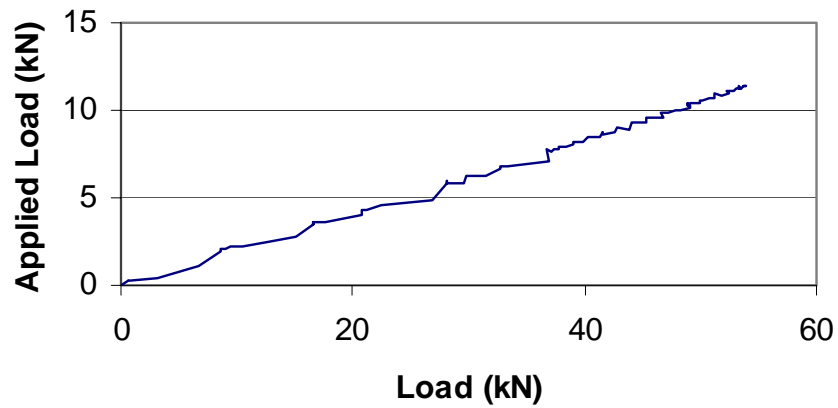


Figure C6.4 Applied Load vs. Load Cell DR15 (Test 6-3/4-4sW-G)

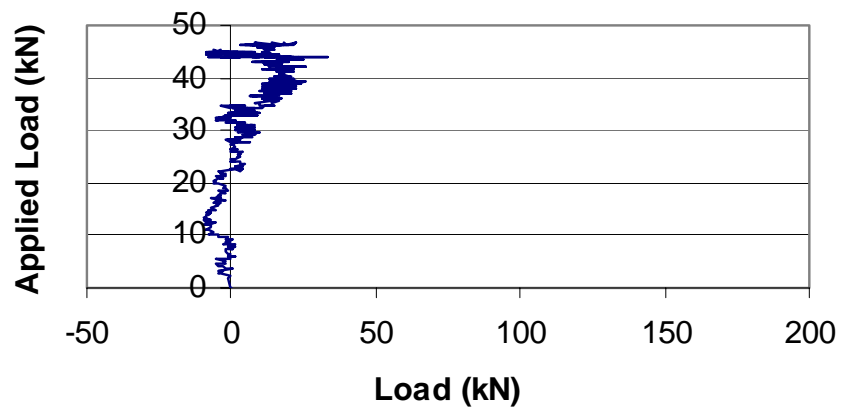


Figure C7.1 Applied Load vs. Load Cell LC5 (Test 6-3/4-4sW-GS)

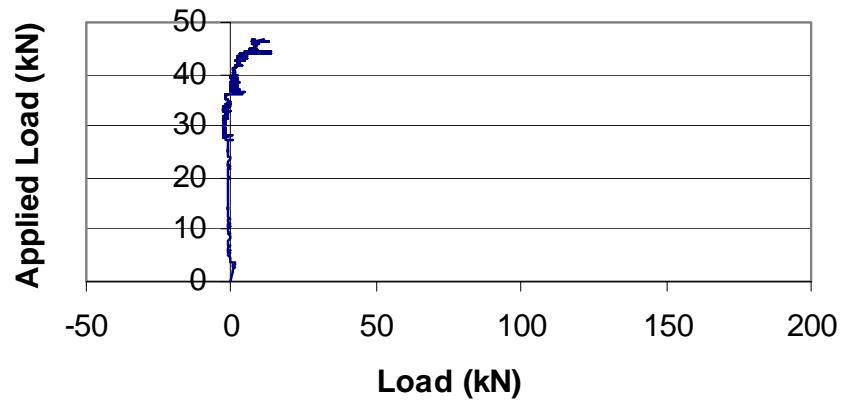


Figure C7.2 Applied Load vs. Load Cell LC4 (Test 6-3/4-4sW-GS)

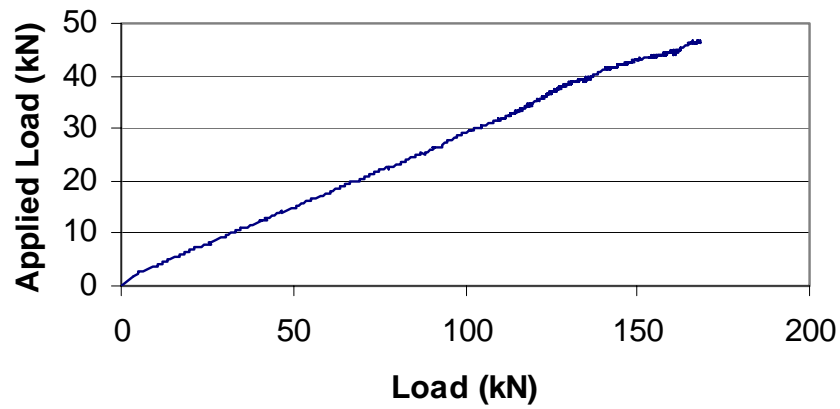


Figure C7.3 Applied Load vs. Load Cell DR04 (Test 6-3/4-4sW-GS)

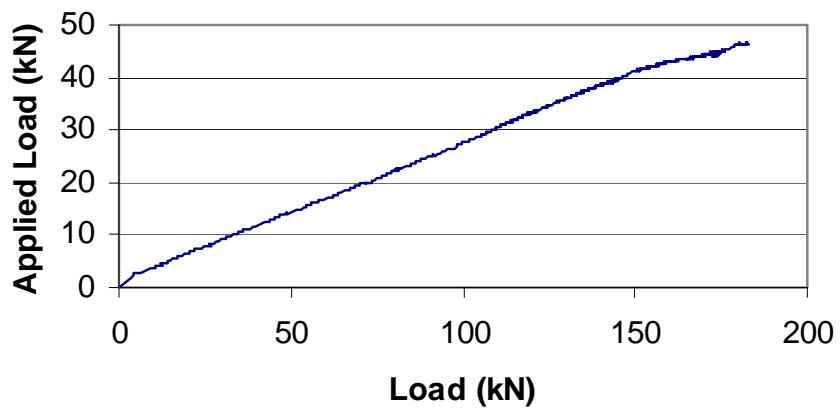


Figure C7.4 Applied Load vs. Load Cell DR15 (Test 6-3/4-4sW-GS)

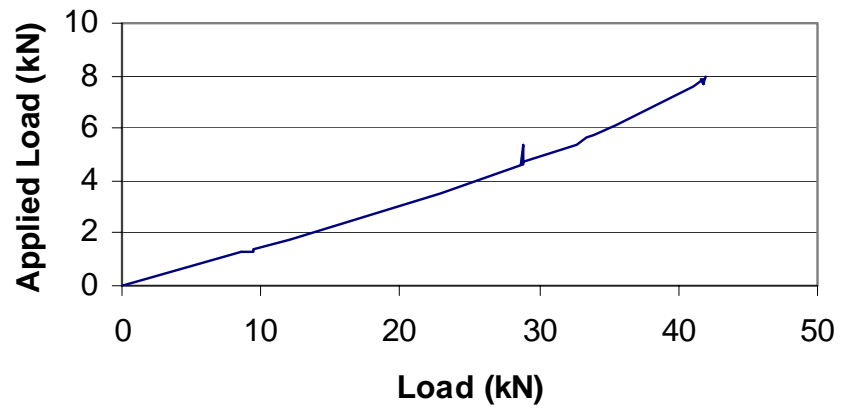


Figure C8.1 Applied Load vs. Load Cell LC3 (Test 6-3/4-4s-U)

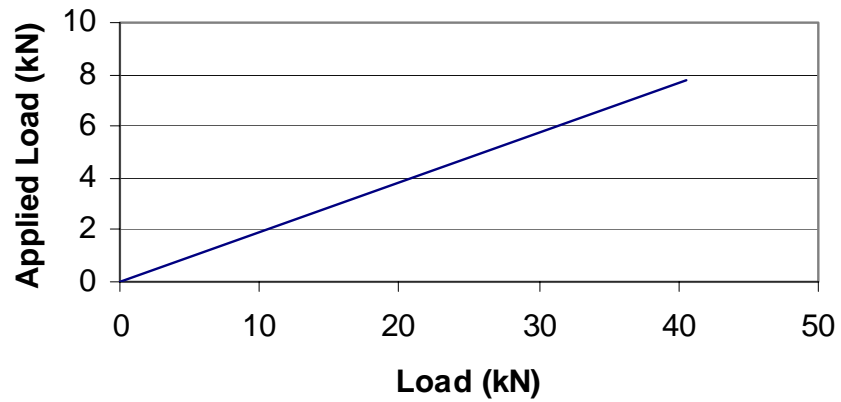


Figure C8.2 Applied Load vs. Load Cell LC6 (Test 6-3/4-4s-U)

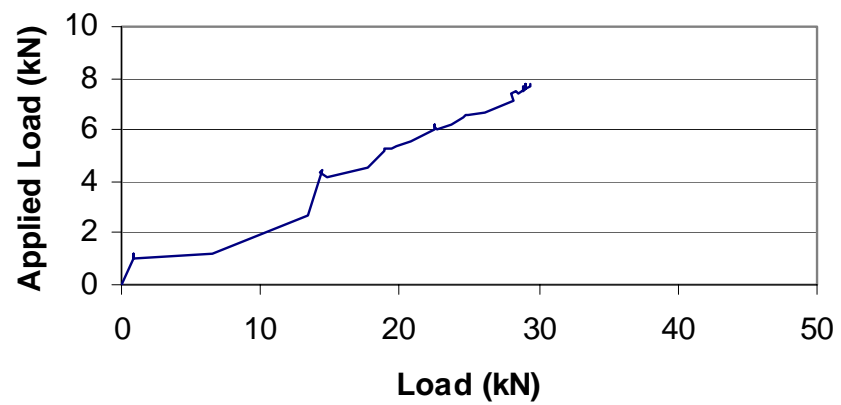


Figure C8.3 Applied Load vs. Load Cell DR17 (Test 6-3/4-4s-U)

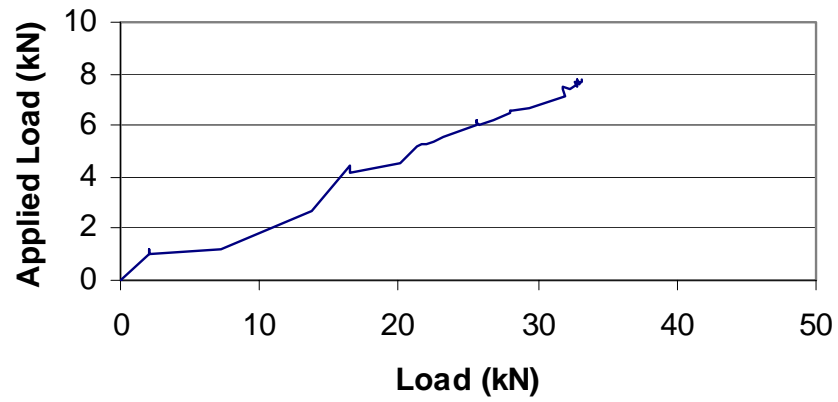


Figure C8.4 Applied Load vs. Load Cell DR21 (Test 6-3/4-4s-U)

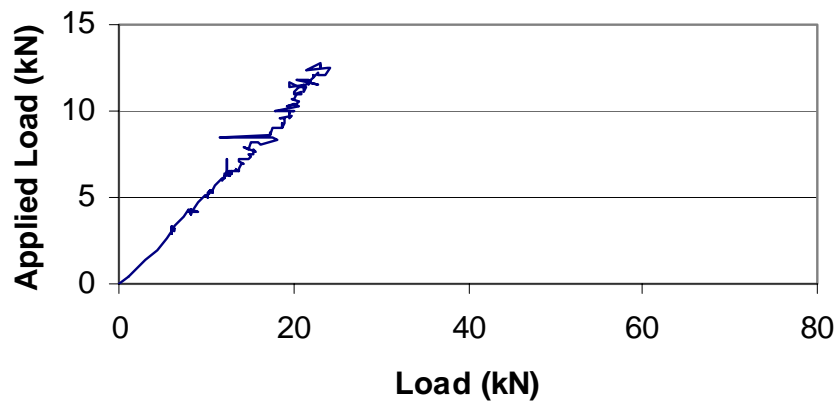


Figure C9.1 Applied Load vs. Load Cell LC3 (Test 6-3/4-4s-G)

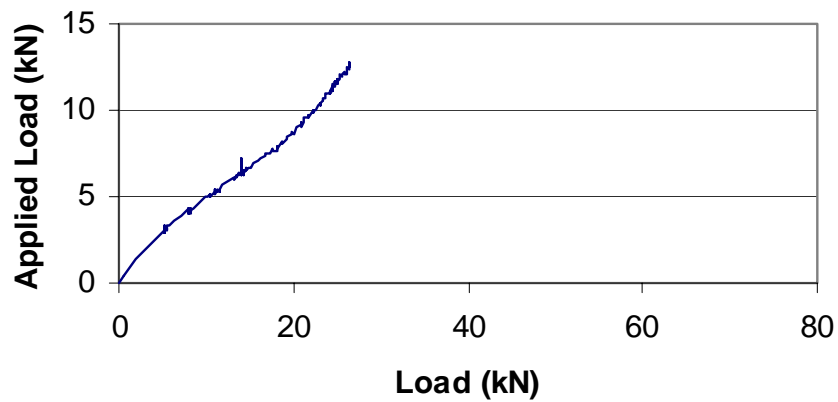


Figure C9.2 Applied Load vs. Load Cell LC6 (Test 6-3/4-4s-G)

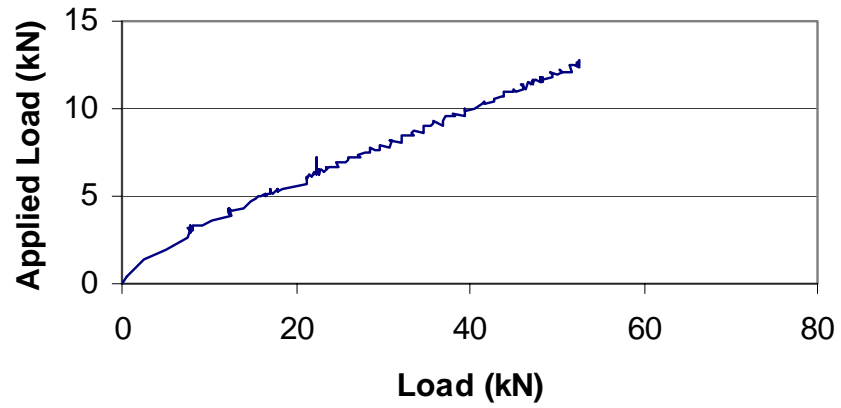


Figure C9.3 Applied Load vs. Load Cell DR17 (Test 6-3/4-4s-G)

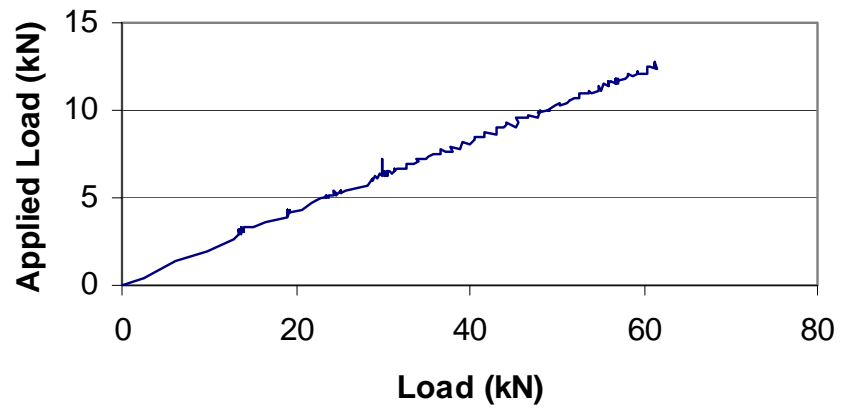


Figure C9.4 Applied Load vs. Load Cell DR21 (Test 6-3/4-4s-G)

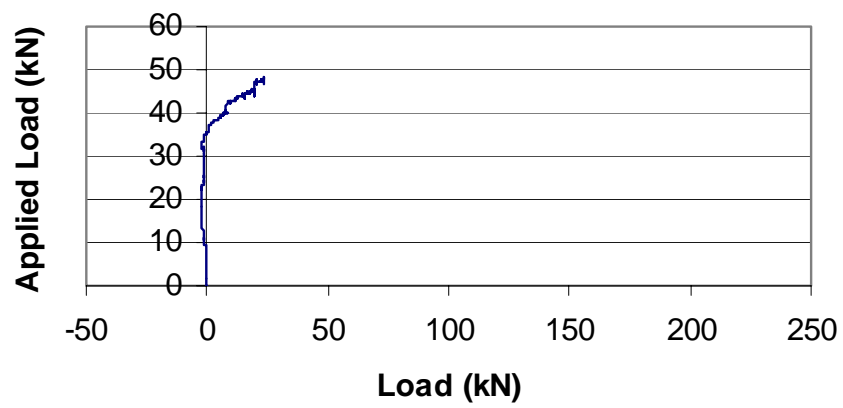


Figure C10.1 Applied Load vs. Load Cell LC3 (Test 6-3/4-4s-GS)

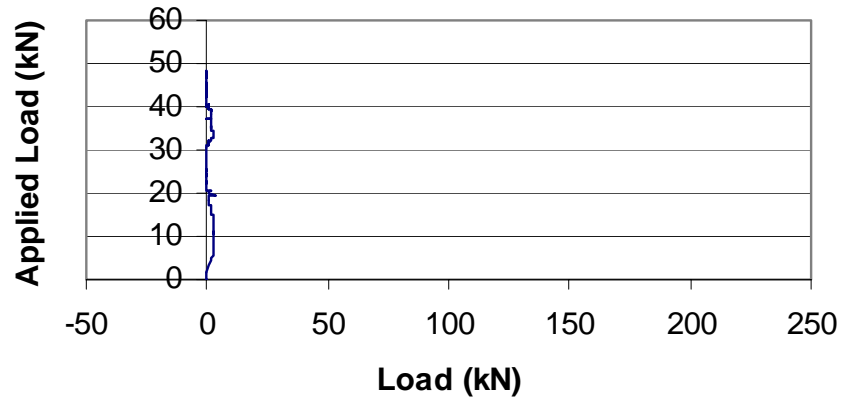


Figure C10.2 Applied Load vs. Load Cell LC6 (Test 6-3/4-4s-GS)

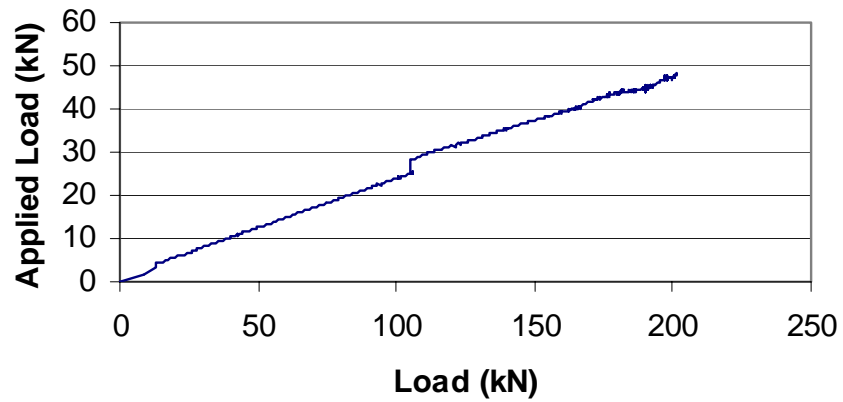


Figure C10.3 Applied Load vs. Load Cell DR17 (Test 6-3/4-4s-GS)

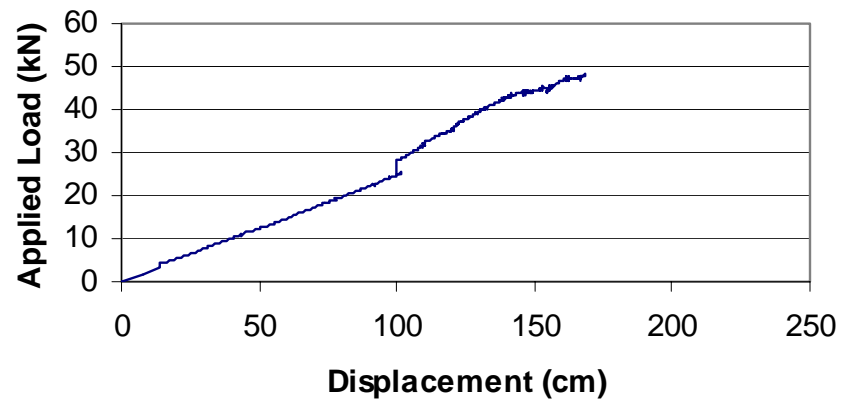


Figure C10.4 Applied Load vs. Load Cell DR21 (Test 6-3/4-4s-GS)

## APPENDIX D: LOAD-DISPLACEMENT GRAPHS

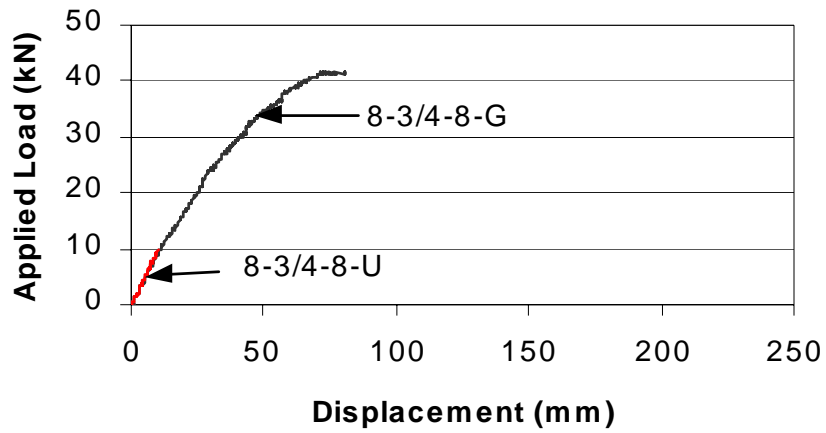


Figure D1 Load-displacement curves for Specimen #1

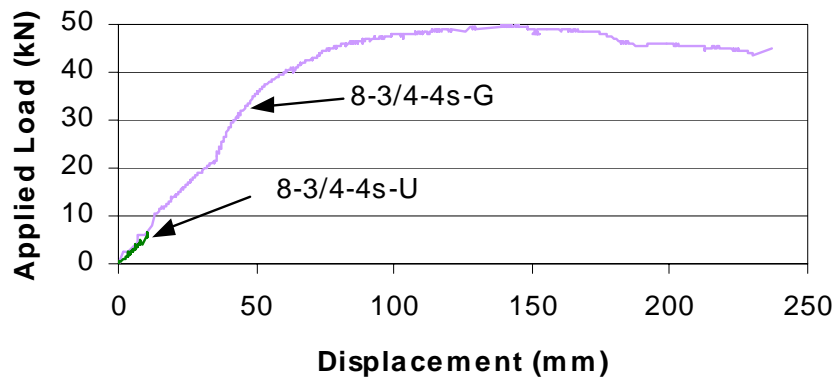


Figure D2 Load-displacement curves for Specimen #2

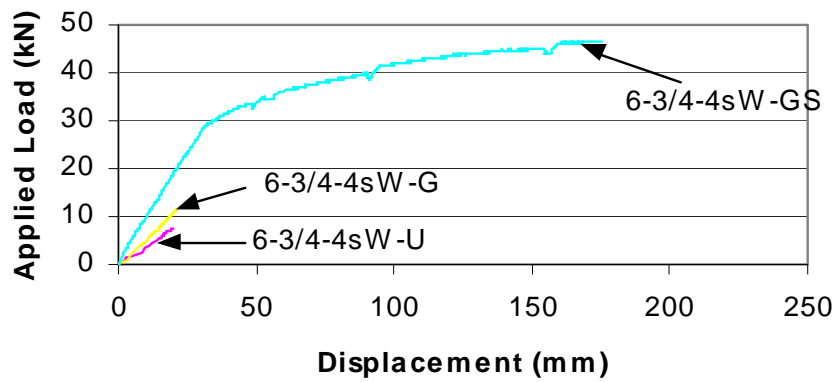


Figure D3 Load-displacement curves for Specimen #3

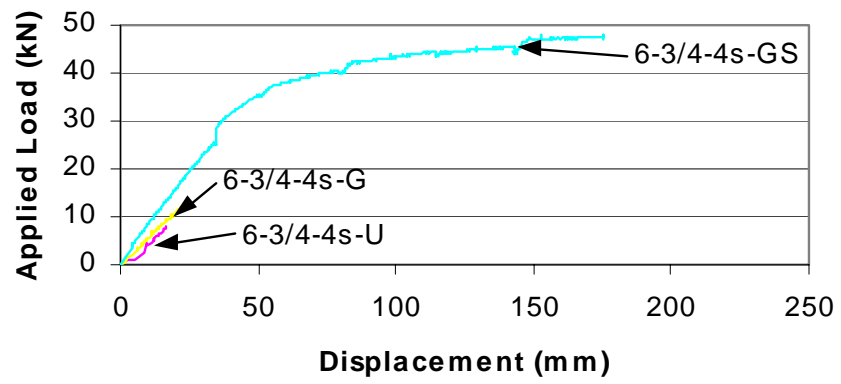


Figure D4 Load-displacement curves for Specimen #4

## APPENDIX E: MOMENT-ROTATION GRAPHS

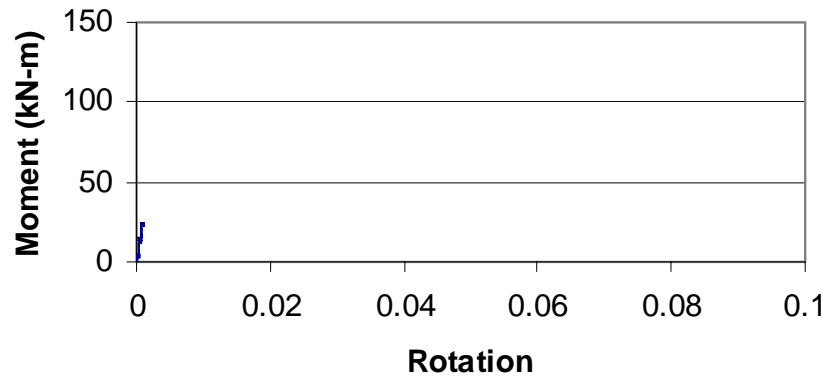


Figure E1 Moment-rotation for Specimen #1, Test 8-3/4-8-U

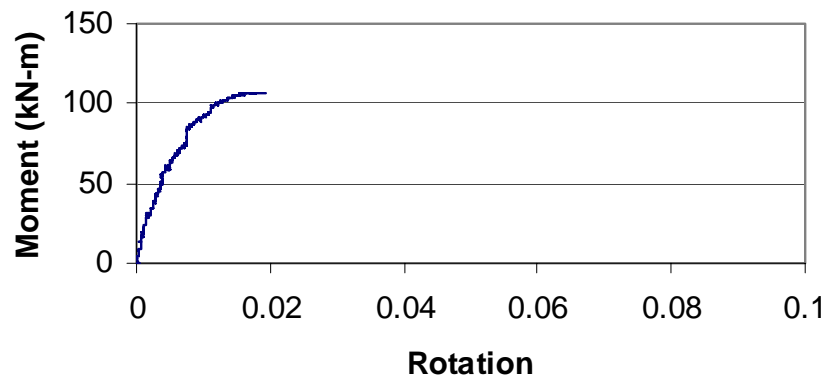


Figure E2 Moment-rotation for Specimen #1, Test 8-3/4-8-G

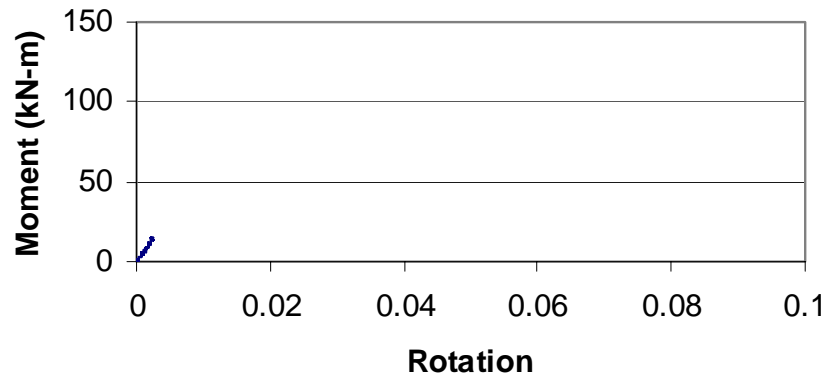


Figure E3 Moment-rotation for Specimen #2, Test 8-3/4-4s-U

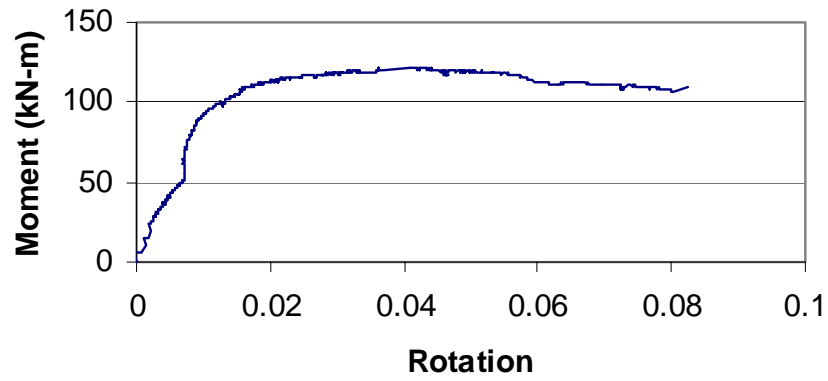


Figure E4 Moment-rotation for Specimen #2, Test 8-3/4-4s-G

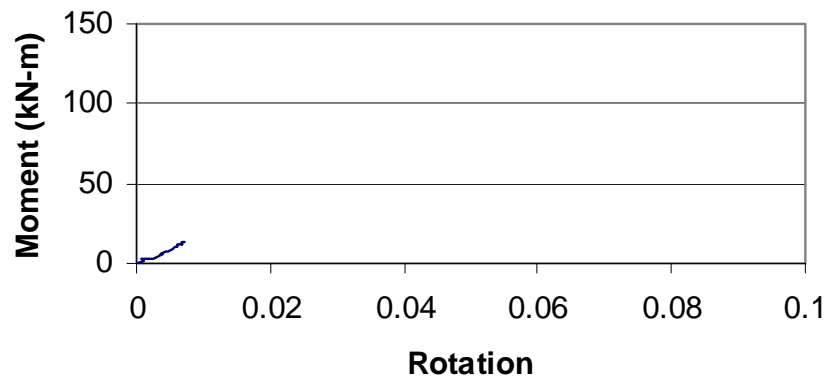


Figure E5 Moment-rotation for Specimen #3, Test 6-3/4-4sW-U

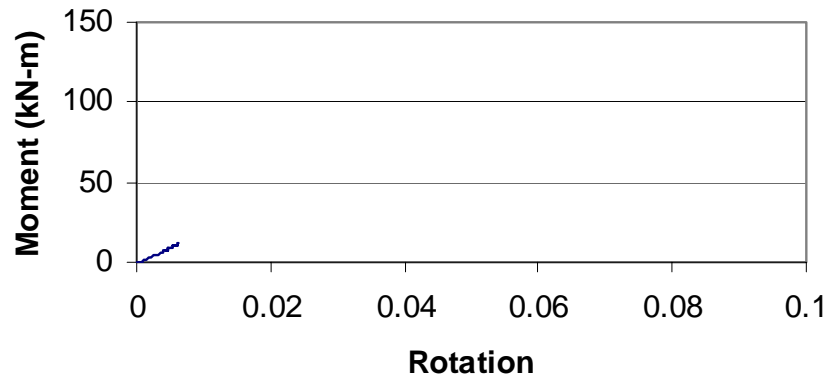


Figure E6 Moment-rotation for Specimen #3, Test 6-3/4-4sW-G

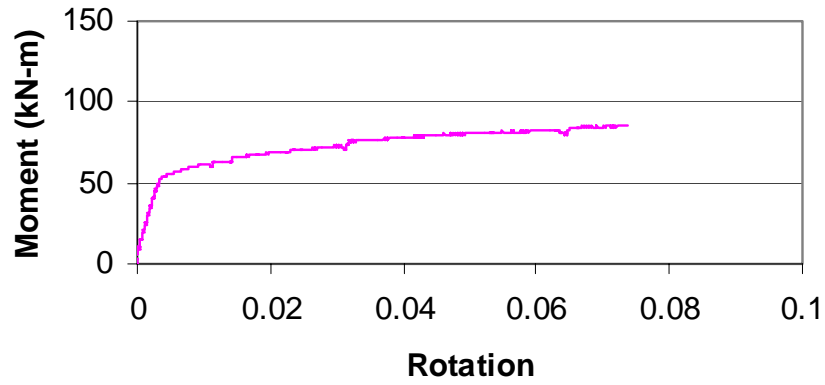


Figure E7 Moment-rotation for Specimen #3, Test 6-3/4-4sW-GS

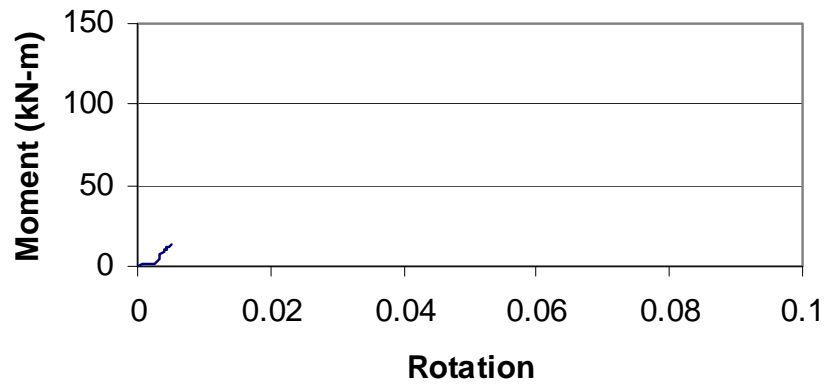


Figure E8 Moment-rotation for Specimen #4, Test 6-3/4-4s-U

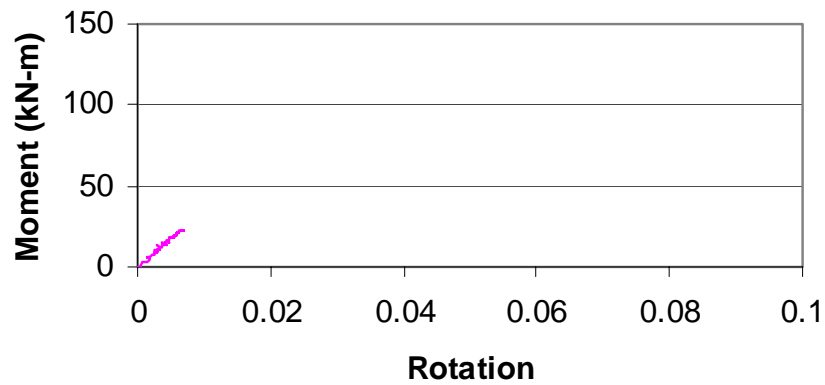


Figure E9 Moment-rotation for Specimen #4, Test 6-3/4-4s-G

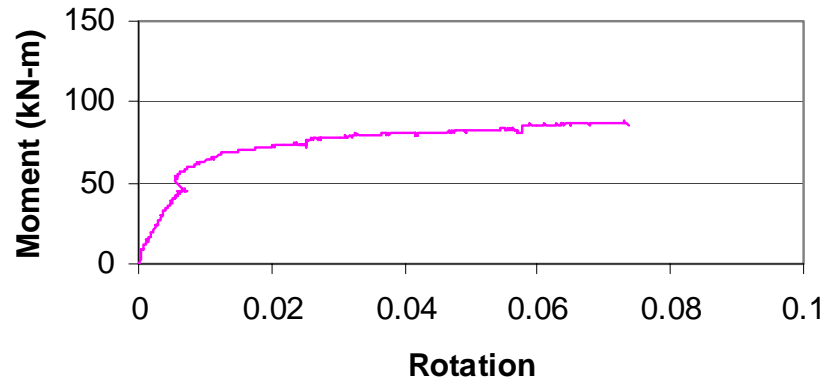


Figure E10 Moment-rotation for Specimen #4, Test 6-3/4-4s-GS

## APPENDIX F: STIFFNESS PLOTS

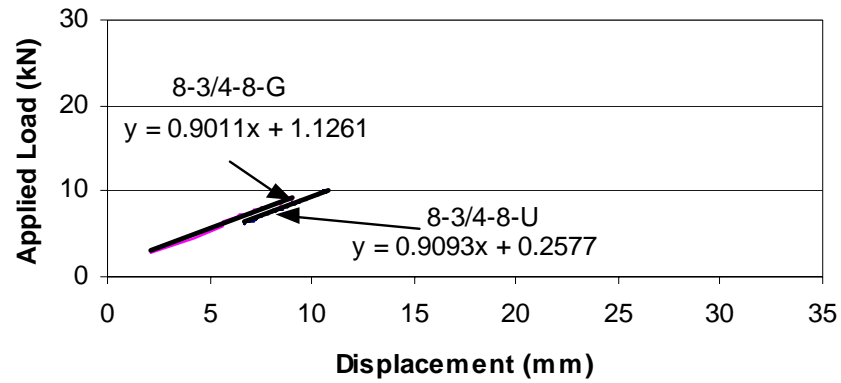


Figure F1 Stiffness plot for Specimen #1 (8-3/4-8)

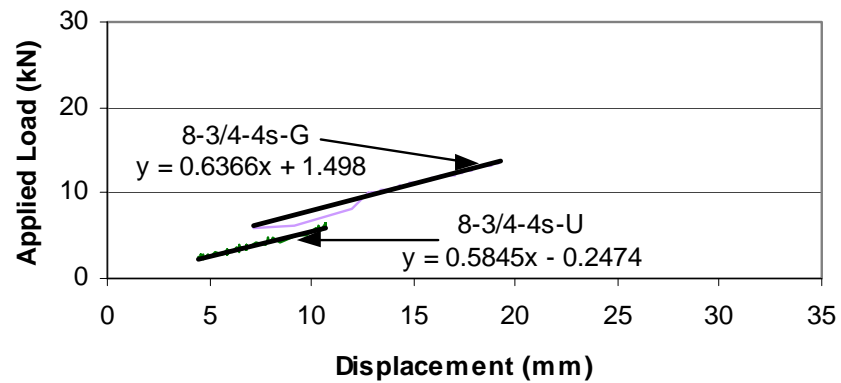


Figure F2 Stiffness plot for Specimen #2 (8-3/4-4s)

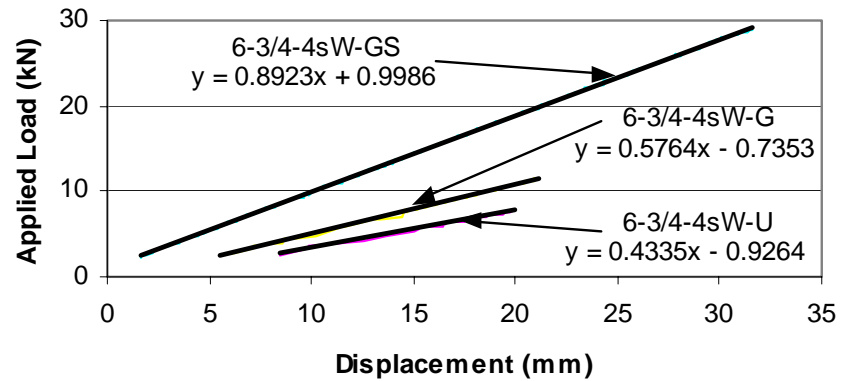


Figure F3 Stiffness plot for Specimen #3 (6-3/4-4sW)

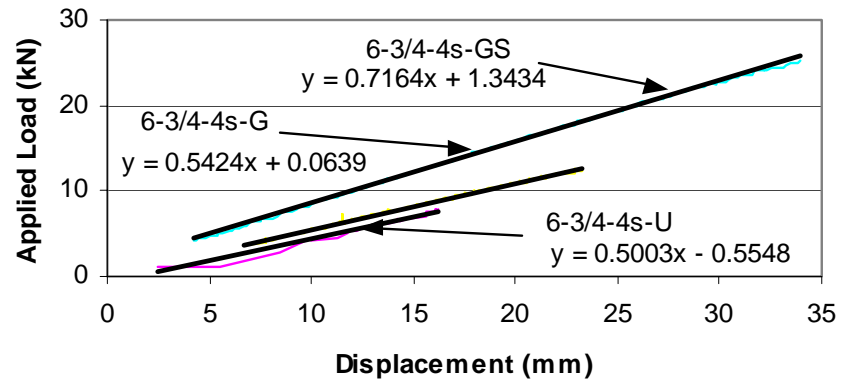


Figure F4 Stiffness plot for Specimen #4 (6-3/4-4s)

APPENDIX G: PLOTTED MOVEMENT OF REACTION ACTING ON GROUT PAD

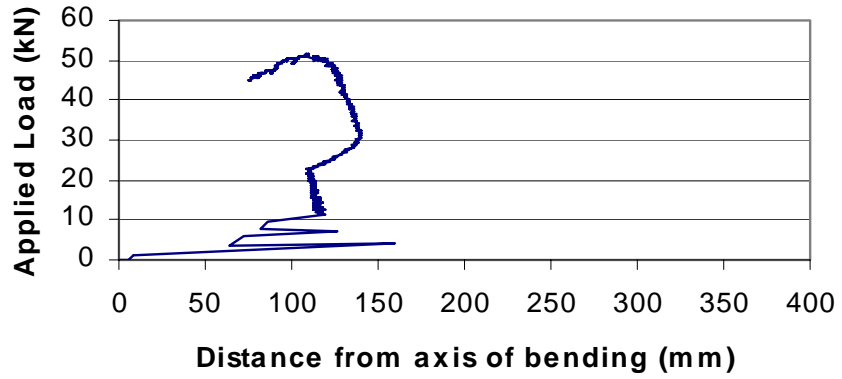


Figure G1 Movement of grout pad reaction for 8-3/4-4s-G

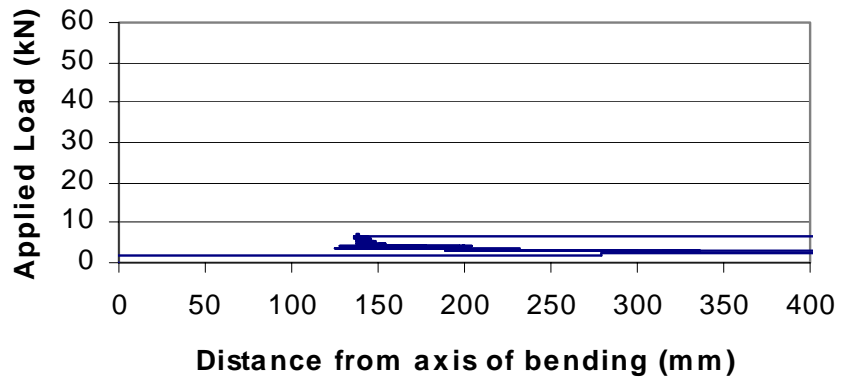


Figure G2 Movement of grout pad reaction for 6-3/4-4sW-G

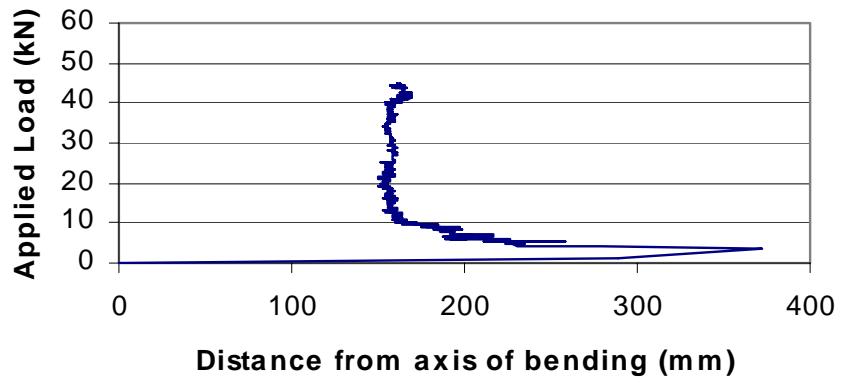


Figure G3 Movement of grout pad reaction for 6-3/4-4sW-GS

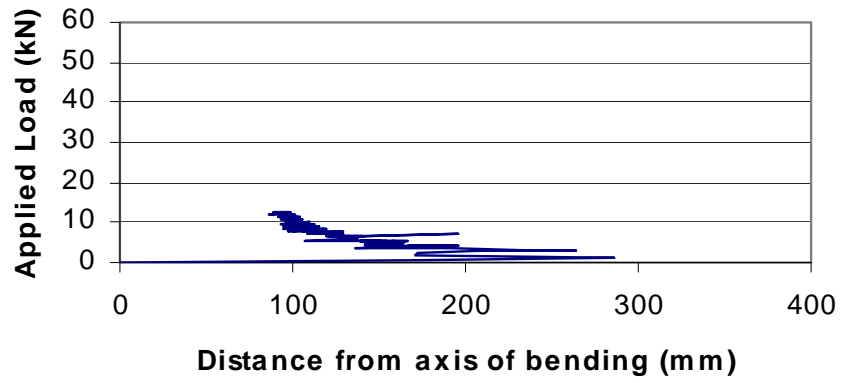


Figure G4 Movement of grout pad reaction for 6-3/4-4s-G

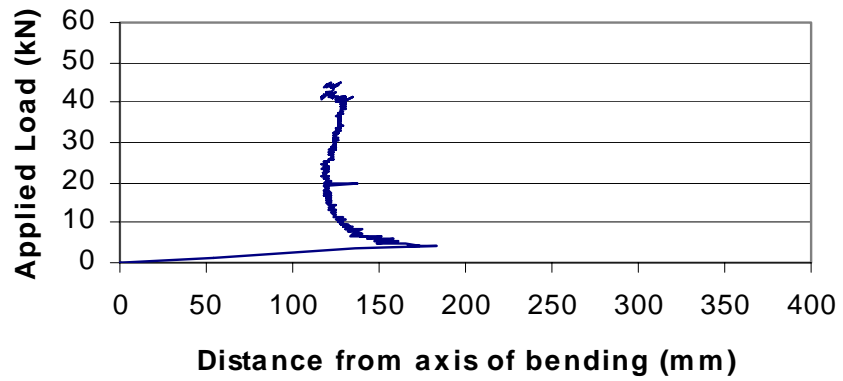


Figure G5 Movement of grout pad reaction for 6-3/4-4s-GS